

ORNL/TM-10723

**OAK RIDGE  
NATIONAL  
LABORATORY**

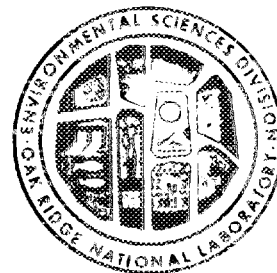
**MARTIN MARIETTA**

**Dynamics of Aquatic Ecosystems and  
Models under Toxicant Stress:  
State Space Analysis, Covariance  
Structure, and Ecological Risk**

A. R. Johnson  
S. M. Bartell

( Environmental Sciences Division  
Publication No. 3073 )

OPERATED BY  
MARTIN MARIETTA ENERGY SYSTEMS, INC.  
FOR THE UNITED STATES  
DEPARTMENT OF ENERGY



Printed in the United States of America. Available from  
National Technical Information Service  
U.S. Department of Commerce  
5285 Port Royal Road, Springfield, Virginia 22161  
NTIS price codes—Printed Copy: A10 Microfiche A01

This report was prepared as an account of work sponsored by an agency of the United States Government. Neither the United States Government nor any agency thereof, nor any of their employees, makes any warranty, express or implied, or assumes any legal liability or responsibility for the accuracy, completeness, or usefulness of any information, apparatus, product, or process disclosed, or represents that its use would not infringe privately owned rights. Reference herein to any specific commercial product, process, or service by trade name, trademark, manufacturer, or otherwise, does not necessarily constitute or imply its endorsement, recommendation, or favoring by the United States Government or any agency thereof. The views and opinions of authors expressed herein do not necessarily state or reflect those of the United States Government or any agency thereof.

ENVIRONMENTAL SCIENCES DIVISION

DYNAMICS OF AQUATIC ECOSYSTEMS AND MODELS UNDER TOXICANT STRESS:  
STATE SPACE ANALYSIS, COVARIANCE STRUCTURE,  
AND ECOLOGICAL RISK\*

A. R. Johnson and S. M. Bartell

Environmental Sciences Division  
Publication No. 3073

---

\*Submitted as a thesis by Alan R. Johnson to the Graduate Council of  
the University of Tennessee, Knoxville, in partial fulfillment of the  
requirements for the degree of Doctor of Philosophy

Date Published -- June 1988

Prepared for the  
Office of Health and Environmental Research  
(Activity No. HA 02 03 01 0)

Prepared by the  
OAK RIDGE NATIONAL LABORATORY  
Oak Ridge, Tennessee 37831  
operated by  
MARTIN MARIETTA ENERGY SYSTEMS, INC.  
for the  
U.S. DEPARTMENT OF ENERGY  
under contract DE-AC05-84OR21400

MARTIN MARIETTA ENERGY SYSTEMS LIBRARIES



3 4456 0280971 7



## TABLE OF CONTENTS

CHAPTER	PAGE
ACKNOWLEDGMENTS . . . . .	xiii
ABSTRACT . . . . .	xv
1. INTRODUCTION . . . . .	1
1.1 STATE SPACE REPRESENTATION OF ECOLOGICAL SYSTEMS . . . . .	1
1.2 CONCEPTS OF ECOLOGICAL STABILITY . . . . .	6
1.3 QUANTIFYING ECOSYSTEM RESPONSE TO PERTURBATION . . . . .	12
1.4 STATE SPACE ANALYSIS AS AN ECOTOXICOLOGICAL TOOL . . . . .	16
2. MATERIALS AND METHODS . . . . .	20
2.1 FLASK MICROCOSMS . . . . .	20
2.1.1 Assembly . . . . .	20
2.1.2 Species Composition . . . . .	21
2.1.3 Measured State Variables . . . . .	23
2.1.4 Experimental Design . . . . .	23
2.2 AQUARIUM MICROCOSMS AND OUTDOOR PONDS . . . . .	25
2.2.1 Assembly . . . . .	25
2.2.2 Species Composition . . . . .	27
2.2.3 Measured State Variables . . . . .	28
2.2.4 Experimental Design . . . . .	31
2.3 COMPUTER SIMULATIONS . . . . .	34
2.3.1 Modifications to SWACOM . . . . .	35
2.3.1.1 Trophic Structure . . . . .	35
2.3.1.2 Dissolved Oxygen . . . . .	36
2.3.1.3 Detritus and Decomposition . . . . .	37
2.3.1.4 Macrophytes . . . . .	39
2.3.2 Modeling Toxic Effects . . . . .	46
2.3.3 Modeling of Uncertainty and Variability . . . . .	48
2.4 STATE SPACE ANALYSIS . . . . .	52
2.4.1 Statistical Estimation of Displacement and Separation . . . . .	53
2.4.2 Distance Metrics and Data Transformation . . . . .	56
2.4.3 Summary Measures . . . . .	61
2.4.4 Computation of State Space Statistics . . . . .	63

CHAPTER	PAGE
3. EXPERIMENTAL RESULTS . . . . .	65
3.1 FLASK MICROCOSMS . . . . .	65
3.1.1 Dynamics of Individual State Variables . . . . .	65
3.1.2 State Space Analysis . . . . .	70
3.1.3 Changes in Covariance Structure . . . . .	75
3.2 AQUARIUM MICROCOSMS AND OUTDOOR PONDS . . . . .	79
3.2.1 Dose-Response Relationships . . . . .	82
3.2.2 Correlation with Original State Variables . . . . .	88
3.2.3 Changes in Covariance Structure . . . . .	88
4. SIMULATION RESULTS . . . . .	94
4.1 RESULTS OF DETERMINISTIC SIMULATIONS . . . . .	95
4.1.1 Model Dynamics in the Absence of Toxicant . . . . .	95
4.1.2 Model Dynamics with Toxicant Effects . . . . .	99
4.2 RESULTS OF STOCHASTIC SIMULATIONS . . . . .	108
4.2.1. Natural Variability . . . . .	108
4.2.1.1 Random initial conditions . . . . .	108
4.2.1.2 Stochastic forcing functions . . . . .	109
4.2.2 Measurement Error . . . . .	109
4.2.3 Combined Sources of Variation . . . . .	109
4.3 STATE SPACE ANALYSIS . . . . .	113
4.3.1 Summary of State Space Dose-Response Relationships . . . . .	113
4.3.1.1 Calculations based on natural variability . . . . .	113
4.3.1.2 Calculations based on measurement error . . . . .	116
4.3.1.3 Calculations based on combined sources of variation . . . . .	119
4.3.2 Statistical Power and Sample Size Requirements . . . . .	123
4.4 CHANGES IN COVARIANCE STRUCTURE . . . . .	131
4.4.1 Changes in Covariance Structure with Time . . . . .	131
4.4.2 Toxicant-Induced Changes in Covariance Structure . . . . .	133
4.5 DIAGNOSTIC VARIABLES . . . . .	137

CHAPTER	PAGE
5. DISCUSSION AND CONCLUSIONS . . . . .	150
5.1 SUMMARY AND EVALUATION OF RESULTS . . . . .	150
5.2 RELATIONSHIP WITH OTHER MULTIVARIATE TECHNIQUES . . . . .	157
5.2.1 Principal Components Analysis . . . . .	158
5.2.2 Discriminant Analysis . . . . .	162
5.3 DIRECTIONS FOR FUTURE RESEARCH . . . . .	165
5.3.1 Use of Alternative Distance Metrics . . . . .	165
5.3.2 Robust Estimation of Covariance Matrix. . . . .	170
5.4 DIAGNOSTIC VARIABLES AND RISK ANALYSIS . . . . .	171
5.5 CONCLUSION . . . . .	183
REFERENCES . . . . .	186



LIST OF TABLES

TABLE	PAGE
1.1. A summary of terminology relating to ecological stability employed in the recent scientific literature . . . . .	7
2.1. Chemical composition of the Taub T82 medium used in the flask microcosms . . . . .	22
2.2. Biotic composition of flask microcosms . . . . .	24
2.3. Toxicant exposure regimes in flask microcosms . . . . .	26
2.4. Biotic composition of the aquarium microcosms (M) and outdoor ponds (P) . . . . .	29
2.5. Toxicant exposure regimes in aquarium microcosms . . . . .	32
2.6. Toxicant exposure regimes in outdoor ponds . . . . .	33
4.1. Standard error of the mean separation as calculated from the empirical sampling distribution . . . . .	125
5.1. Type II error rates associated with the use of separation and of individual state variables to test the hypothesis of no effect on day 21 of the ecosystem simulation . . .	154



## LIST OF FIGURES

FIGURE	PAGE
2.1 Typical results of detailed <u>Elodea</u> growth model . . . . .	43
2.2 Comparison of simplified and detailed <u>Elodea</u> growth models . . . . .	45
2.3 Typical realizations of stochastic forcing functions . . . . .	50
2.4 State space trajectories showing displacement vector as the difference between perturbed and control state vectors . . . . .	54
2.5 An illustration of the Mahalanobis transformation . . . . .	60
3.1 Dynamics of pH in flask microcosms . . . . .	67
3.2 Dynamics of dissolved oxygen in flask microcosms . . . . .	68
3.3 Dynamics of conductivity in flask microcosms . . . . .	69
3.4 State space separation as a function of time and treatment level for flask microcosm experiment . . . . .	71
3.5 Correlation of state variables with separation as a function of time following toxicant addition . . . . .	72
3.6 Dose-response curves for flask microcosms exposed to 2,4-dimethylphenol . . . . .	74
3.7 Square root of the generalized variance of the control microcosms as a function of time . . . . .	76
3.8 State variable correlations as a function of time . . . . .	78
3.9 State variable correlations in microcosm data pooled over time . . . . .	80
3.10 Summary of responses observed in aquarium microcosm and outdoor pond experiments . . . . .	81
3.11 State space separation as a function of time and treatment level . . . . .	83

FIGURE	PAGE
3.12 Dose-response curves for outdoor ponds exposed to synthetic oil . . . . .	85
3.13 Dose-response curves for aquarium microcosms exposed to synthetic oil . . . . .	86
3.14 Percentage of state variable correlations greater than 0.7 in absolute value as a function of treatment level . . . . .	90
3.15 Eigenvectors associated with first principal component of correlated data . . . . .	91
3.16 Changes in covariance structure of state variables as a function of treatment level in pond experiment . . . . .	93
4.1 Biomasses of pelagic trophic levels in deterministic simulations at various toxicant concentrations . . . . .	96
4.2 Macrophyte biomass dynamics in deterministic simulations at various toxicant concentrations . . . . .	97
4.3 Detritus dynamics in deterministic simulations at various toxicant concentrations . . . . .	98
4.4 Dynamics of macrophyte net photosynthesis in deterministic simulations at various toxicant concentrations . . . . .	100
4.5 Dynamics of phytoplankton net photosynthesis in deterministic simulations at various toxicant concentrations . . . . .	101
4.6 Dissolved oxygen dynamics in deterministic simulations at various toxicant concentrations . . . . .	102
4.7 Nutrient dynamics in deterministic simulations at various toxicant concentrations . . . . .	103
4.8 Dynamics of representative state variables in Monte Carlo simulations with random initial conditions . . . . .	110
4.9 Dynamics of representative state variables in Monte Carlo simulations with stochastic forcing functions . . . . .	111

FIGURE	PAGE
4.10 Dynamics of representative state variables in Monte Carlo simulations with measurement error . . . . .	112
4.11 Dynamics of representative state variables in Monte Carlo simulations with combined sources of variability . . . . .	114
4.12 State space separation as a function of time and treatment level for ecosystem simulation model with natural variability alone . . . . .	115
4.13 Dose-response curves for ecosystem simulation model with natural variability alone . . . . .	117
4.14 State space separation as a function of time and treatment level for ecosystem simulation model with measurement error alone . . . . .	118
4.15 Dose-response curves for ecosystem simulation model with measurement error alone . . . . .	120
4.16 State space separation as a function of time and treatment level for ecosystem simulation model with combined sources of variability . . . . .	121
4.17 Dose-response curves for ecosystem simulation model with combined sources of variability . . . . .	122
4.18 Mean separation for 20 independent samples of size N (N=1,2,4,8,16,32,64) at various toxicant concentrations . . . . .	126
4.19 Mean separation as a function of toxicant concentration for a sample size of N=1 . . . . .	127
4.20 Operating characteristic curves for mean separation for samples of size N=1 and N=2 . . . . .	130
4.21 Changes in covariance structure of state variables over time in the simulation model . . . . .	132
4.22 Changes in selected state variable correlations over time in the simulation model . . . . .	134
4.23 Changes in covariance structure of state variables as a function of treatment level in the simulation model . . . . .	136

FIGURE	PAGE
4.24 Rates of occurrence of type I and type II errors as a function of numerical criterion using total zooplankton as a diagnostic variable . . . . .	143
4.25 Simulation results projected into two-dimensional diagnostic space defined by $P_{\text{blugrn}}$ and $P_{\text{spring}}$ . . . . .	147
5.1 Results of analysis of hypothetical data set . . . . .	159
5.2 Illustration of geometric interpretation of discriminant analysis . . . . .	164
5.3 Minkowski circles for $p = 1, 2,$ and $\infty$ . . . . .	169
5.4 Total zooplankton as a diagnostic variable . . . . .	176
5.5 Blue-green and spring dominant phytoplankton as diagnostic variables based on linear regression . . . . .	177
5.6 Blue-green and spring dominant phytoplankton as diagnostic variables based on discriminant analysis . . . . .	178
5.7 Blue-green and spring dominant phytoplankton as diagnostic variables based on ad-hoc nonlinear criterion . . . . .	179

## ACKNOWLEDGMENTS

Several persons were directly involved in the guidance of this research, including Gary Sayler, Tom Hallam, Walter Farkas, Jeff Giddings, Barbara Walton and Roger Minear. Many others were involved in discussions which stimulated the development of the ideas presented in this work; we are particularly indebted to Bob O'Neill, Tony King and Dean Urban in this regard.

Finally we thank the ESD word processing staff and the graphics staff for their able contributions to the production of this manuscript. This research was conducted at the Environmental Sciences Division, Oak Ridge National Laboratory, Oak Ridge, Tennessee, and was sponsored by the Office of Health and Environmental Research, U.S. Department of Energy, under contract DE-AC05-84OR21400 with Martin Marietta Energy Systems, Inc.



## ABSTRACT

JOHNSON, A. R. and S. M. BARTELL. 1988. Dynamics of aquatic ecosystems and models under toxicant stress: state space analysis, covariance structure, and ecological risk. ORNL/TM-10723. Oak Ridge National Laboratory, Oak Ridge, Tennessee. 212 pp.

The state of an ecosystem at any time  $t$  may be characterized by a multidimensional state vector  $x(t)$ . Changes in state are represented by the trajectory traced out by  $x(t)$  over time. The effects of toxicant stress are summarized by the displacement of a perturbed state vector,  $x_p(t)$ , relative to an appropriate control,  $x_c(t)$ . Within a multivariate statistical framework, the response of an ecosystem to perturbation is conveniently quantified by the distance separating  $x_p(t)$  from  $x_c(t)$  as measured by a Mahalanobis metric. Use of the Mahalanobis metric requires that the covariance matrix associated with the control state vector be estimated.

State space displacement analysis was applied to data on the response of aquatic microcosms and outdoor ponds to alkylphenols. Dose-response relationships were derived using calculated state space separations as integrated measures of the ecological effects of toxicant exposure. Inspection of the data also revealed that the covariance structure varied both with time and with toxicant exposure, suggesting that analysis of such changes might be a useful tool for probing control mechanisms underlying ecosystem dynamics.

State space displacement analysis was further investigated in the context of an ecological simulation model. Replicate state space trajectories, incorporating both natural variability (random initial conditions and stochastic forcings) and measurement error, were produced using Monte Carlo techniques. It was demonstrated that although quantitative estimates of state space separation vary with the estimated covariance matrix, qualitative features of the dose-response relationships are relatively robust to variation in the covariance estimates. Furthermore, the state space methodology was demonstrated to have high statistical power: effects at the lowest simulated dose could readily be detected with as few as one or two Monte Carlo replicates per treatment.

Finally, the problem of selecting a small set of diagnostic variables which reflect ecosystem state was examined. The adequacy of diagnostic variables as predictors of ecological risk is a function of the probabilities of the associated type I and type II statistical errors. A cost-benefit approach for choosing an optimal balance between these error rates was developed.

## Chapter 1

## INTRODUCTION

This thesis is concerned with the development of a practical methodology for applying the state space approach to the analysis of ecotoxicological data. The objectives of the research are (1) to distinguish the response to stress from other aspects of ecosystem behavior, and (2) to develop a methodology for describing this response, both qualitatively and quantitatively. The work presented here represents a significant extension of many of the preliminary applications of state space techniques which will be reviewed in sections 1.1 and 1.3. Specifically, a methodology is developed which fits neatly into the framework of modern multivariate statistical analysis.

## 1.1 STATE SPACE REPRESENTATION OF ECOLOGICAL SYSTEMS

This study employs a "state space" or "phase space" representation of ecological systems. The state space approach can be given a simple geometric interpretation, and thereby facilitates mathematical analysis of system behavior. The state space approach is a widely used mathematical tool, particularly in the study of the dynamic behavior of systems of differential equations (see, for example, Zadeh and Desoer 1963). As such it has found frequent

application in modeling real world systems, particularly in such fields as physics and engineering, and increasingly in the biological sciences, including ecology.

At any instant in time, an ecosystem can be defined to be in a "state" described by a set of observable quantities called state variables. It may be that the state variables are not themselves directly measured, but rather a set of output variables which bear some mathematical relationship to the state variables. This does not affect our ability to apply the state space approach as long as the functional relationships between the state variables and the output variables are known.

A state space is defined by constructing a coordinate system in which a separate axis is taken to represent each state variable,  $x_i$ . The dimensionality of the state space is therefore equal to the number of state variables,  $n$ . Any set of values for the state variables corresponds to a point, or equivalently a vector, in the state space:  $x(t) = (x_1, x_2, \dots, x_n)'$ . As changes in the state of the ecosystem occur, the location of the corresponding vector in the state space changes. The path traced out by the state vector is referred to as a state trajectory. When the dimensionality is low (two or three state variables) the state space representation leads to a graphical display of the data. State space trajectories of higher dimensionality are not accessible to direct visual inspection,

but quantities related to distance or direction can be defined algebraically, and interpreted by analogy to lower dimensional systems.

The concepts of a state space and state trajectories are quite general. They can be applied to either continuous or discrete state variables. In the case of discrete state variables, such as numbers of individuals (which is restricted to integer values), the state vector is constrained to lie on a multidimensional grid. Similarly, the state space representation is valid whether time is considered as a continuous variable (as in models based on differential equations) or a discrete variable (as in models based on difference equations). State space analysis can be applied to systems that are linear or nonlinear, deterministic or stochastic, stable or unstable, near or far from equilibrium. To place the present study in perspective, a brief overview is presented of some applications of the state space representation drawn from the recent ecological literature, with an emphasis on experimental studies.

Two dimensional state space diagrams have been used as a graphical device for presenting data. Heath (1980) plotted trajectories of nitrate concentration versus phosphate concentration for a series of small, flask-type aquatic microcosms. Marmorek (1984) plotted trajectories of zooplankton biomass versus chlorophyll for lake enclosures used in an acidification study. Woltering (1985) plotted guppy biomass versus amphipod biomass trajectories to display

results obtained in his multispecies toxicity test system. Waide et al. (1980) displayed regions of a pH-dissolved oxygen state space occupied by their aquatic microcosms. In this last case, the choice of state variables is given the theoretical justification that they serve as surrogates for hydrogen ion activity and electron activity, two master variables controlling biogeochemical systems.

Often higher dimensional data are presented as trajectories projected into a two dimensional subspace defined by principal components. Principal components analysis is a statistical technique used to find lower dimensional representations which often explain most of the variance in the original multivariate data set. This was the approach taken by Gates (1983) in analyzing changes in the size distribution for the protozoan Tetrahymena grown in batch culture. Cell volume distribution, as quantified by a 100-channel electronic particle counter, was seen to change as the cultures aged, and these changes took the form of a simple circular trajectory in the space defined by the first two principal components. Gates et al. (1983) applied the same technique to analyze biomass distributions for plankton samples collected from a series of lakes in Ontario, Canada. The technique was found to be useful in summarizing both seasonal and year-to-year changes in the plankton community, and suggested several hypotheses about processes controlling plankton dynamics in lake ecosystems.

Bartell et al. (1978) explored the use of trajectories in principal components space as a method of describing phytoplankton periodicity in Lake Wingra. More recently, Allen et al. (1984) analyzed patterns emerging from trajectories of phytoplankton data submitted to various transformations prior to principal components analysis. These techniques were able to uncover different aspects of phytoplankton dynamics operating at different time scales. Allen and Shugart (1983) analyzed by principal components the community trajectories generated by a forest succession model. This analysis revealed a decoupling of overstory versus understory dynamics which had not been explicitly built into the model, but which could be explained in hindsight. Allen et al. (1977) studied patterns of phytoplankton succession in a state space based on "first differences" in species abundance. The first difference, which is the difference in abundance between two successive observations, gives an indication of the rate of change of species abundance. It was shown that over the course of a year, the state vector migrates in a cyclic fashion through a set of relatively stable configurations.

Ecological observations can be expressed in state vector form to facilitate mathematical calculations. Ollason (1977) studied the population densities of algae, rotifers and protozoans in freshwater microcosms, calculating the speed at which the state vector moved along its trajectory as a measure of the overall rate of community change. Leffler (1980) adopted the same approach for analyzing the

nutrient input-output dynamics of flow-through microcosms. Using a more elaborate mathematical approach, Morkoc et al. (1985) employed the state space approach to statistically model spatial and temporal variations in soil water content and temperature.

## 1.2 CONCEPTS OF ECOLOGICAL STABILITY

Central to the study of ecosystem dynamics, both in the unperturbed state and in response to toxicant stress, are a number of concepts related to stability. These concepts are relevant to this study because they can be used to describe the range of dynamic systems to which state space methodology is best applied. The state space method used in this study requires comparing the state trajectory of a toxicant-perturbed system with some reference trajectory representing the dynamics of an unperturbed system. The meaningfulness of such a comparison is a function of the stability characteristics of the system.

The use of various stability related terms in the recent ecological literature is summarized in Table 1.1. Various authors have obviously attached different meanings or shades of meaning to these terms, but in many cases have failed to provide explicit definitions, making reconstruction of their intent a difficult task. The groupings shown in Table 1.1 are intended to represent constellations of related ideas, but not necessarily strict synonymy.

Table 1.1. A summary of terminology relating to ecological stability employed in the recent scientific literature.

<u>Term(s)</u>	<u>References</u>	<u>Approximate Definition</u>
Constancy	4,6	The degree to which an ecosystem tends to remain in a fixed state.
Variability	7,8	Inversely related to constancy.
Resistance Interia Resilience?	1,7,8 2,4,5,6 3	The capacity of an ecosystem to resist changes in state in the face of external disturbance.
Resilience Elasticity Stability	1,7,8 2,4,5,6 3	The rate of (or time to) recovery following a perturbation.
Amplitude Resiliency Fragility	2,4,6 5 9	The extent to which an ecosystem can be perturbed and still be capable of recovery.
Persistence Resilience?	4,6,7,8 3	The capacity for continued survival of an ecosystem in the face of disturbance, although perhaps in an altered state.

- 1 - Webster, Waide and Patten (1975)  
 2 - Westman (1978)  
 3 - Holling (1973)  
 4 - Orians (1975)  
 5 - Cairns and Dickson (1977)  
 6 - Sheehan (1984)  
 7 - Pimm (1984)  
 8 - Harrison (1979)  
 9 - May (1975)

In many respects the simplest, but also the most restrictive definition of stability is that of constancy. An ecosystem which displays little change over time is regarded, in some sense, as more stable than a continually changing one. It is apparent that the natural variability of an ecosystem is an inverse measure of its constancy. Furthermore, the notions of constancy and variability may be generalized (though none of the authors reviewed explicitly do this) to apply not only in a static sense, but also in a relative sense to systems undergoing periodic or other predictable changes of state. In this case, a system which faithfully repeats a cyclical pattern with only minor deviations is exhibiting a high degree of constancy relative to that cycle, even if the changes in the state variables over time is great (low constancy in an absolute sense).

The shortcoming of using constancy (or variability) alone as a measure of ecosystem stability is that no distinction can be made between systems that exhibit little change due to a lack of disturbance as opposed to systems that are able to maintain a degree of constancy despite disturbance. This necessitates the definition of a third concept of stability, variously referred to as resistance or inertia. Ideally the relative resistance (inertia) of different ecosystems could be quantified by measuring the differing amounts of change in state variables given the same disturbance.

Frequently contrasted with resistance is the concept of resilience, which is a measure of the rate of recovery following perturbation. The term elasticity is also used in an apparently synonymous fashion by several authors. Resistance has been related to the presence of large components with slow turnover, such as detritus, whereas resilience is a function of rate regulation, particularly by heterotrophs (O'Neill et al. 1975, O'Neill 1976). Webster et al. (1975) proposed a generally inverse relationship between resistance and resilience, but empirical tests of this hypothesis are lacking.

The concept of amplitude has been introduced as a measure of the maximum disturbance an ecosystem can withstand while retaining the capacity for recovery to the original state. Similar concepts are expressed as resiliency by Cairns and Dickson (1977), and as dynamic fragility by May (1975). Imposed disturbances can be thought of as a direct perturbation of the state variables, or as changes in parameters which control the dynamics of the state variables. Orians (1975) defines amplitude with respect to displacement in the state space, whereas May (1975) explicitly relates fragility to changes in the parameters. Therefore, these may be regarded as different concepts, but since the decision as to whether a particular quantity is treated as a parameter or as a state variable is frequently equivocal, these concepts have been grouped together.

Persistence is alternately defined as the capability of an ecosystem to survive for an indefinite time span, or in terms of the expected survival time for the the system (or its individual components). In either case, persistence is related to the ability to survive in the face of disturbance, although not necessarily in the same state.

The terminology employed by C. S. Holling deserves special attention. In an important and influential review paper, Holling (1973) uses the term *stability* to express the concept referred to above as resilience. Unfortunately, he also uses the term *resilience*, but with a very different connotation. According to Holling, resilience "determines the persistence of relationships within a system and is a measure of the ability of these systems to absorb changes of state variables, and parameters, and still persist". Orians (1975) and Westman (1978) equate Holling's concept of resilience with their use of the term *inertia*. However, a careful inspection of Holling's definition appears to show a greater affinity with the concept of persistence. In actuality, Holling's precise meaning is elusive, and his concept of resilience may not fit neatly into any of the categories of Table 1.1.

Having introduced the subject of ecological stability, it is now necessary to examine the implications for state space analysis. Clearly, a state space analysis is not well suited to systems which

are unstable in the sense of lacking persistence. Systems which fail to persist will be characterized by state variables going to zero or to other trivial values. Such a system may reorganize, but in general this will entail the appearance of new state variables replacing the now irrelevant original state variables. Simple comparison of perturbed and unperturbed trajectories in such a situation becomes fruitless. Fortunately, an observer usually has considerable latitude in the choice of state variables used to describe an ecosystem. Frequently a judicious selection of state variables will yield a description in which the system is persistent.

However, if persistence is the only form of stability displayed by the system, the application of state space analysis may still be problematical. Persistent systems may have the property that trajectories differing only slightly in initial conditions will diverge greatly over time (even in the absence of toxicant stress). In such cases, distinguishing between endogenous system dynamics and true toxicant-induced displacement would be difficult at best. It is possible that valid distinctions could be made in terms of the long term statistical properties of the trajectories (i.e., the distribution of states visited), but such methods are not employed in this study.

State space displacement analysis is most readily applied in cases where (1) the unperturbed system follows a well-defined reference trajectory, and (2) a perturbed system tends to return

toward the reference trajectory, at least for displacements over some noninfinitesimal magnitude range. If the unperturbed reference trajectory is in fact a static equilibrium point, such a system is referred to as homeostatic. In the more general situation of a dynamic reference trajectory, the system is said to be homeorhetic. The stability concepts of resistance, resilience, and amplitude are all applicable to homeorhetic systems, and can be quantified using the state space methodology. The constancy (or variability) of the system is important in determining the sampling protocol necessary to adequately characterize the system dynamics.

### 1.3 QUANTIFYING ECOSYSTEM RESPONSE TO PERTURBATION

Within the state space representation, the response of an ecosystem to perturbation is reflected by the displacement of the state vector away from its original location. It is thus convenient to use some measurement of the distance the state vector is displaced to quantify the response to perturbation. Several researchers have in fact explicitly used this approach. Others have used measures which are equivalent to a state space distance, although not defined in those terms. Several approaches to quantifying ecosystem response to perturbation, explicitly or implicitly based on state space displacements, are discussed below.

Ulanowicz (1978) distinguished between ecological stress and ecological strain using terminology borrowed from mechanical

engineering. Stress was defined as an external force or pressure exerted on the system, while strain is the response of the system to the imposed stress. Then, following Innis (1975), Ulanowicz adopted the the following index of ecological strain. Taking  $H^*$  as the value of some vector function describing an ecosystem in an unstressed condition, and  $H$  as the corresponding value of the function for a stressed ecosystem, ecological strain was quantified as

$$S = |H - H^*| \quad (1.1)$$

which is an Euclidean distance measure.

Leffler (1978, 1980) defined several measures of the relative stability of ecosystem dynamics in response to perturbation. Constancy was defined in terms of the normal range of fluctuations of a measured ecosystem parameter over time. A response to perturbation was considered significant if the parameter moved outside this normal operating range. Resistance was measured by the largest excursion beyond the normal operating range, and resilience by the time required to return to the normal operating range. Leffler applied these stability measures to aquatic microcosms, concentrating particularly on nutrient input/output ratios. More recently, Shannon et al. (1986) employed Leffler's definitions in the analysis of other aquatic microcosms. These applications were restricted to the

univariate case, but the methodology developed in this study can be regarded as an extension of the technique to a multivariate state space.

O'Neill (1976) investigated the properties of a three compartment (producer-heterotroph-detritus) simulation model using different sets of parameter values to represent various types of ecosystems. One aspect of this simulation involves perturbing the system by removing 10% of the equilibrium producer biomass. In all cases, the systems tended to return to the original equilibrium, and the rate of recovery was summarized by calculating the "sum of the squared deviations" for all three components over time. This measure is equivalent to the squared Euclidean distance in the three dimensional state space.

Finally, consideration is given to the method for quantifying community recovery developed by Bloom (1980). Bloom addressed the problem of analyzing of data consisting of repeated observations of the abundance of various taxa over a time interval prior to and subsequent to perturbation. The data (either raw or suitably transformed) were analyzed by principal components to reduce the dimensionality of the state space. Then, working in the space defined by the first two or three principal components, a cluster of state vectors corresponding to the "preperturbation" samples was identified. A rejection envelope was defined such that any vector

outside the envelope was considered to be significantly displaced from the preperturbation cluster, i.e., to be in a stressed condition. The envelope was defined by calculating the distance of each vector from the cluster centroid on each axis, and then calculating a confidence interval for each axis. Confidence intervals were calculated either on a parametric basis (using a Student's *t* statistic) and on a nonparametric basis (using a Mann-Whitney *U* statistic). The recovery of a community following perturbation was monitored by calculating the distance from the postperturbation state vectors to the nearest face of the rejection envelope.

Although Bloom's work is significant in terms of attempting to employ multivariate techniques to study the trajectories of perturbed communities, there are significant problems with his methodology. Bloom specifies that the boundaries of the rejection envelope be determined by independent confidence intervals on each of the axes, but this method yields a true type I error rate that may be substantially different than the  $\alpha$  value chosen for the univariate confidence intervals. This problem can be corrected by using established techniques for simultaneous statistical inference, such as a maximum modulus, a Bonferroni, or a Scheffé approximation (Miller 1966, pp. 12-22). More importantly, because of the computational complexity of determining the distance from an arbitrary point to the nearest face of a multidimensional rectangular

solid, Bloom reports that the method is effectively limited to three or fewer dimensions. This is his motivation for the initial principal components analysis, to approximate a system of high dimensionality by one of low dimensionality. Furthermore, by defining the rejection envelope as a static region of the state space based on pre-perturbation samples, Bloom's method is restricted to systems displaying homeostatic behavior. The methodology developed in the present study is applicable in more general situations, and overcomes Bloom's computational limitations.

#### 1.4 STATE SPACE ANALYSIS AS AN ECOTOXICOLOGICAL TOOL

The objective of this thesis is to present a state space representation of ecosystem dynamics which is appropriate for evaluating the response of such systems to inputs of toxic materials. The preceding discussion has demonstrated that this response can be conceptualized as a displacement of the state vector away from its original trajectory. Thus, the response can be described by displacement vector,  $u(t)$ , defined as

$$u(t) = x(t) - x_0(t) \quad (1.2)$$

where  $x(t)$  represents the state vector of the perturbed ecosystem, and  $x_0(t)$  represents the state vector which would have been realized if the ecosystem had not been perturbed. In experimental

situations  $x(t)$  is directly observable, but  $x_0(t)$  must be inferred from observation of an appropriate reference system. In this study comparisons are always made between replicate experimental ecosystems (microcosms or ponds) randomly assigned to control (untreated) or to perturbed (toxicant-treated) groups.

The displacement vector measures the magnitude and the direction of perturbation to the state variables at a given time  $t$ . If  $u(t)$  is plotted as a function of time in its own multidimensional space (the displacement space), the resulting trajectory contains all the information available in the original state variables about the dynamics of the system's response to the toxicant. It captures all the information necessary to evaluate the various aspects of ecosystem stability, notably resistance, resilience, and amplitude. Resistance can be related to the maximum magnitude of the displacement vector following introduction of the toxicant. Resilience can be quantified in terms of the rate at which the displacement vector returns to the origin of the displacement space once exposure to the toxicant ceases. The boundaries of the domain of attraction associated with the unperturbed state, and therefore the amplitude of the system, can be determined by identifying those displacements which do not yield a return to the control state.

The magnitude of the displacement vector is of considerable importance in establishing the stability properties of perturbed

ecosystems. This quantity will be referred to by the term separation. Separation is a scalar quantity which describes how far an ecosystem has been displaced without regard to direction. This does not mean that the directional information contained in the displacement vector is superfluous, however. Only the displacement vector reflects how the response of individual state variables varies with time, from which the mechanisms of ecosystem response might be elucidated.

Applying the state space approach to the analysis of ecological data requires consideration of two factors frequently excluded from purely mathematical discussions. First, although their underlying dynamics may be effectively continuous, ecological variables are usually sampled at discrete time intervals. Second, ecological state variables cannot be quantified with absolute precision. Uncertainty may arise due to measurement error or due to natural variability caused either by endogenous dynamics or by external forcing of the system. Application of the state space approach to the analysis of discretely sampled state vectors in the presence of noise is a multivariate statistical estimation problem.

The statistical approach taken to state space analysis is explained in detail in chapter 2 (see especially section 2.4). Chapter 2 also contains methodological details on the experimental systems and the simulation model to which state space analysis is

applied. Chapter 3 is devoted to the analysis of experimental data collected from freshwater ecosystems (microcosms and ponds) exposed to phenolic toxicants, providing an opportunity to assess its effectiveness and utility. In chapter 4 the method is applied in the analysis of the output from a computer simulation of a lentic ecosystem exposed to a toxicant. This allows an evaluation of the performance of the methodology in cases where the true response of the system (i.e., in absence of measurement error) is known, and where the number of replicates can be varied arbitrarily, allowing an investigation of the statistical power and other properties of the method. This chapter also presents an application of the state space approach to ecological risk analysis in the context of defining diagnostic variables which can be used as predictors of ecological risk. Finally, chapter 5 attempts to summarize the strengths and weaknesses of the methodology as applied in the two preceding chapters, and to suggest directions for future research.

## Chapter 2

## MATERIALS AND METHODS

The focus of this research is the application of state space displacement analysis to both experimental data and simulation results. Sections 2.1 and 2.2 describe the experimental systems and the methods used in their study. I conducted the experimental studies using the flask microcosms as described in section 2.1, whereas the studies with aquarium microcosms and ponds described in section 2.2 were conducted by others (Franco et al. 1985, Giddings et al. 1985) and I subsequently performed the state space analysis of their data. Section 2.3 describes the computer model used to produce the simulation results. The model used in this study is based on the Standard Water Column Model (SWACOM) developed by O'Neill et al. (1982). However, SWACOM as originally conceived represents a pelagic ecosystem, and I introduced substantial modifications, described in section 2.3, to produce a model more appropriate to littoral ecosystems. Finally, section 2.4 provides a detailed description of the state space analytical techniques developed and employed in this study.

## 2.1 FLASK MICROCOSMS

### 2.1.1 Assembly

Twenty-four microcosms were established in 2-L Erlenmeyer flasks as follows. Each flask received 600 mL of freshly prepared, Taub TB2

nutrient medium (Taub and Read 1982), the composition of which is described in Table 2.1. The microcosms were then inoculated with a mixture of natural materials, described below, bringing the total volume to approximately 800 mL. The microcosms were kept on a table at room temperature, under a light bank providing approximately  $200 \mu\text{Ei m}^{-2} \text{ s}^{-1}$  of photosynthetically active radiation on a 10h:14h light-dark schedule.

The sources for the inocula were two 80-L aquaria containing water, detritus, and biota taken from a local fish pond and a drainage ditch, respectively. These aquaria had been maintained under laboratory conditions for nearly three months prior to the beginning of the microcosm experiment. Each microcosm received: (1) 100 mL of a detritus suspension siphoned from the bottoms of both aquaria, (2) approximately 0.5 g drained fresh weight of the aquatic moss Amblystegium, (3) approximately 1.5 g drained fresh weight of filamentous algae dominated by Spirogyra, (4) 10 mL of zooplankton suspension concentrated from the ditch aquarium, and (5) sufficient water, equal parts from both aquaria, to bring to total microcosm volume to 800 mL.

### 2.1.2 Species Composition

The microcosms contained a diverse assemblage of organisms typical of a freshwater littoral ecosystem. Because the microcosms were stocked with natural materials, the resulting species

Table 2.1. Chemical composition of the Taub T82 medium used in the flask microcosms.

---

<u>Chemical Species</u>	<u>Molar Concentration</u>
major cations:	
Na <sup>+</sup>	2.2 x 10 <sup>-3</sup>
K <sup>+</sup>	4.0 x 10 <sup>-5</sup>
Ca <sup>2+</sup>	1.0 x 10 <sup>-3</sup>
Mg <sup>2+</sup>	1.0 x 10 <sup>-4</sup>
Al <sup>3+</sup>	1.0 x 10 <sup>-5</sup>
major anions:	
NO <sub>3</sub> <sup>-</sup>	5.0 x 10 <sup>-4</sup>
PO <sub>4</sub> <sup>3-</sup>	4.0 x 10 <sup>-5</sup>
SO <sub>4</sub> <sup>2-</sup>	1.2 x 10 <sup>-4</sup>
SiO <sub>3</sub> <sup>2-</sup>	1.0 x 10 <sup>-4</sup>
Cl <sup>-</sup>	3.5 x 10 <sup>-3</sup>
trace elements:	
B	7.5 x 10 <sup>-7</sup>
Co	2.5 x 10 <sup>-9</sup>
Cu	5.0 x 10 <sup>-9</sup>
Fe	7.5 x 10 <sup>-7</sup>
Mn	2.5 x 10 <sup>-7</sup>
Zn	2.5 x 10 <sup>-8</sup>
chelating agent:	
EDTA	1.4 x 10 <sup>-6</sup>

---

composition was neither precisely controlled nor completely known. Since the focus in this experiment was on integrative measures of ecosystem dynamics, the advantages of using a complex, naturally-derived community were felt to outweigh the disadvantage of an incompletely specified taxonomic composition. A general characterization of the biotic composition is given in Table 2.2.

#### 2.1.3 Measured State Variables

Dissolved oxygen, pH and conductivity were monitored routinely at three day intervals throughout the course of the experiment. Dissolved oxygen was measured in the morning immediately after the lights came on using an oxygen electrode. Subsequently, the contents of each microcosm were gently mixed, and 100 mL samples were removed for pH and conductivity determinations. Following these measurements, each water sample was returned to the microcosm from which it was taken. Small volumes of distilled water were added to the microcosms as needed to compensate for evaporation.

#### 2.1.4 Experimental Design

The experiment lasted for a total of 38 days. Initially, 24 replicate microcosms were established and maintained under laboratory conditions for 17 days. At this point, one microcosm which deviated

Table 2.2. Biotic composition of flask microcosms.

---

Plants:

Amblystegium (aquatic moss)  
Lemna minor (duckweed)

Filamentous Algae:

Spirogyra  
Oedogonium  
Oscillatoria  
Anabaena

Diatoms:

Cocconeis  
Navicula  
Achanthes

Other Algae:

Scenedesmus  
Pediastrum

Protozoa:

various ciliates (including Colpoda)  
various flagellates (including Euglena)  
various peritrichs  
occasional sarcodines

Invertebrates:

Cypridopsis vidua (ostracod)  
Chydorus sphaericus (cladoceran)  
cyclopoid copepods  
rotifers (including Philodina)  
juvenile snails (probably Helisoma)  
midges (probably Calopsectra)

---

the most in terms of appearance and measured state space dynamics was removed from the experiment. The remaining microcosms were randomly assigned to control and treatment groups.

The toxicant used in this experiment was 2,4-dimethylphenol (2,4-DMP). Each treated microcosm received 100 mL of an aqueous 2,4-DMP solution calculated to produce specified nominal concentrations in a geometric series spanning two orders of magnitude (see Table 2.3). The control microcosms each received 100 mL of distilled water. There were five replicate control microcosms, and three microcosms at each of six treatment levels.

## 2.2 AQUARIUM MICROCOSMS AND OUTDOOR PONDS

An abbreviated account of the materials and experimental methods used in the aquarium microcosm and the pond studies is presented here for the convenience of the reader. For details, the reports of the original investigators should be consulted (Franco et al. 1984, Giddings et al. 1984).

### 2.2.1 Assembly

Aquatic microcosms were assembled in 72-L glass aquaria, using materials collected from a shallow, 0.04-ha pond. Each microcosm was filled to a depth of about 10 cm with sediment and then received 55

Table 2.3. Toxicant exposure regimes in flask microcosms.

---

<u>Treatment Level</u>	<u>Nominal Concentration of 2,4-DMP (mg/L)</u>
controls	0.0
1	1.0
2	2.5
3	6.3
4	16
5	39
6	98

---

liters of pond water and 100 g (drained wet weight) of the submerged aquatic macrophyte Elodea canadensis. The microcosms were maintained in a growth chamber under combined fluorescent and incandescent illumination (12 h light:12 h dark), with photosynthetically active radiation ranging from 160 to 215  $\mu\text{Ei m}^{-2}\text{s}^{-1}$  at the water surface. Air temperature was regulated at 21°C during the light period and at 15°C during the dark period.

In late April 1982, outdoor experimental ponds were assembled in 1-m-deep excavated depressions with sloping sides (5 x 5-m perimeter, 3.5 x 3.5-m bottom) lined with sheets of 0.036-in reinforced potable-grade Hypolon (DuPont). Fine-grained sediment from a fish pond was placed on the bottom of each experimental pond to a depth of 15 cm. Water from the fish pond was pumped into the ponds to a depth of 80 to 90 cm (about 15 m<sup>3</sup> per pond). One week later 8 L of Elodea canadensis from a natural pond was added to each pond. On June 8, 35 immature and 4 adult mosquitofish (Gambusia affinis) were added to each pond.

### 2.2.2 Species Composition

Since both the microcosms and the ponds were stocked with natural materials from the same source, the resulting species assemblages were similar. The major difference was that the ponds were stocked with Gambusia affinis, whereas fish were excluded from

the microcosms. A general characterization of the biotic composition of the aquarium microcosms and the ponds is presented in Table 2.4. Note is made as to which taxa were reported in the microcosms, in the ponds, or in both, but since efforts to describe the biota were not extensive, the lack of a reported observation is not necessarily evidence for the absence of a taxon.

### 2.2.3 Measured State Variables

The response of a wide variety of physical, chemical, and biological variables was monitored throughout the experiments. For the state space analysis, a subset of these variables was selected based upon two criteria: (1) only those variables which were routinely measured at weekly intervals during the dosing period were included, and (2) variables with values frequently missing or below detection limits were excluded. The few missing values in this subset were replaced by values linearly interpolated from preceding and subsequent observations. The response variables analyzed from the pond experiment were pH, dissolved oxygen, conductivity, alkalinity, ammonium concentration, chlorophyll a in phytoplankton and in periphyton, and total abundance values of cladocerans, copepods, and rotifers. In the microcosm experiment, the same variables were analyzed, with the exception of alkalinity and periphyton chlorophyll.

Table 2.4. Biotic composition of the aquarium microcosms (M) and outdoor ponds (P).

---

Plants:

Elodea canadensis M,P  
 Potamogeton M,P  
 Nitella M,P

Filamentous Algae:

Spirogyra M,P  
 Oscillatoria M  
 Gloeotrichia M

Diatoms:

Eunotia M  
 Gomphonema M  
 Navicula M

Other Algae:

Gonium M,P  
 Coleochaeta M  
 Scenedesmus P

Flagellates:

Euglena M,P  
 Phacus M,P

Zooplankton:

cladocera-

Simocephalus vetulus M,P  
 Chydorus sphaericus M,P  
 Alona costata M,P

copepoda-

Cyclops vernalis M,P  
 Cyclops varicans M,P  
 Eucyclops agilis M,P  
 Macrocyclus albidus M,P

Table 2.4. (Continued)

---

rotifera-

Platyias patulus P  
Mytilina M  
Euchlanis P  
Lecane P  
Brachionus quadridentata P

Insects:

diptera (primarily Chironomidae and Ceratopogonidae) P  
ephemeroptera (Caenidae and Baetidae) P  
trichoptera (Hydroptilidae and Leptoceridae) P  
odonata (Coenagrionidae) P

Other Invertebrates:

Physa (snails) M,P  
oligochaetes M  
leeches M

Fish:

Gambusia affinis P

---

#### 2.2.4 Experimental Design

The toxicant used in this experiment was an unrefined, coal-derived middle distillate from an H-Coal process, identified in the Oak Ridge National Laboratory repository as ACD No. 887. By weight, 12.4% of the oil consisted of water-soluble compounds. Approximately 95% of this water-soluble fraction was composed of phenolic compounds, particularly cresols, dimethylphenols, and other alkylphenols.

Both microcosms and ponds were subjected to chronic oil contamination over a 56-d exposure period, beginning July 13, 1982. Duplicate microcosms were randomly assigned to controls or to one of seven treatment levels (M1-M7). Within each treatment level, one microcosm was dosed weekly and one was dosed daily, although the total amount of oil added per week was the same. Ponds were randomly assigned to controls or to one of five treatment levels (P1-P5), with two replicates at each level both dosed daily. Oiling rates in the ponds ranged from 1 to 16 mL m<sup>-3</sup>d<sup>-1</sup>, resulting in measured total phenol concentrations ranging from approximately 0.05 to 8 mg/L, averaged over the 56-d exposure period (Table 2.5). Oiling rates in the microcosms encompassed a range from 0.07 to 18 mL m<sup>-3</sup>d<sup>-1</sup>, resulting in 56-d average total phenol concentrations of 0.01 to 10 mg/L (Table 2.6).

Table 2.5. Toxicant exposure regimes in aquarium microcosms.

---

Treatment Level	Oil Input Rate (mL m <sup>-3</sup> d <sup>-1</sup> )	Measured Peak Concentration of Phenols (mg/L)
Controls	0.0	not detectable
M1	0.067	not detectable
M2	0.17	0.032
M3	0.43	0.052
M4	1.1	0.23
M5	2.7	0.92
M6	6.7	1.2
M7	17	18

---

Table 2.6. Toxicant exposure regimes in outdoor ponds.

Treatment Level	Oil Input Rate ( $\text{mL m}^{-3} \text{d}^{-1}$ )	Measured Peak Concentration of Phenols (mg/L)
Controls	0.0	0.26
P1	1.0	0.46
P2	2.0	0.90
P3	4.0	3.6
P4	8.0	4.5
P5	16	28

### 2.3 COMPUTER SIMULATIONS

A computer simulation model was developed in order to investigate certain aspects of the state space methodology in greater detail than could practically be accomplished in the experimental systems. It was hoped that explorations of the dynamics of the simulation model would lead to the generation of hypotheses which could be checked against the available experimental data or more rigorously tested in future experiments. A model of a typical freshwater, littoral ecosystem was developed for this purpose.

The Standard Water Column Model (SWACOM) described by O'Neill et al. (1982) served as a point of departure for building the model. SWACOM is a generalized freshwater ecosystem model designed to represent a temperate, dimictic lake. The dynamics of a pelagic food web are governed by phenomenological equations incorporating, as appropriate, processes such as photosynthesis, respiration, prey capture and assimilation, and excretion. These processes are modified by light, temperature, and nutrient conditions, as well as toxicant concentration, all of which are treated as external forcing functions. Mathematically, the model consists of a set of linked first order nonlinear difference equations implemented in a FORTRAN code and iterated with a one day time step.

A number of modifications were made to the original version of SWACOM to make it more suitable for comparison with the shallow,

littoral ecosystems which are the focus of this study. The trophic structure was altered to reflect the fewer trophic levels present in the experimental ponds. Since dissolved oxygen appeared to be a sensitive indicator of stress in the pond experiments, dissolved oxygen was incorporated as a state variable in the model. Detritus and the dynamics of its decomposition were also added to the model, primarily because of the potential importance in affecting oxygen balance. Finally, considerable effort was made to model macrophyte dynamics in a simple but realistic fashion because of their dominating influence in the systems under consideration, both in terms of biomass and productivity. These modifications are described in detail below.

### 2.3.1 Modifications to SWACOM

#### 2.3.1.1 Trophic Structure

SWACOM contains a food web including 10 phytoplankton species, 5 zooplankton species, 3 species of forage fish, and 1 carnivorous game fish. For the purposes of this study the structure of the food web was altered by elimination of the top predator and by reducing the number of forage fish species from three to one. This simplified trophic structure is representative of the experimental ponds, in which the only fish species present was a planktivore.

### 2.3.1.2 Dissolved Oxygen

Since the experimental data included measurements of dissolved oxygen, which proved to be a sensitive indicator of ecosystem response to the toxicant, it was decided to include dissolved oxygen as a state variable in the model. The processes considered to affect dissolved oxygen levels were (1) exchange with the atmosphere, (2) net photosynthetic oxygen production, (3) oxygen consumption by zooplankton and fish respiration, and (4) oxygen demand due to the decomposition of detritus.

Atmospheric exchange was modeled using an algorithm developed by Bloomfield (1975) in his model of microbial decomposition and carbon cycling in Lake George, New York. Daily net oxygen flux is taken to be the sum of  $X_L$ , oxygen evolution from supersaturated solution, and of  $X_D$ , exchange due to turbulent diffusion.  $X_L$  is a linear function of the degree of supersaturation, calculated with respect to an empirical relationship for temperature-dependent oxygen solubility:

$$X_L = \begin{cases} 0 \\ R_o([O_2] - [O_2]_{sat}) \end{cases} \quad (2.1)$$

where

$$[O_2]_{sat} = (13.17 - 0.18 T)Z \quad (2.2)$$

where  $[O_2]$  is (epilimnetic) dissolved oxygen,  $[O_2]_{sat}$  is the oxygen solubility,  $T$  is temperature in degrees Celsius,  $Z$  is the

depth of the euphotic zone in meters, and  $R_0$  is a rate constant.

Turbulent diffusion is also governed by a set of empirical equations:

$$X_D = R_1 Q ([O_2]_{\text{sat}} - [O_2]) \quad (2.3)$$

$$Q = \begin{cases} 1 + R_2 \left( \frac{T - 3.5}{1.5} \right) & 3.5 < T < 5.0 \\ 1 + R_2 \left( \frac{6.5 - T}{1.5} \right) & 5.0 < T < 6.5 \\ 1 & \text{otherwise} \end{cases} \quad (2.4)$$

where  $R_1$  and  $R_2$  are constants.

Photosynthetic oxygen production was calculated as being proportional to biomass production on the basis of stoichiometry. In the case of the macrophytes, experimental data on oxygen production and consumption was available (see section 2.3.1.4). Oxygen consumption by zooplankton and fish was likewise calculated on the basis of stoichiometric proportionality (1.42 g  $O_2$  consumed per g respired biomass). Finally, oxygen demand in decomposition, presumably due to microbial respiration, was calculated as being proportional to the current rate of decomposition (see section 2.3.1.3).

### 2.3.1.3 Detritus and Decomposition

The major source of detritus in the ecosystems under consideration is dead macrophytes, in this case primarily Elodea. There have been numerous studies of the decomposition of plant

materials in aquatic systems. Notably, Jewell (1971) investigated weight loss, oxygen utilization, and nutrient regeneration in the decomposition of a variety of aquatic plants, including Elodea. He concluded that the kinetics of decomposition could be adequately represented by an exponential disappearance of a labile fraction, and no significant decomposition of the remaining refractory material. Subsequently, Godshalk and Wetzel (1978), after a thorough investigation of the decomposition of five aquatic angiosperms (not including Elodea), argued for a kinetic equation of the form:

$$\frac{dW}{dt} = -ae^{-bt} W \quad (2.5)$$

where  $W$  is the weight of detritus remaining, and  $a$  and  $b$  are constants. At any time  $t$ , this is equivalent to a first-order kinetic equation, but the apparent rate "constant" itself exponentially decays with time.

Carpenter (1982) examined the decomposition of leaf litter in laboratory microcosms, and evaluated the adequacy several possible kinetic equations, including those discussed above. He concluded that the most satisfactory was a composite exponential decay, conceptually dividing the detritus into a rapidly decaying labile fraction and a slowly decaying refractory fraction. This approach was incorporated into the model by the equations

$$\Delta D_L = k_L H(T) D_L \quad (2.6)$$

$$\Delta D_R = k_R H(T) D_R \quad (2.7)$$

where  $\Delta D_L$  and  $\Delta D_R$  are the losses due to decomposition for the labile and refractory fractions,  $D_L$  and  $D_R$  are the current amounts of labile and refractory detritus, and  $k_L$  and  $k_R$  are the associated decay rate constants.  $H(T)$  is a generalized temperature response function that modifies the decomposition rate as a function of temperature,  $T$ , with a maximum rate at 25°C. For a description of the temperature function see Shugart et al. (1974). Parameter values were chosen primarily on the basis of the data in Jewell (1971).

#### 2.3.1.4 Macrophytes

Shallow littoral ecosystems are frequently dominated by macrophyte beds which can exert considerable control over the physical and chemical characteristics of the water column. Because of this, inclusion of macrophytes in the model seemed desirable. Unfortunately, most previous attempts at modeling macrophytes have focused on physiological aspects of plant growth and on the distribution of biomass with depth, details which are difficult to incorporate within the context of the ecosystem model. On the other hand, it was not initially apparent how a simpler macrophyte model might be formulated or parameterized. Therefore, the strategy adopted was to first build a separate, detailed macrophyte model, and then to empirically arrive at a simplified model which could mimic the behavior of the detailed model (at least under the conditions of interest), and to incorporate this empirical formulation within the ecosystem model.

The detailed model was developed following the approach used by Titus et al. (1975) in modeling the aquatic macrophyte Myriophyllum. A similar model was also developed for Ceratophyllum by Best (1981). The model partitions the water column into 10-cm depth intervals, and keeps track of both leaf biomass and stem biomass in each depth interval. Additionally, the model includes a root biomass compartment and a labile carbohydrate pool. The model incorporates the processes of photosynthesis, respiration, growth, leaf sloughing, and excretion of dissolved organic material.

Within each each depth interval, net photosynthesis was calculated as

$$P_i = \left( \frac{P_{\max} E_i B_{\text{leaf},i}}{K_E + E_i} \right) F(T) - R_l B_{\text{leaf},i} \quad (2.8)$$

where  $B_{\text{leaf}}$  is leaf biomass,  $E_i$  is the incident light,  $P_{\max}$  and  $K_E$  are maximum photosynthetic rate and light half-saturation constants,  $F(T)$  is a function which modifies photosynthesis by temperature, and  $R_l$  is a respiration rate coefficient. Field and laboratory data from which parameter estimates could be derived are presented by Pokorny et al. (1984), Ondok et al. (1984), and Simpson and Eaton (1986). Light attenuation due to water and to macrophytes was modeled as a composite exponential reduction with depth using the parameters derived by Ikusima (1970) in a field study of the light regime in a bed of Elodea nuttallii.

The direct result of photosynthesis was an augmentation of the available carbohydrate pool. Growth was then modeled by the following equations for leaves, stems, and roots, respectively.

$$\Delta B_{\text{leaf},i} = G_l \left( \frac{1 - B_{\text{leaf},i}}{F_{\text{opt}} B_{\text{max}}} \right) \left( \frac{P_i}{P_{\text{max}}} \right) \left( \frac{C}{K_c + C} \right) \quad (2.9)$$

$$\Delta B_{\text{stem},i} = G_s \left( \frac{1 - B_{\text{stem},i}}{F_{\text{opt}} B_{\text{max}}} \right) \left( \frac{P_i}{P_{\text{max}}} \right) \left( \frac{C}{K_c + C} \right) \quad (2.10)$$

$$\Delta B_{\text{root}} = G_r \left( \frac{1 - B_{\text{root}}}{B_{\text{rmax}}} \right) \left( \frac{C}{K_c + C} \right) \quad (2.11)$$

In equation 2.9,  $G_l$  represents the maximum rate of production for leafy biomass under optimal conditions. This is modified by a Michaelis-Menten function representing limitations in available carbohydrates ( $C$ ), a term expressing the ratio of the current photosynthetic rate to the maximal rate ( $P_i/P_{\text{max}}$ ), and a term expressing density dependent limitation. This last term is derived by assuming a maximum total leaf biomass of  $B_{\text{max}}$ , and assuming that the optimal vertical distribution is a concentration of photosynthetic biomass at the surface, declining exponentially with depth; which leads to  $F_{\text{opt}}$ , the calculated fraction of total biomass optimally allocated to the  $i$ th depth interval. Equation 2.10 is a completely analogous expression for the growth of stem biomass ( $B_{\text{stem},i}$ ), and equation 2.11 expresses root biomass growth as a function of current root biomass and available carbohydrates.

The vertical distribution of shoot biomass is determined by the combined processes of growth and sloughing. In addition to growth within a given depth interval, governed by the equations described above, vacant depth intervals receive a pulse of shoot biomass whenever the biomass in the next deeper interval exceeds a set threshold. Sloughing occurs at a constant rate whenever the shoot biomass exceeds the current optimum for that depth interval. Finally, dissolved organic material is excreted a rate proportional to the size of the carbohydrate pool.

Few quantitative data are available from which estimates of the parameters in the growth, sloughing, and excretion equations can be estimated. The values used in the simulations represent informed guesses chosen to produce a pattern of growth consistent with those reported in field studies of Elodea beds (Pokorný et al. 1984, Kunii 1984, Bowmer et al. 1984).

Simulations were run with this model under a variety of constant temperature and light conditions covering the range likely to be encountered in a shallow pond during the growing season (Pokorný et al. 1984, Dale and Gillespie 1977). Typical results from such simulations are shown in Fig. 2.1. It was discovered that, under any given set of constant light and temperature conditions, the growth of total macrophyte biomass could be closely approximated by a logistic model. The parameters of the logistic model, however, varied as a function of light and temperature. On the basis of these simulations, the following modified logistic model was derived for total macrophyte growth:

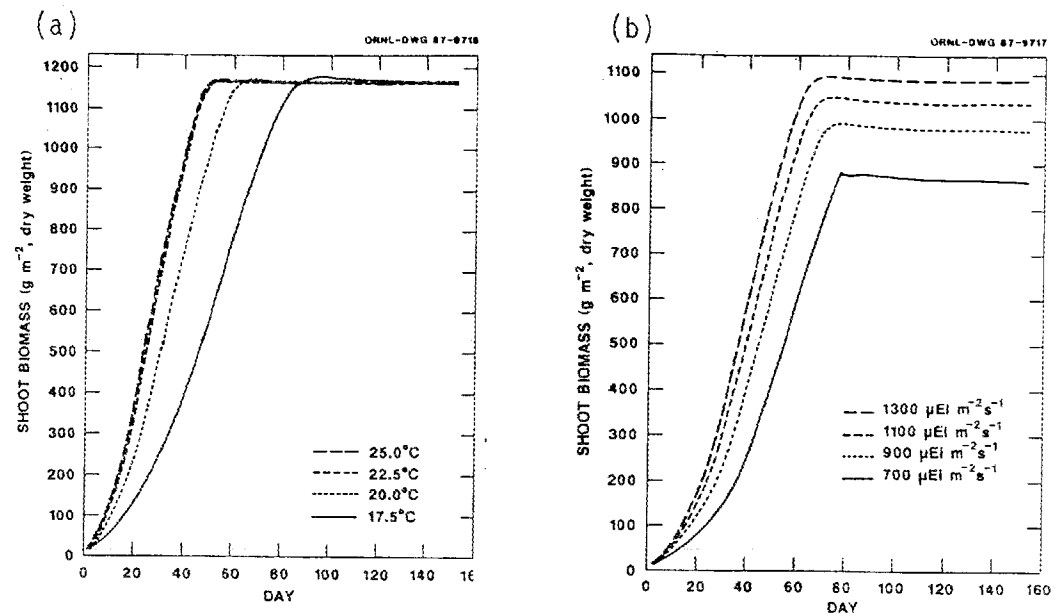


Figure 2.1 Typical results of detailed Elodea growth model.  
 (a) Shoot biomass dynamics under  $1700 \mu\text{Ei m}^{-2} \text{s}^{-1}$  illumination at various temperatures. (b) Shoot biomass dynamics at  $20^\circ\text{C}$  under various light conditions.

$$\frac{dB}{dt} = -r B (1 - B/K) \quad (2.12)$$

$$r = \min [0.122, -0.142 + 2 \times 10^{-5}E_0 + 1.05 \times 10^{-2}T] \quad (2.13)$$

$$K = 690 + 0.3 E_0 \quad (2.14)$$

where  $dB/dt$  is the growth rate of macrophytes,  $B$  is their current biomass,  $r$  is the intrinsic rate of increase,  $K$  is the carrying capacity,  $E_0$  is the photosynthetically active radiation incident at the water surface (in  $\mu\text{Ei m}^{-2} \text{s}^{-1}$ ), and  $T$  is the water temperature in degrees Celsius. It should be noted that although the expression for  $r$  has a negative intercept, under the range of conditions occurring in any of the simulations in this study (where the temperature exceeds  $15^\circ\text{C}$ ), this quantity is always positive.

As a partial test of the above simplified model, both the detailed and the simplified models were run under time-varying light and temperature conditions typical of those to be used in the ecosystem model. These time-varying conditions included an excursion outside the range of constant conditions explored in parameterizing the simplified model. Despite this, the overall agreement between the predictions of the simplified model and the detailed model was good (Fig. 2.2). A discrete-time version of the simplified model was therefore incorporated into the ecosystem model.

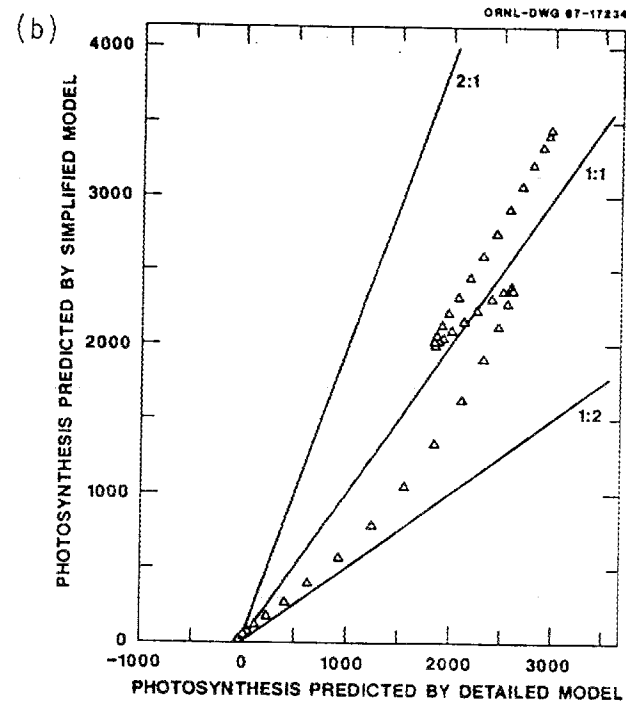
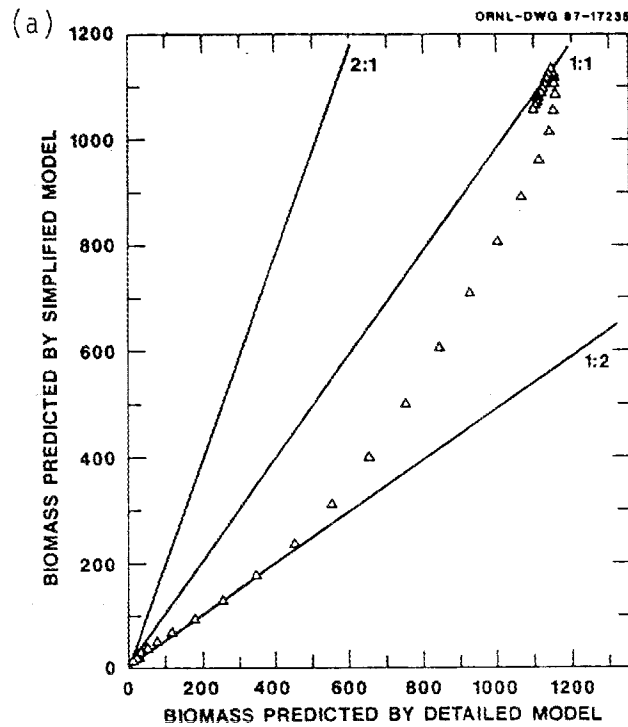


Figure 2.2 Comparison of simplified and detailed Elodea growth models. (a) Ratio of shoot biomass predicted by simplified model to that predicted by detailed model. (b) Ratio of net photosynthesis predicted by simplified model to that predicted by detailed model.

### 2.3.2 Modeling Toxic Effects

The ecological effects of toxicant exposure were modeled through changes in the parameters of the model. Specifically, each parameter of the model was multiplied by a toxic effects factor. If this factor equals 1.0, the parameter value remains unchanged, indicating no toxicity. Inhibitory effects, such as a reduction in photosynthetic rate, are indicated by factors less than 1.0, and stimulatory effects, such as increased respiration, are indicated by factors exceeding 1.0. Within the model, the parameters are stored within a two dimensional array (the parameter matrix), so the effects can also be summarized in a corresponding array (the effects matrix). For each run including toxicant effects, the model is reparameterized by multiplying each parameter by the corresponding element of the effects matrix.

The entries in the effects matrix must be estimated as a function of toxicant concentration using available toxicity data. In most cases this involves an extrapolation from single species, laboratory bioassay data. A general protocol for making such an extrapolation is outlined by O'Neill et al. (1982, 1983). In the absence of more detailed information regarding a toxicant's mode of action, changes in the effects factors are assumed to be predictable on the basis of a general stress syndrome. For autotrophic organisms, the general stress syndrome predicts a lowering of maximum photosynthetic rate, increased respiration, lower light saturation

point, and increased Michaelis-Menten constant as a result of exposure to the toxicant. For heterotrophs, a decrease in grazing rate, increased respiration, lowered temperature optimum, and increased mortality and susceptibility to predation are assumed. Laboratory bioassays were simulated by mimicking laboratory conditions (i.e., constant optimal light and temperature, ample food and no grazing or predation losses), and then varying the remaining parameters in accordance with the general stress syndrome until the model predictions matched the experimental results (e.g., a 50% reduction in biomass on day 4 to correspond to a 96-h LC50). Effects factors which could not be estimated on the basis of available experimental data, such as susceptibility to predation, were assumed to be of the same magnitude as the factors calculated for the other processes.

In this study, the laboratory toxicity data used to estimate the sensitivities of the pelagic species consisted of the results of a series of bioassays with the water-soluble fraction of the oil added to the ponds (Giddings et al. 1985). Acute bioassays were conducted with the cladoceran Daphnia magna, the fathead minnow Pimephales promelas, the mosquitofish Gambusia affinis, the midge Chironomus tentans, and the green alga Selenastrum capricornutum. A chronic bioassay was also conducted with Daphnia magna. Details of these tests are presented in Giddings et al. (1985). The effect of the toxicant on macrophytes was extrapolated from laboratory bioassays which examined the changes in photosynthesis and respiration of

Elodea canadensis shoot tips exposed to an equimolar mixture of 2,4-dimethylphenol, 2-isopropylphenol, and 2-sec-butylphenol (Moore, 1985).

### 2.3.3 Modeling of Uncertainty and Variability

Experimentally, it is impossible for ecosystem state variables to be known with complete accuracy and precision. In order to more realistically evaluate the potential applicability of state space analysis to experimental data, it was necessary to incorporate statistical errors into the model output similar to those that would be inherent in an actual observation set. It was assumed that such errors could be partitioned into two categories depending upon the source of the error: (1) errors due to the natural variability of ecological systems, and (2) errors introduced in the measurement process. Natural variability was incorporated into the model by choosing random initial values for the state variables, and by running the model with stochastic forcing functions. Measurement errors were added to the output after the model was run.

In terms of the experimental ponds the model was designed to simulate, randomized initial conditions can be interpreted as reflecting the lack of homogeneity between individual ponds arising from differences in construction and from non-uniform stocking and colonization. For each model run, a vector of initial values for the state variables was selected from a multivariate normal distribution

by latin hypercube sampling using a FORTRAN computer code called PRISM (Gardner et al. 1983). Latin hypercube sampling is a stratified random sampling scheme which allows statistical distributions to be reliably approximated with substantially fewer Monte Carlo replicates than would be required by simple random sampling (McKay et al. 1979, Iman and Conover 1982). The initial values were chosen as independently distributed normal random variables with means equal to their deterministic values and 10% coefficients of variation.

Stochastic forcing functions were used to model the spatiotemporal variability in environmental conditions experienced by individual ponds. In the model, both light and temperature were modeled as stochastic functions consisting of a random walk superimposed on a deterministic seasonal trend (Fig. 2.3). Although air temperature and incident light at the surface of a set of experimental ponds may not vary greatly from pond to pond, it is frequently observed that there is considerable variability in the color and turbidity of individual ponds, resulting in greater variability in the light and temperature regimes within the ponds. The stochastic forcing functions were generated such that random deviates with small variance were added daily, and deviates with progressively larger variance were added every 3, 9, and 27 days. This produced a pattern of autocorrelations which favored runs of days with similar conditions, as is frequently encountered in actual meteorological data. The ensemble of stochastic forcing functions

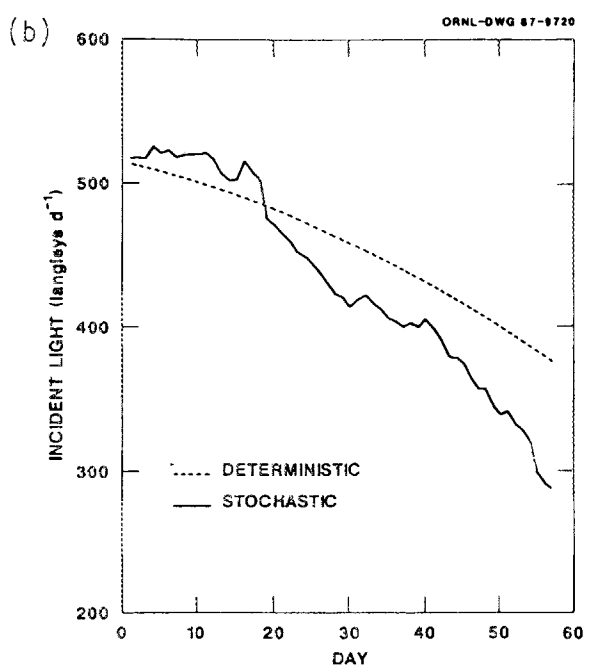
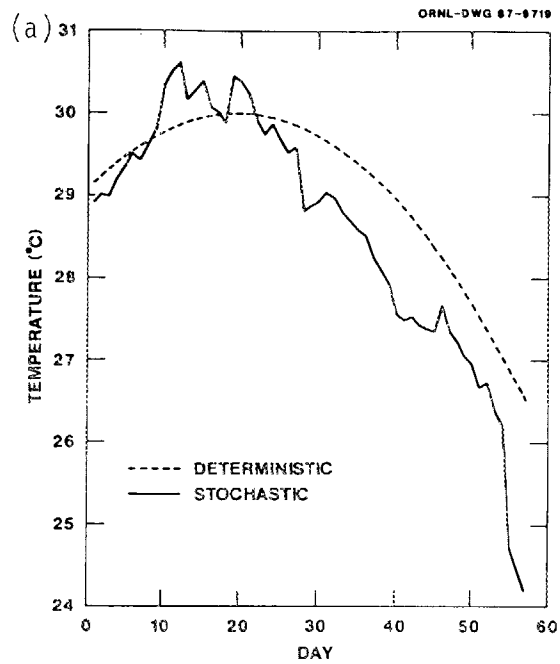


Figure 2.3 Typical realizations of stochastic forcing functions.  
 (a) Temperature. (b) Incident light.

averaged over all 200 Monte Carlo replicates did not exhibit any systematic deviation from the deterministic mean.

Other sources of natural variability could, of course, be imagined. Variations in other forcing functions, such as nutrient inputs to the system, could be considered. In the case of the experimental ponds, it seems likely that nutrient inputs from external sources, although they do occur, play a subordinate role relative to nutrient regeneration within the pond. Also, previous modeling studies using SWACOM have demonstrated a greater sensitivity to changes in light and temperature than to nutrient inputs, further supporting the emphasis on light and temperature as sources of natural variability. Other types of natural variability, such as differences in species composition, genetic variability, differences in microbial activity, local extinctions and invasion by new species, undoubtedly occur in the real world but are not explicitly incorporated in the model. It is argued that at the level of resolution of the current modeling effort, which is primarily exploratory in nature, such phenomena may be neglected.

Measurement errors were introduced as independent, normally distributed random numbers added to the values of the state variables. The biomasses and detritus variables were transformed by taking the natural logarithm prior to the addition of measurement errors and then transformed back to the original scale; all other variables received measurement errors directly (i.e., without prior

transformation). The variances of the errors were chosen to approximate a level of precision technically attainable in the absence of any variability other than measurement errors. Standard deviations of the measurement errors were as follows: 0.20 for the log-phytoplankton and the log-zooplankton biomasses, 0.30 for the log-fish biomass, log-elodea biomass and log-detrital masses, 0.10 for phytoplankton productivity, 0.50 for macrophyte productivity, 0.10 for dissolved oxygen, and 0.30 for nutrient concentration. This resulted in coefficients of variation generally within the range of 20-30% for all except the physicochemical variables (dissolved oxygen and nutrient concentration) which had coefficients of variation of 2-4%.

#### 2.4 STATE SPACE ANALYSIS

As discussed in Chapter 1, the response of an ecosystem to toxicant stress can be quantified by the displacement of the state vector away from some reference state (see section 1.4). In the situations considered in this study, the reference states are measured states in replicate control ecosystems (i.e., those to which no toxicant is added). Changes induced by the toxicant can be described by calculating a displacement vector,  $u(t)$ , defined as the vector difference between the perturbed and control state vectors:

$$u(t) = x_p(t) - x_c(t) \quad (2.15)$$

as illustrated in Fig. 2.4. This equation is precisely equivalent to equation 1.4, except that the subscripts now explicitly reflect the comparison between perturbed and control ecosystems. The word "displacement", as used here, refers to a vector quantity, possessing both magnitude and direction. The word "separation" is used to denote the associated scalar quantity, defined as the distance between perturbed and control state vectors or, equivalently, as the magnitude of the displacement vector.

#### 2.4.1 Statistical Estimation of Displacement and Separation

In experimental situations, the true state space trajectories and displacement vectors are not known, but must be estimated from discrete samples in the presence of natural variability, measurement error, and other uncertainties. At any sampling time,  $t$ , the displacement vector  $u(t)$  must be estimated based on observations of  $m$  replicate control ecosystems and  $n$  replicate perturbed ecosystems. The situation can be visualized as two clusters, of  $m$  and  $n$  points respectively, distributed in state space. In the absence of systematic bias these points will tend to be centered around the true population centroids,  $\mu_c(t)$  and  $\mu_p(t)$ . The statistical problem is one of finding an appropriate estimator of the distance between the centroids of the two (statistical) populations.

ORNL-DWG 86-1727

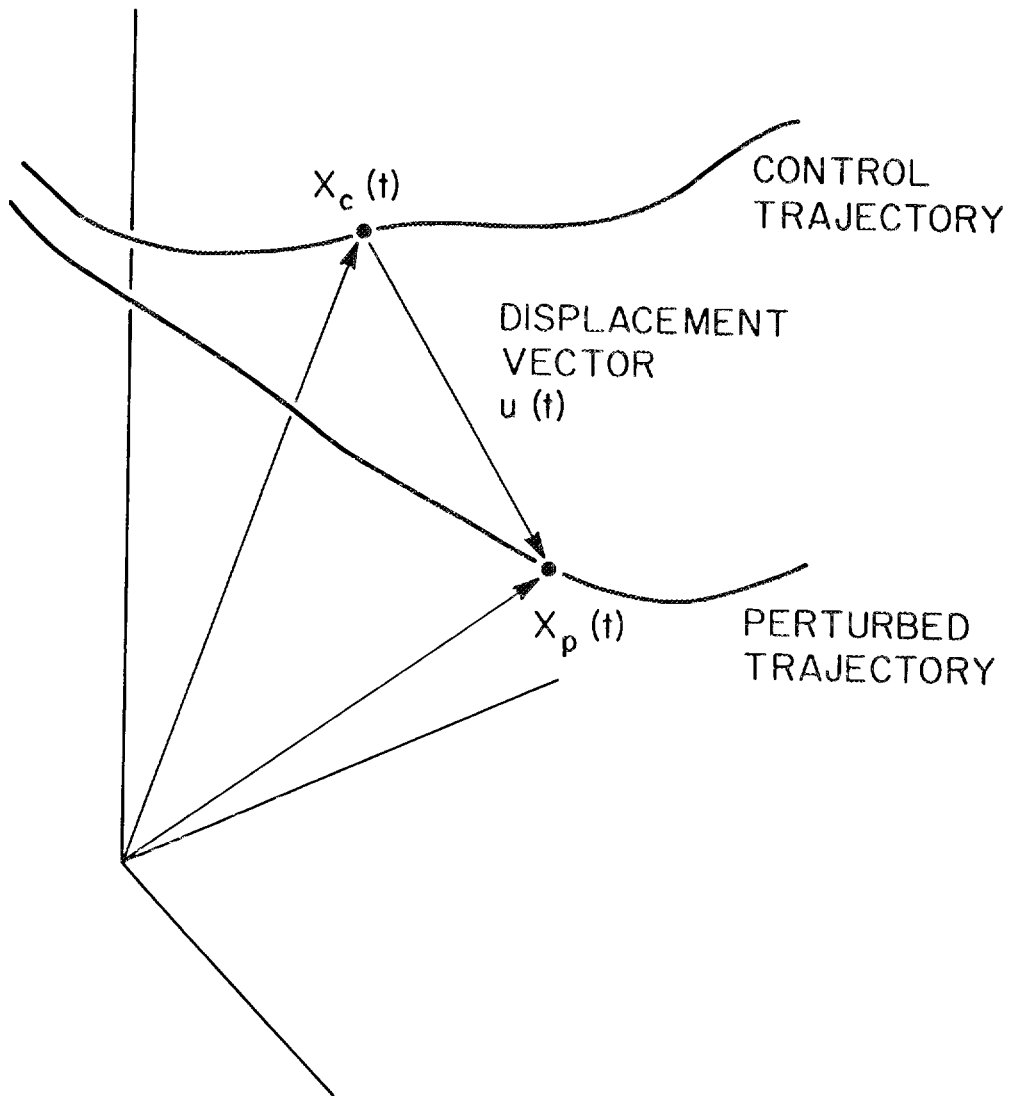


Figure 2.4 State space trajectories showing displacement vector as the difference between perturbed and control state vectors.

One such estimator is the distance between the two sample centroids,  $\mu_c(t)$  and  $\mu_p(t)$ . This is an unbiased estimator of the desired population quantity. The major disadvantage of this estimator is that it is difficult to assess its statistical accuracy (i.e., to compute its standard error or to construct a confidence interval). An alternative estimator is the average of the distances calculated from all pairwise comparisons between clusters. This is not an unbiased estimator of the true distance between population centroids, as can be seen by considering the case where  $\mu_c(t) = \mu_p(t)$ , such that the true distance between centroids is zero, but the estimator yields a positive value related to the variance of the measured states about their centroids. In practice however, two considerations favor the use of this biased estimator: (1) the bias becomes less important as the distance between  $\mu_c(t)$  and  $\mu_p(t)$  becomes large relative to the within group variance (i.e., as the ecosystem responds to the toxicant), and (2) the variability among the pairwise estimates gives an indication of the degree of uncertainty in the estimate of centroid separation. Furthermore, calculating the average distance between replicate control states provides a measure of the degree of bias in the estimator.

In cases where the number of replicates is small, it is feasible to calculate the distances between all possible pairs. When comparing controls with perturbed states, there are  $mn$  such pairs, whereas  $m(m-1)$  comparisons can be made between nonidentical

controls. If these numbers are large, it is possible to compute the estimator on the basis of a smaller number of randomly matched pairs. Once a distribution of calculated pairwise distances is obtained, a confidence interval can be estimated. If the original state vectors follow a multivariate normal distribution with an identity covariance matrix, then under the null hypothesis that  $\mu_c(t) = \mu_p(t)$ , the squared distances will follow a chi-squared distribution with  $p$  degrees of freedom, where  $p$  is the dimensionality of the state space. A transformation which will convert an arbitrary multivariate normal distribution into one with an identity covariance matrix will be discussed in the next section. Confidence limits can then be calculated from the appropriate percentage points in the chi-squared distribution. If such parametric assumptions are not warranted, a confidence interval could be derived by means of nonparametric resampling methods, such as the bootstrap procedure (Efron and Tibshirani 1986).

#### 2.4.2 Distance Metrics and Data Transformation

In the previous section emphasis was placed on estimation of the distance between state vectors or between the centroids of groups of state vectors. Explicit consideration will now be given to how distances may be measured in the state space. The issue at hand is the selection of an appropriate metric, or mathematical yardstick, for making such distance measurements.

The most straightforward mathematical analog of the intuitive notion of distance is that employed in Euclidean geometry. The Euclidean distance metric is based on a generalization of the Pythagorean Theorem. Given two vectors in  $n$ -dimensional space,  $v = (v_1, v_2, \dots, v_n)'$  and  $w = (w_1, w_2, \dots, w_n)'$ , the Euclidean distance between them is

$$d_E(v, w) = \left[ \sum_{i=1}^n (v_i - w_i)^2 \right]^{1/2} \quad (2.16)$$

or, in vector notation,

$$d_E(v, w) = [(v-w)'(v-w)]^{1/2} \quad (2.17)$$

A problem that frequently arises in using Euclidean distance to measure state space separations is that the various axes of the state space are often scaled in incommensurate units. For instance, in the flask microcosm experiment to be discussed in Chapter 3, both pH and conductivity were included as measured state variables. In the controls, pH was typically observed to vary over a range of approximately 1 pH unit, whereas conductivity, measured in different units, typically spanned about 50 units. Clearly a displacement of 5 units along the pH axis would be seen as a major perturbation while a 5 unit change in conductivity would be insignificant, but both are equivalent in terms of Euclidean distance! One obvious solution would be to rescale the axes in some way to make the units commensurable. That option will be discussed later, but first an alternative distance metric will be considered.

A distance metric commonly employed in multivariate statistics is the Mahalanobis distance (Mahalanobis 1936, Mardia 1977). Given two random vectors,  $v$  and  $w$ , the Mahalanobis distance between them is

$$d_M(v, w) = [(v-w)' \Sigma^{-1} (v-w)]^{1/2} \quad (2.18)$$

where  $\Sigma^{-1}$  is the inverse of the covariance matrix for the distribution from which the vectors were drawn<sup>1</sup>. The interpretation of this distance measure can be seen by considering a cloud of data points distributed with centroid  $\mu$  and covariance matrix  $\Sigma$  as shown in Fig. 2.5a. If the underlying distribution is multivariate normal, an elliptical joint confidence region can be defined (Fig. 2.5b). The Mahalanobis distance from the centroid to any point on the ellipse is a constant. Thus, equally probable deviations from the centroid are equally distant when measured by the Mahalanobis metric.

An alternative to the use of the Mahalanobis distance metric is to transform the state space. The appropriate transformation involves the Cholesky decomposition (sometimes called the symmetric square root) of  $\Sigma^{-1}$ . Given an arbitrary matrix<sup>2</sup>  $M$ , its Cholesky decomposition

---

<sup>1</sup>The quantity Mahalanobis actually considered in his original paper was the square of that given in equation 2.18, and the term Mahalanobis distance has been ambiguously used to refer to both quantities ever since. The usage adopted here parallels the traditional definition of Euclidean distance, and is equivalent to the standard distance proposed by Flury and Riedwyl (1986).

<sup>2</sup>Strictly speaking, the Cholesky decomposition is only defined for positive definite matrices. This requirement is satisfied by any nonsingular covariance matrix. In practice, singular covariance matrices are seldom encountered except for situations where fewer degrees of freedom are available than the number of state variables.

(often written as  $M^{-1/2}$ ) is a matrix  $A$  such that

$A'A = M$ . It is useful to transform the data such that a vector  $x$  in the original state space is mapped into a vector  $y$  in the transformed space, where

$$y = Ax \quad (2.19)$$

and

$$A = (\Sigma^{-1})^{1/2} = (\Sigma^{1/2})^{-1} = \Sigma^{-1/2} \quad (2.20)$$

It can be easily demonstrated that the Euclidean distance between two vectors in the transformed space is equal to the Mahalanobis distance between the corresponding vectors in the original space. Furthermore, the covariance matrix of the transformed data is an identity matrix.

In essence the transformation can be seen as simultaneously standardizing the data and removing the effects of any correlations. This results in a transformed state space in which the axes are orthogonal and have been appropriately rescaled in commensurable units. This is illustrated graphically in Fig 2.5c and d. Fig. 2.5c shows a concentration ellipse in the original state space. Points A and B are equally distant from the data centroid, as measured by the Euclidean metric, but point B clearly represents a larger deviation from the normal range of variability. In the transformed space, shown in Fig. 2.5d, the concentration ellipse becomes a circle, and the Euclidean distances of A' and B' from the centroid reflect the

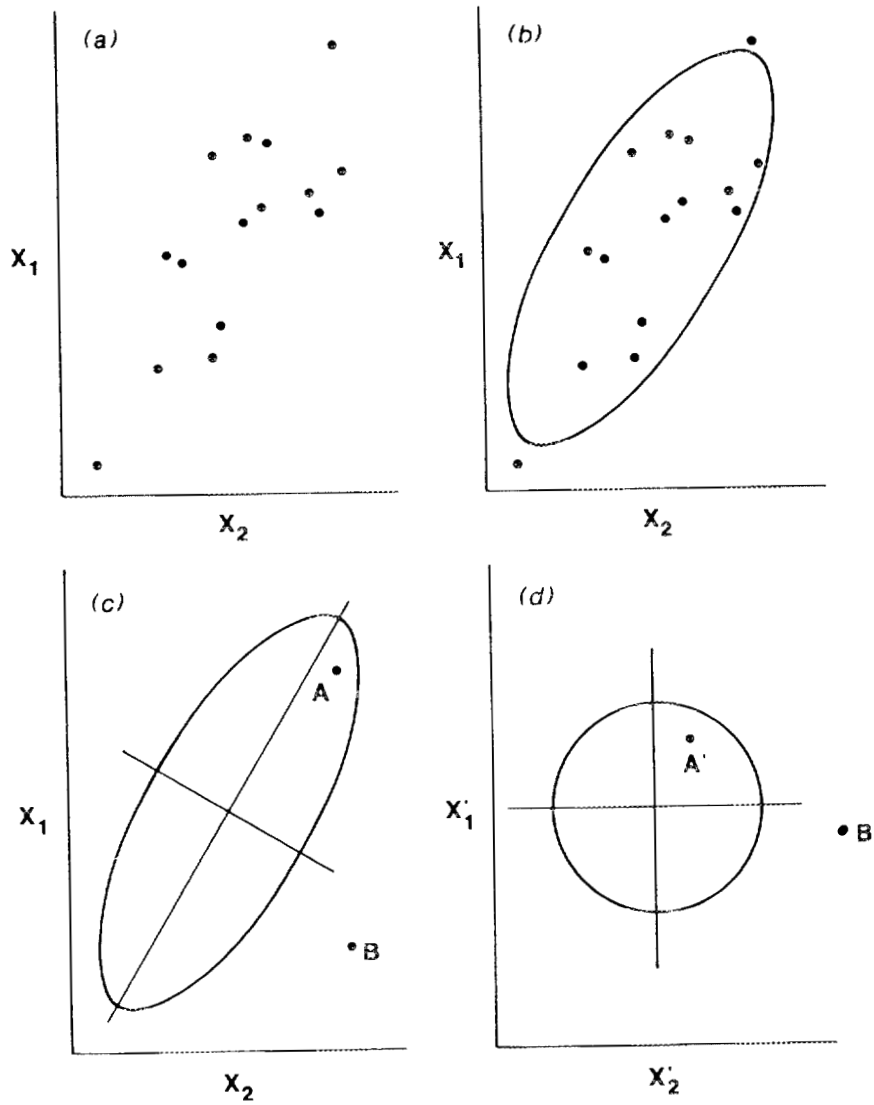


Figure 2.5 An illustration of the Mahalanobis transformation. (a) A sample of bivariate observations. (b) The corresponding concentration ellipse. (c) Two points, A and B, equidistant from the centroid in the original data space. (d) The locations of the two points in the transformed data space (A' and B').

Mahalanobis distances for the corresponding points in the original space.

In this study, the sample covariance matrix for the control (unperturbed) systems was calculated from experimental data or Monte Carlo simulations. This was used to perform the data transformation described above. Euclidean distances were calculated in the transformed space between control and perturbed state vectors, and between replicate control state vectors. The separations thus calculated can equivalently be regarded as Mahalanobis distances between the original state vector standardized to the variability of the controls.

#### 2.4.3 Summary Measures

The techniques outlined in the preceding sections will provide an estimate of the displacement vector, and of the corresponding state space separation, between control and perturbed ecosystem at each point in time. It is often desirable to summarize this detailed information by some set of integrated measures that typify ecosystem response over a specified time interval. The following integrated measures are proposed which, when taken together, effectively summarize much of the information contained in the full set of displacement vectors.

##### 1. Maximum Displacement or Separation

The maximum displacement vector is simply the largest displacement vector,  $u(t)$ , encountered over the specified time

interval. The maximum separation is defined as the magnitude of the maximum displacement vector.

## 2. Mean Separation

Over a time interval beginning at  $t_1$  and ending at  $t_2$ , the mean separation is defined as

$$\frac{1}{t_2 - t_1} \int_{t_1}^{t_2} |u(t)| dt \quad (2.21)$$

where  $|u(t)|$  represents the magnitude of the displacement vector  $u(t)$ .

## 3. Mean Displacement

The mean displacement vector is defined as

$$\frac{1}{t_2 - t_1} \int_{t_1}^{t_2} u(t) dt \quad (2.22)$$

Note that in general the magnitude of the mean displacement vector will not equal the mean separation because a partial cancellation occurs as the vector  $u(t)$  changes direction.

The integral formulae for mean separation and mean displacement were approximated by summations calculated from the discretely sampled data or simulation results. Comparisons among these measures may reflect aspects of the behavior of the displacement vector over time. For example, if the response of the system remains fairly constant over a given time interval, the mean displacement will approach the maximum displacement. Similarly, a comparison of the magnitude of the mean displacement with the mean separation measures the degree to which  $u(t)$  wanders over time, since these quantities will be equal only if the direction of  $u(t)$  is constant. Changes

in direction will decrease the value of the mean displacement magnitude. This might be expected, for example, in systems which show a biphasic response to a toxicant, such as an initial decline in primary productivity due to direct phytotoxic effects, followed by indirect effects at higher trophic levels. The details of such a response can be reconstructed from an analysis of the displacement trajectory.

#### 2.4.4 Computation of State Space Statistics

All analyses of both experimental data and simulation results were performed using the Statistical Analysis System (SAS). The calculation of displacement vectors and state space separations was accomplished by an algorithm written using PROC MATRIX (SAS 1985a). The summary indices were subsequently computed using PROC MEANS or PROC SUMMARY (SAS 1985b). Other SAS procedures were used in the course of the study, notably for regression analysis (PROC REG), for principal components analysis (PROC PRINCOMP and PROC FACTOR), and for discriminant analysis (PROC DISCRIM, PROC CANDISC and PROC STEPDISC) (SAS 1985c).

The methods of data analysis developed in this chapter are applied to experimental microcosm and pond data in chapter 3. Chapter 4 presents the results of similar analyses of the output of an ecosystem model. Because of the large number of Monte Carlo replicates produced by the model, certain statistical properties of the method can be addressed using the simulated data set.

Subsampling of the the simulated data allows the robustness of the method to the smaller, experimentally feasible sample sizes to be assessed.

## Chapter 3

## EXPERIMENTAL RESULTS

This chapter presents the results of applying the state space methodology developed in chapter 2 to experimental data. The data were collected in a series of studies of the response of freshwater ecosystems to the introduction of alkylphenols. The flask microcosm experiment investigated the effects of an acute dose of a single phenolic compound, 2,4-dimethylphenol. The aquarium microcosms and outdoor ponds were used to investigate the effects of chronic exposure to a coal-derived complex mixture. These systems, and the experimental methods used to gather the data, are discussed in greater detail in chapter 2 (sections 2.1 and 2.2).

## 3.1 FLASK MICROCOSMS

## 3.1.1 Dynamics of Individual State Variables

After inoculation, the microcosms underwent a period of growth and development. This transient phase was characterized by an initial rapid rise followed by decline in pH (from 8.01 to 9.24 to 8.24) and dissolved oxygen (from 7.9 to 9.0 to 6.8 ppm), and by a steady decline in conductivity (from 447 to 391  $\mu\text{mho cm}^{-1}$ ). After approximately three weeks, coinciding with the time at which the toxicant was introduced, the untreated microcosms appeared to enter a quasi-steady state, in which the three state variables

fluctuated around a relatively constant value for the rest of the experiment. Within the quasi-steady state there seemed to be greater variability between replicates than during the transient phase, especially for pH and conductivity.

The nominal concentration of 2,4-dimethylphenol at each of the treatment levels is summarized in Table 2.3. The dynamics of the toxicant-perturbed microcosms was compared to that of the controls on the basis of least significant differences with a comparisonwise type I error rate of 0.05, computed by the formula

$$|y_c - y_p| \geq t_{\alpha, v} \left( \frac{1}{n_c} + \frac{1}{n_p} \right) s \quad (3.1)$$

where  $y_c$  and  $y_p$  are the control and the perturbed means,  $n_c$  and  $n_p$  are the numbers of control and perturbed replicates,  $s$  is the root mean square error, and  $t_{\alpha, v}$  is the Student's  $t$  value with  $\alpha = .05$  and  $v$  degrees of freedom. The interval not significantly different from the controls was taken to represent the normal operating range for each variable. No significant differences were found for any of the state variables at the three lowest doses. The results for the higher treatment levels are summarized in Figs. 3.1, 3.2 and 3.3. The mean pH at the two highest doses drops slightly below the normal operating range immediately after the perturbation, but quickly recovers. Dissolved oxygen is depressed well below the normal range, but again recovers rapidly. Conductivity, by comparison, shows a delayed but sustained response, significantly increasing in all three of the higher treatment levels.

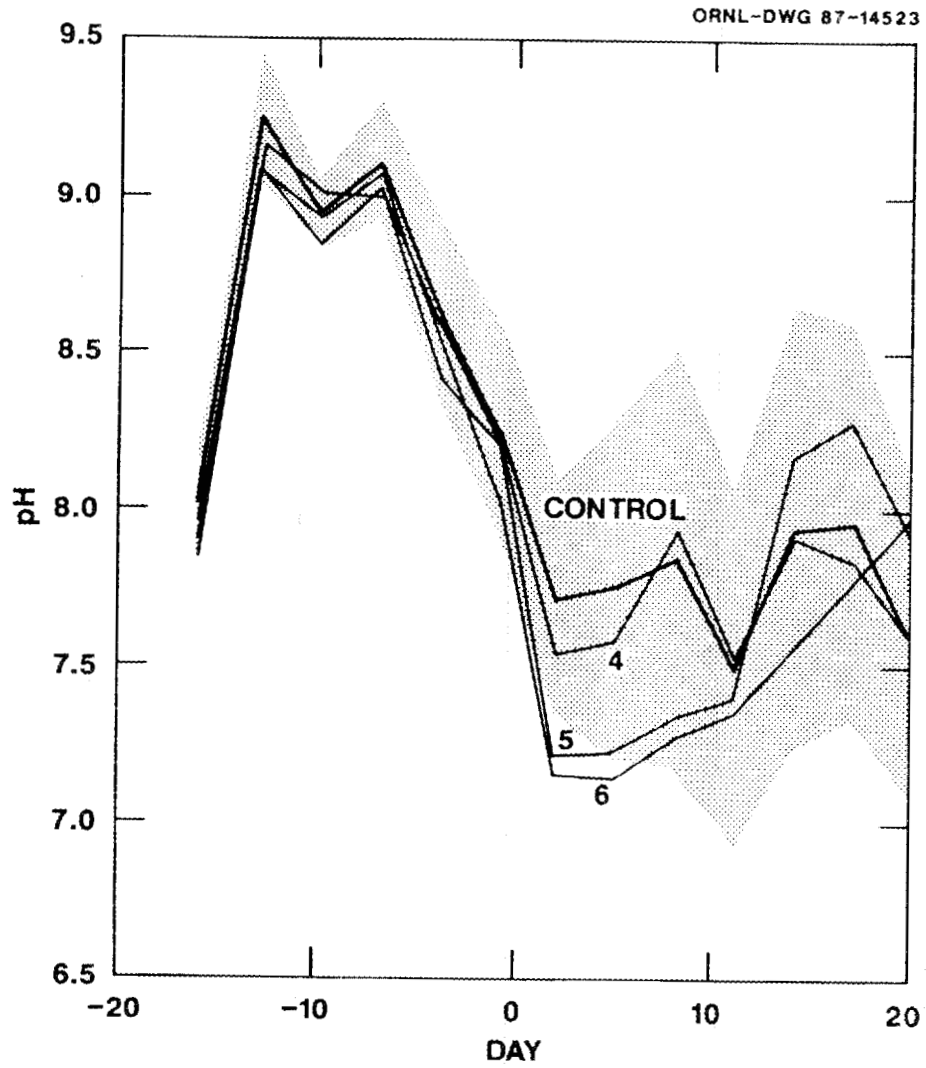


Figure 3.1 Dynamics of pH in flask microcosms. Shaded region indicates least significant difference interval ( $\alpha=0.05$ ). Treatment levels 1-3 (not shown) did not significantly differ from controls.

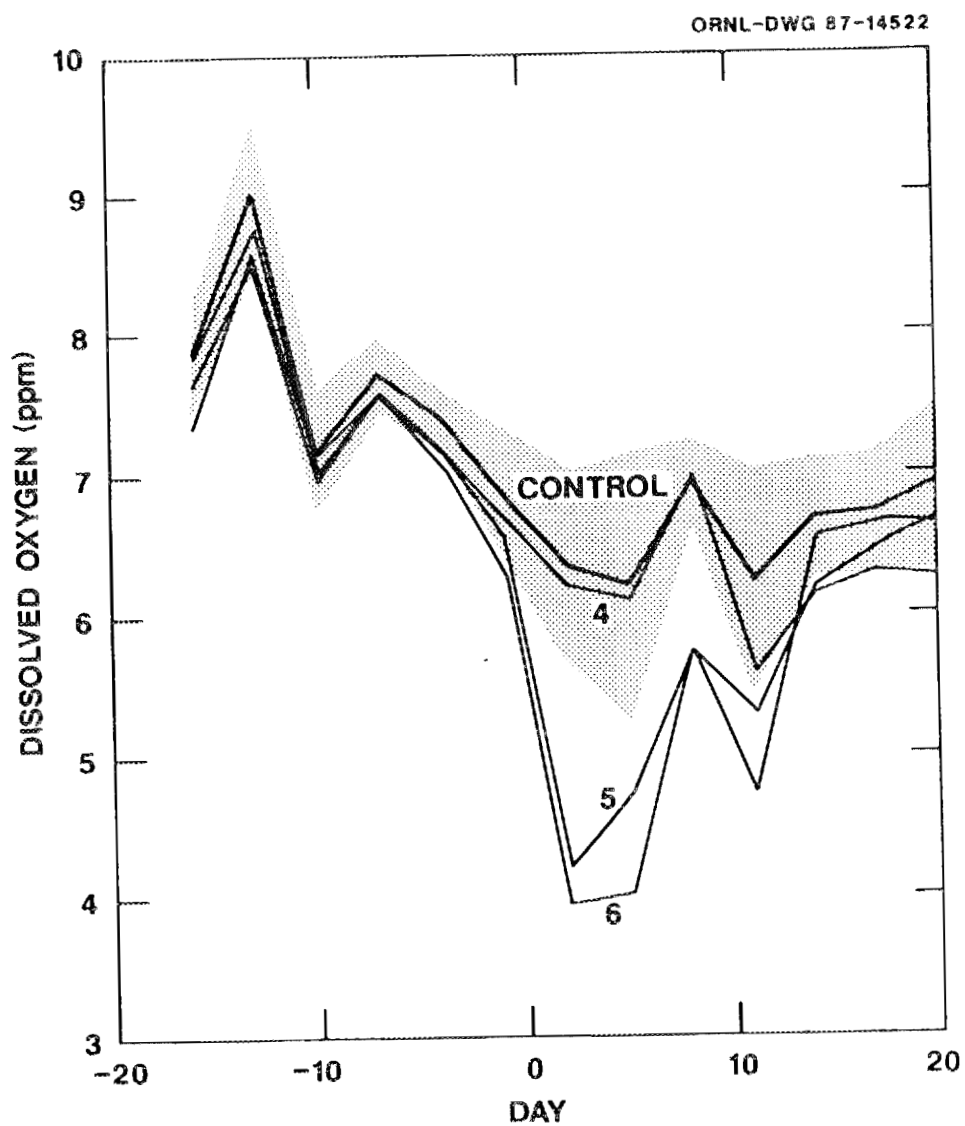


Figure 3.2 Dynamics of dissolved oxygen in flask microcosms. Shaded region indicates least significant difference interval ( $\alpha = .05$ ). Treatment levels 1-3 (not shown) did not significantly differ from controls.

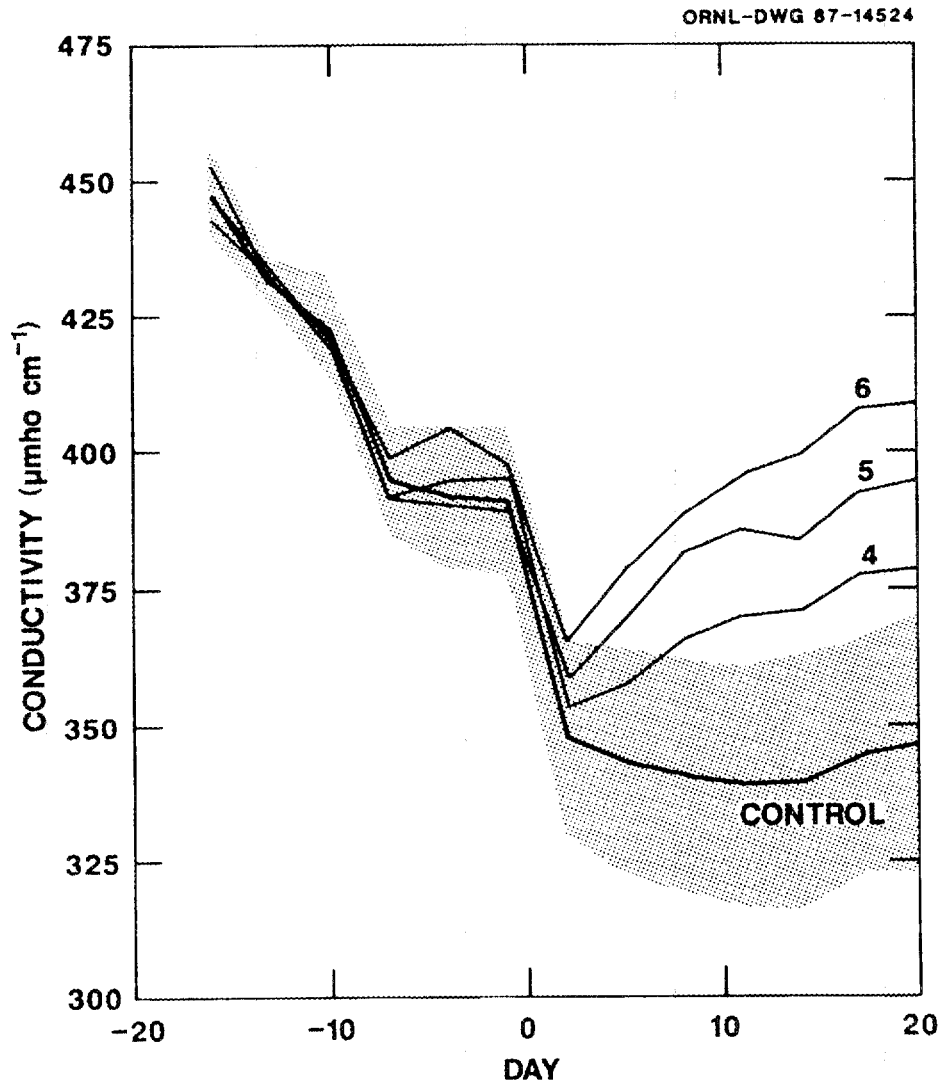


Figure 3.3 Dynamics of conductivity in flask microcosms. Shaded region indicates least significant difference interval ( $\alpha=.05$ ). Treatment levels 1-3 (not shown) did not significantly differ from controls.

### 3.1.2 State Space Analysis

The separation between treatment group centroids, as defined in sections 2.4.1 and 2.4.2, is shown as a function of time in Fig. 3.4. The separation was estimated by the mean separation of all nonidentical pairwise comparisons of state vectors. The rapid response at treatment levels 5 and 6 is clearly shown. At treatment level 4 a smaller, delayed response is detectable. As was the case when examining the state variables individually, no discernable response is observed at any of the lower toxicant exposures as compared to the controls. It is also apparent that the separation between replicate controls was not constant over time. Some of this variability is probably due to random sampling error, but there is a pattern of consistently higher control variability in the second half of the experiment.

As an aid to interpretation, the correlations between state space separations and changes in each of the individual state variable were examined. These correlations change over time, as shown in Fig. 3.5. Immediately following the introduction of the toxicant, there is a strong negative correlation between state space separation and changes in dissolved oxygen. Subsequently, the magnitude of this correlation decreases, while the correlation with changes in conductivity increases. The patterns revealed by these correlations are in accordance with the temporal patterns of response observed in the original data (Figs. 3.1 - 3.3), lending support to the use of such correlations for interpreting the results of state

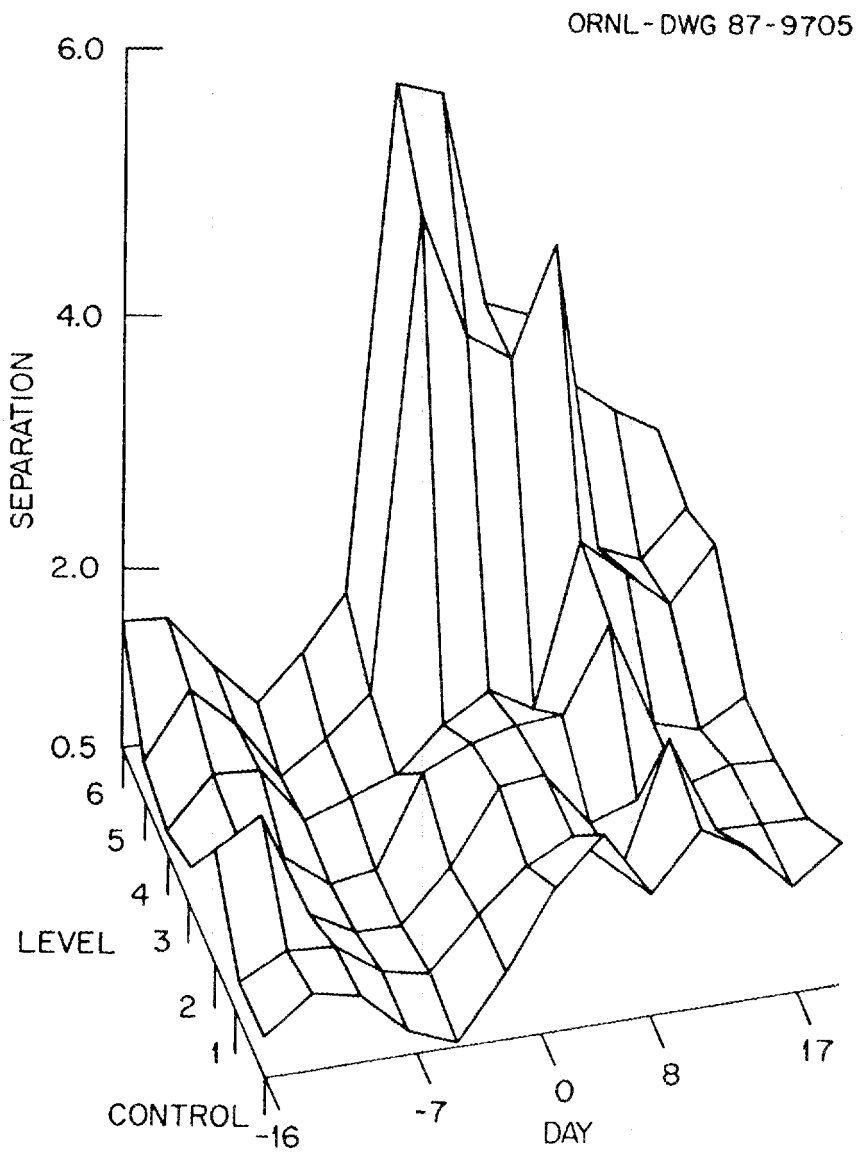


Figure 3.4 State space separation as a function of time and treatment level for flask microcosm experiment.

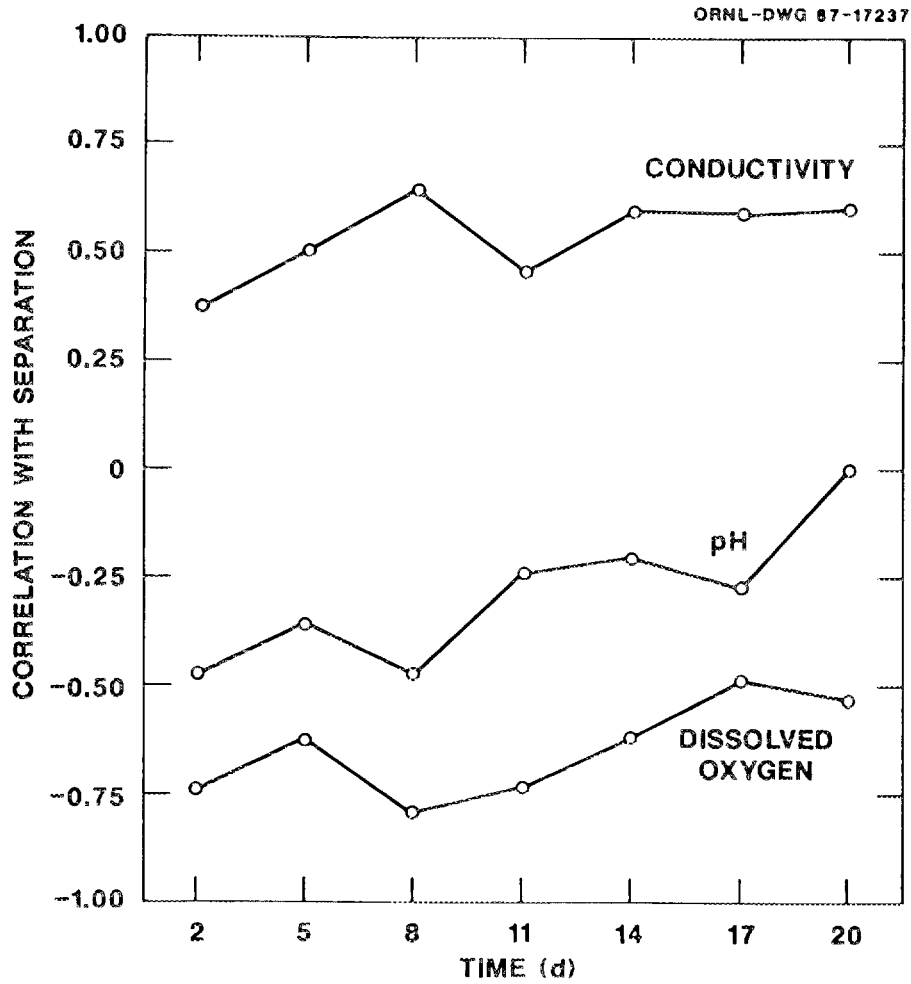


Figure 3.5 Correlation of state variables with separation as a function of time following toxicant addition.

space analysis. At the same time, it may be noted that since the correlations are not strong ( $|r|$  seldom  $> 0.7$ ), the multivariate response contains information not captured by individual variables, providing support for the use of state space analysis.

The response of the microcosms during the post-treatment period, as characterized by the summary indices described in section 2.4.3 (maximum separation, mean separation, and mean displacement magnitude), is shown in Fig. 3.6. All three curves increased significantly at the two highest toxicant concentrations, but showed little or no response at lower doses. The wide divergence of mean separation and mean displacement magnitude values at the low doses is compatible with a relatively random, non-directional differences between microcosms, as would be expected if the dynamics of these systems is dominated by inherent natural variability or by stochastic factors affecting each microcosm differently. As response to the toxicant becomes the dominant influence on ecosystem dynamics, these indices converge toward the same value, indicating a more directed displacement.

Ninety-five percent confidence intervals for maximum separation were calculated on the basis of an assumed normal distribution. These intervals are shown as bars in Fig. 3.6. The normality assumption was tested using the Shapiro-Wilk statistic (Shapiro and Wilk 1965), and was rejected only for the controls. Further inspection of the control distribution indicated that it was lighter in the tails than a normal distribution, so that a confidence

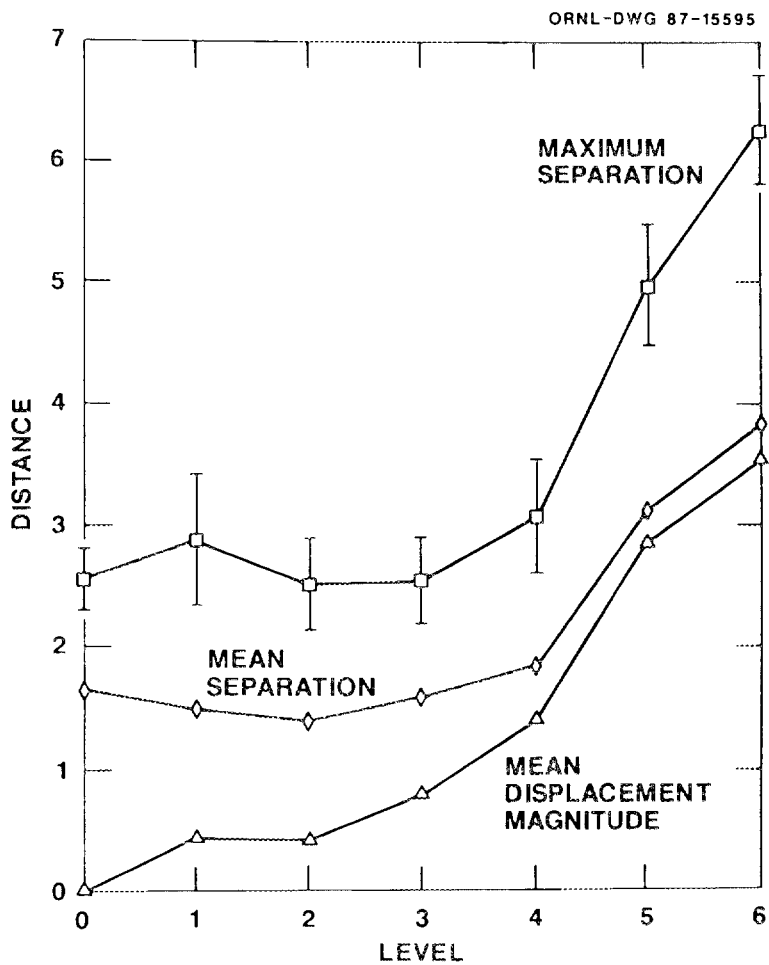


Figure 3.6 Dose-response curves for flask microcosms exposed to 2,4-dimethylphenol. Squares represent maximum separation, diamonds mean separation, triangles mean displacement magnitude. Bars represent calculated 95% confidence intervals.

interval based on a normal approximation is likely to be larger than required. Confidence intervals are not shown for mean separation or mean displacement magnitude. For these indices the assumption of a normal distribution was frequently violated, but inspection of the empirical frequency distributions indicated that appropriate confidence intervals would be somewhat asymmetric and of a size comparable to those for maximum separation.

### 3.1.3 Changes in Covariance Structure

Since the state space analysis is based on a data transformation which is a function of the sample covariance matrix, it is of interest to observe changes in the covariance structure that occur over time. The covariance structure was investigated in two ways: (1) the generalized variance, defined as the determinant of the covariance matrix, was calculated for each sample over the course of the experiment, and (2) the correlations between state variables were also calculated for each sample.

The square root of the generalized variance, which can be regarded as a generalized standard deviation, is plotted for the control microcosms in Fig. 3.7. There is a substantial increase in the variability of the controls coinciding with the beginning of the treatment period. The reasons for this are not entirely clear, but it should be remembered that the controls did receive an addition 100 mL of distilled water, corresponding the addition of 100 mL of toxicant solution in the perturbed systems. It is possible that the

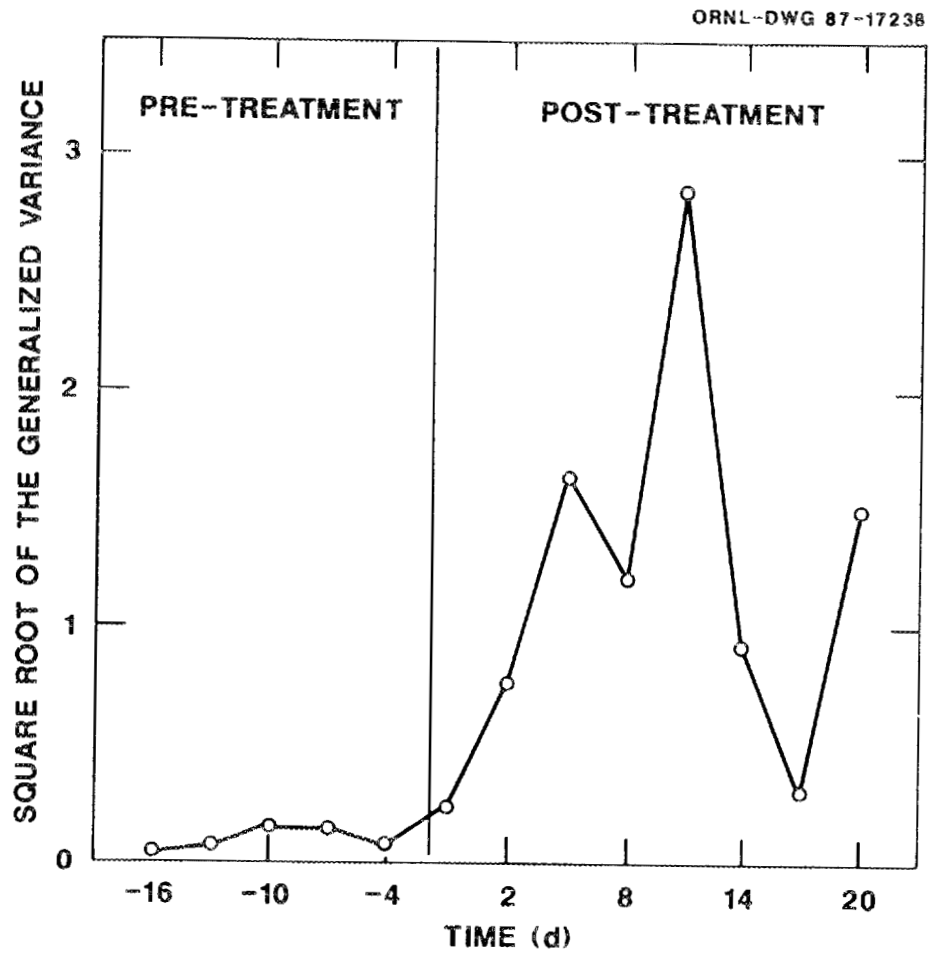


Figure 3.7 Square root of the generalized variance of the control microcosms as a function of time.

dilution caused by adding distilled water was itself not an inconsequential perturbation to the system.

It is important to evaluate the extent to which the temporal variations in calculated correlations represent true changes in the underlying correlation structure as opposed to random sample variation. This is examined in Fig. 3.8, where, correlations between state variables in the microcosms are plotted as a function of time. After addition of the toxicant to the treated microcosms, the correlation structure must be calculated on the basis of the five remaining control microcosms. Prior to treatment with the toxicant, however, all 24 microcosms are effectively controls. The correlation structure based on all 24 microcosms was calculated for each sampling date in the pretreatment period. These correlations can be compared with those calculated on the basis of the five controls. The correlation between pH and dissolved oxygen is generally strong ( $|r| > 0.6$ ), and the estimates based on the five controls agree well with those based on all 24 microcosms. The pH-conductivity and dissolved oxygen-conductivity correlations, however, are generally weaker and the concordance between the  $n = 5$  and  $n = 24$  estimates is poor, so that little can be inferred about the actual temporal dynamics of these correlations.

In addition to temporal changes in the covariance structure of unperturbed microcosms, the covariance structure might be expected to change in response to toxicant exposure. The accuracy in estimation of a correlation matrix is improved as more degrees of freedom are

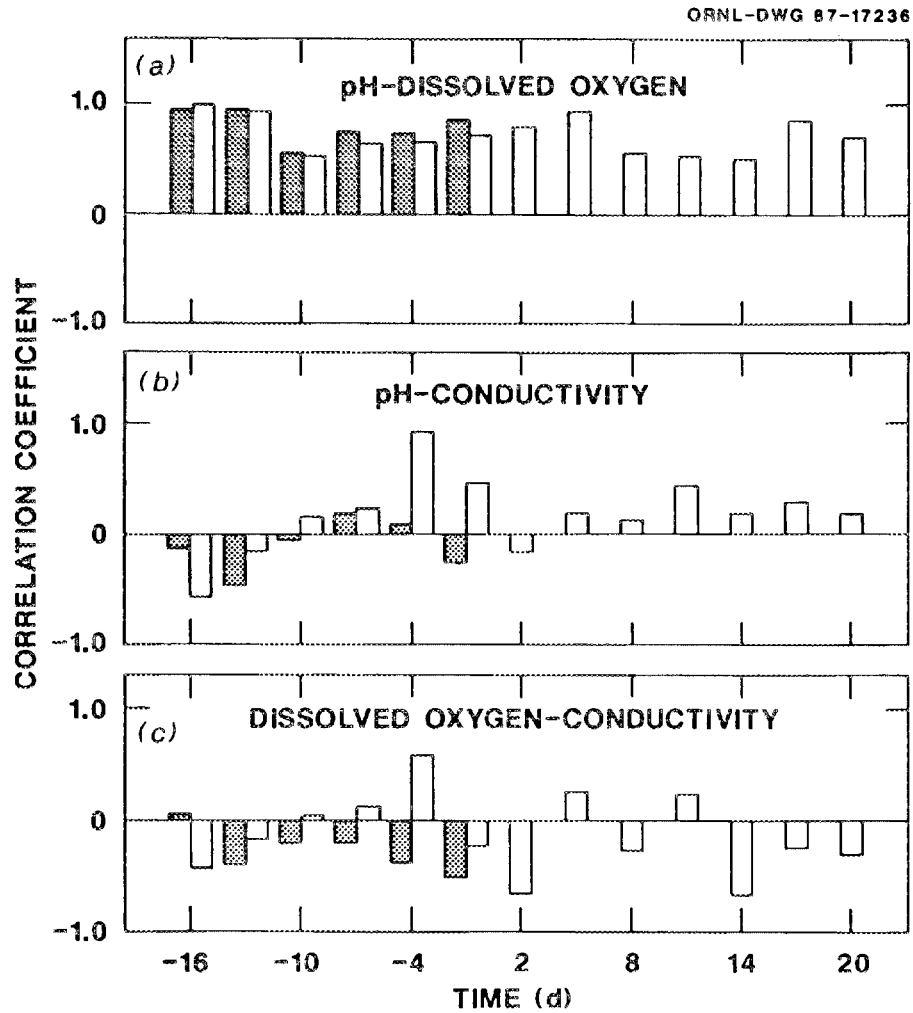


Figure 3.8 State variable correlations as a function of time. Shaded bars, correlations calculated from all microcosms prior to toxicant addition. Open bars, correlations calculated from control microcosms only.

available relative to the rank of the matrix, so correlations among state variables were calculated at each treatment level from data pooled over two time periods: before and after addition of the toxicant. The results are shown in Fig. 3.9. The pH-dissolved oxygen correlations were moderately strong ( $> 0.4$ ) and positive during the pre-treatment phase, and became generally stronger ( $> 0.5$ ) in the post-treatment phase, but no dose-related response was observed. The pH-conductivity correlations were weak (mostly  $|r| < 0.3$ ) and negative in the pre-treatment phase, becoming positive in the post-treatment phase ( $r = 0.8$  at the highest dose). In this case, a clear dose-related pattern is discernible, with markedly stronger correlations at the higher doses. A dose-related response is also evident in the dissolved oxygen-conductivity correlations. Before treatment, these correlations were moderately positive, taking on near zero values following treatment, except at the two highest doses, where the correlations were strongly positive ( $> 0.7$ ).

### 3.2 AQUARIUM MICROCOSMS AND OUTDOOR PONDS

The responses of both ponds and microcosms to the synthetic oil are summarized in Fig. 3.10. More detailed accounts of the response of individual state variables have been published by Franco et al. (1985) and Giddings et al. (1985). This section focuses on the results of an analysis of their data using the state space approach.

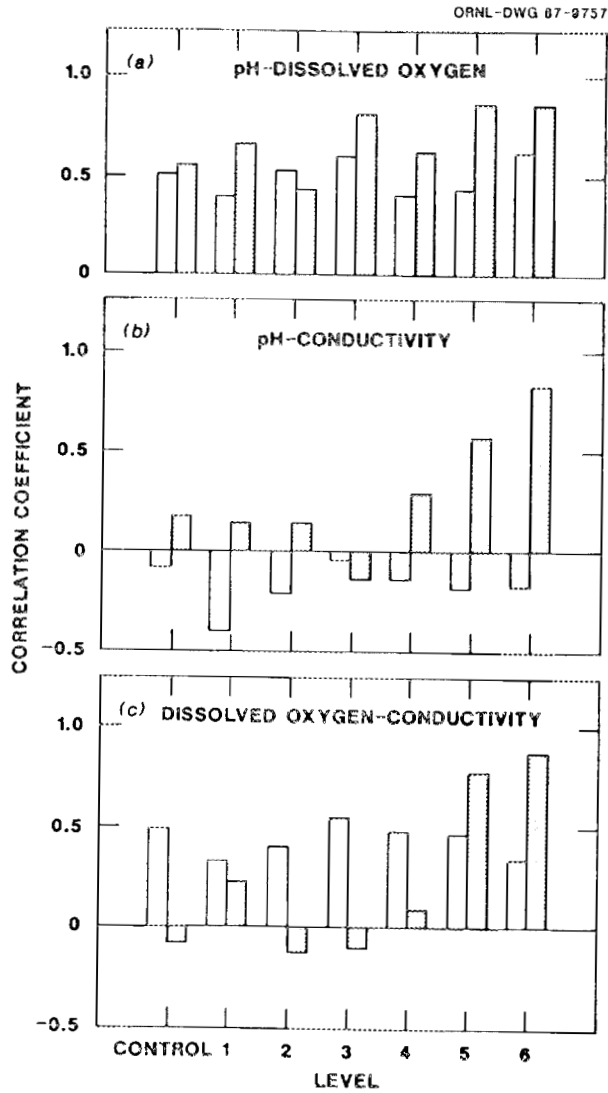


Figure 3.9 State variable correlations in microcosm data pooled over time. Open bars = prior to toxicant addition. Shaded bars = after toxicant addition.

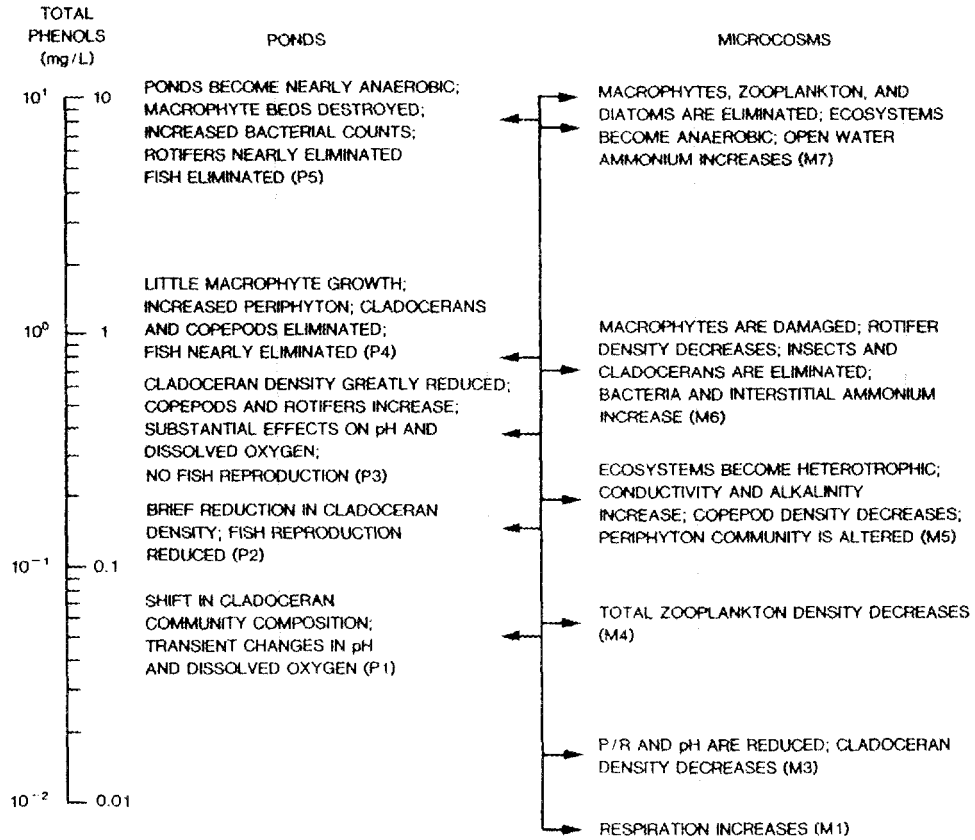


Figure 3.10 Summary of responses observed in aquarium microcosm and outdoor pond experiments.

### 3.2.1 Dose-Response Relationships

Separation was plotted as a function of oil input rate and length of exposure for both ponds (Fig. 3.11a) and microcosms (Fig. 3.11b). For this analysis, daily- and weekly-dosed microcosms at each treatment level were treated as replicates, as justified by previous statistical analysis (Franco et al. 1984, p.451). Additionally, the transformations of both pond and microcosm data before state space trajectory analysis were based on sample covariance matrices for control data pooled over the entire exposure period. This procedure is valid as long as the covariance structure of the state variables was reasonably constant over the 56-d interval. The assumptions made in the analysis are necessitated by the low degree of replication provided by this experimental design, but could be relaxed for studies with greater replication.

The relationship between separation, oil input rate, and length of exposure were qualitatively similar for both ponds and microcosms. Specifically, (1) there is a generally monotonic increase in response with increasing dose or time of exposure; (2) exposure conditions exist below which response is negligible; and (3) there is a suggestion of a response plateau at higher doses or with prolonged exposure. The major apparent difference is the smoother texture of the microcosm response surface. In part this apparent difference may be partly a consequence of the longer time interval between observations in the microcosm data. If observations are deleted from the pond data to produce the same sampling frequency, the resulting

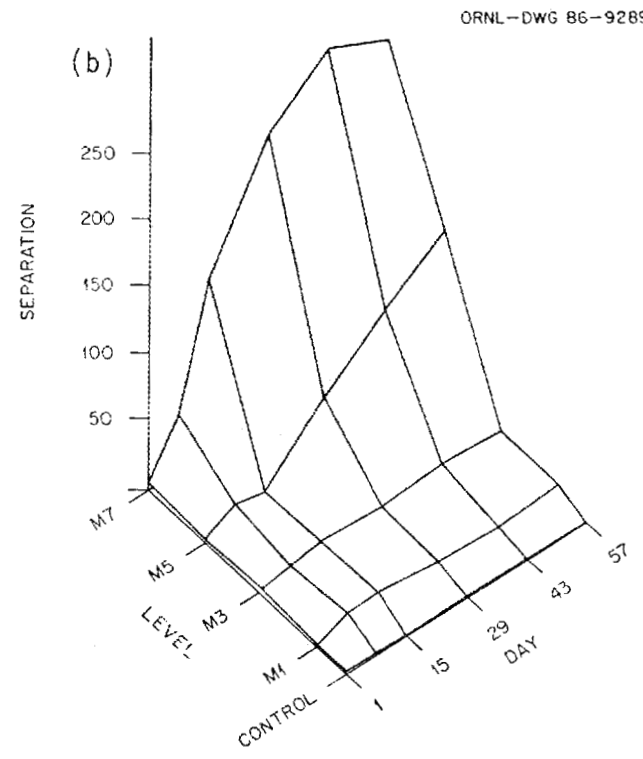
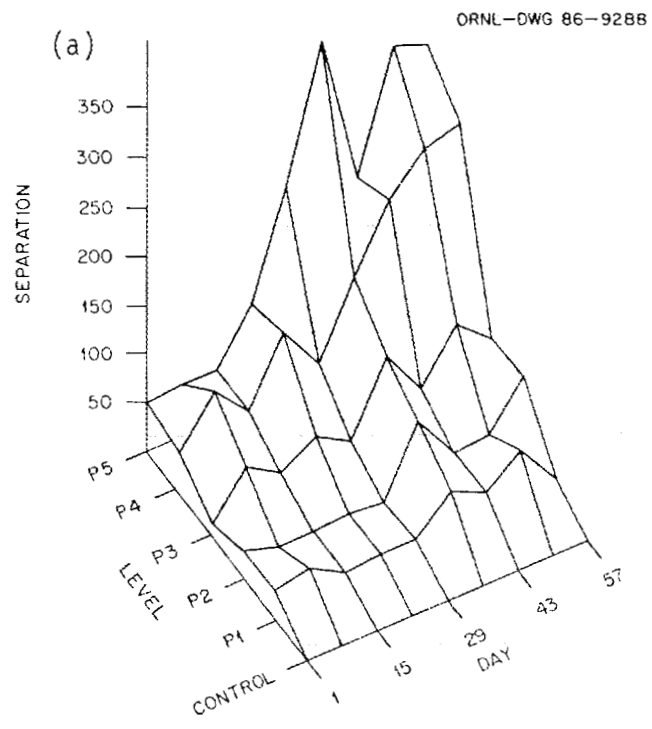


Figure 3.11 State space separation as a function of time and treatment level. (a) Outdoor pond experiment. (b) Aquarium microcosm experiment.

surface also appears substantially smoother. However, the greater roughness of the pond response surface is not completely artifactual, and may reflect the greater environmental variability to which the outdoor ponds were exposed in contrast to the controlled laboratory environment of the microcosms.

Dose-response curves calculated over the 56-d exposure period for each of the three summary state space indices are shown in Figs. 3.12 and 3.13. As expected, the summary indices increase with increasing dose. The error bars on the maximum separation curve represent the range of values over all pairwise comparisons. Error bars for the other curves are of comparable size. The error bars associated with the pond data were substantially larger than for the microcosm data, reflecting the greater variability of the ponds. Since the degree of replication at each treatment was identical in both pond and microcosm experiments ( $n = 2$ ), this is not an effect of sample size. It seems likely to be primarily a reflection of the greater environmental variability to which the ponds were subjected, although it is also possible that larger aquatic ecosystems differ organizationally from their smaller counterparts in ways which affect their dynamic variability.

A comparison of maximum separation with mean separation indicates that the magnitude of the displacement vector changed substantially over the exposure period, as can be seen in the response surfaces. This is simply a reflection of the divergence of

ORNL-DWG 86-9287

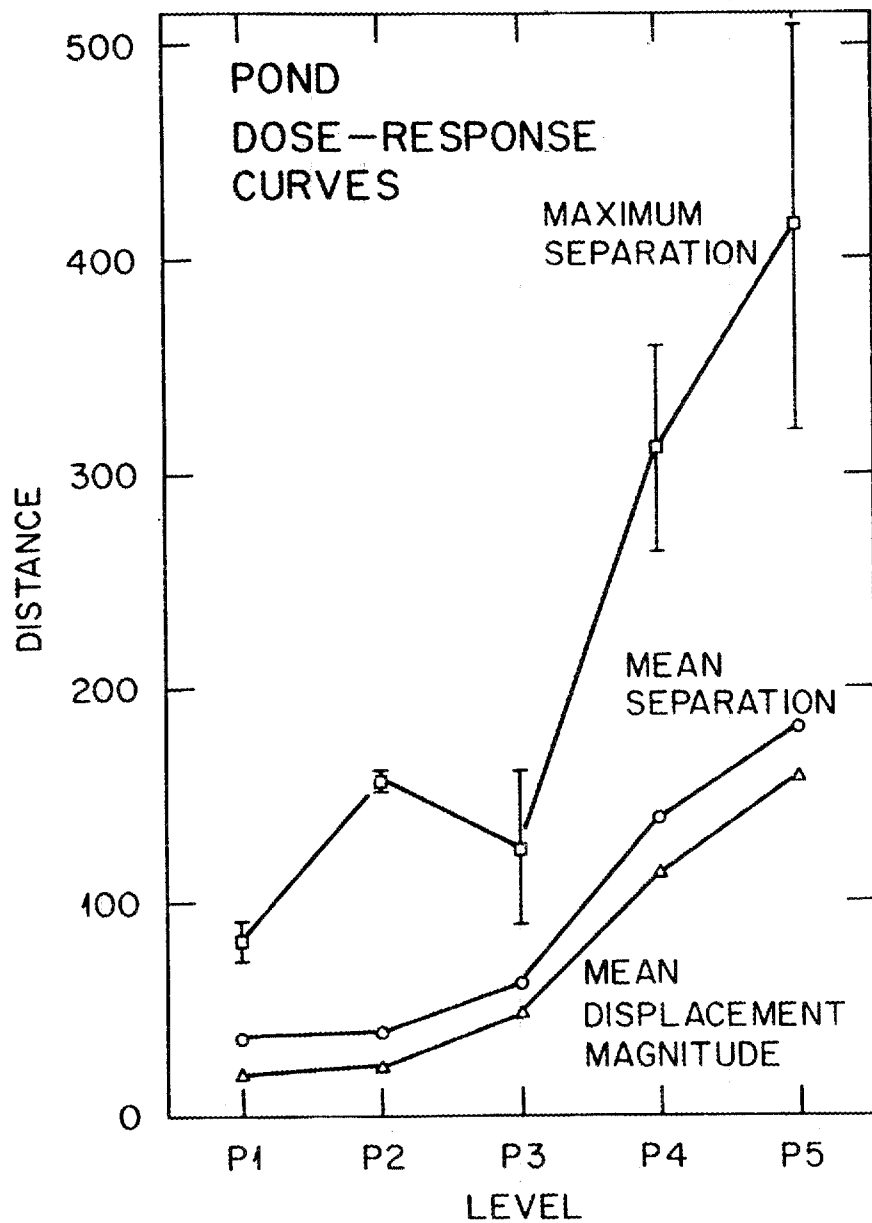


Figure 3.12 Dose-response curves for outdoor ponds exposed to synthetic oil. Squares represent maximum separation, diamonds mean separation, triangles mean displacement magnitude. Bars represent range of maximum separation values observed.

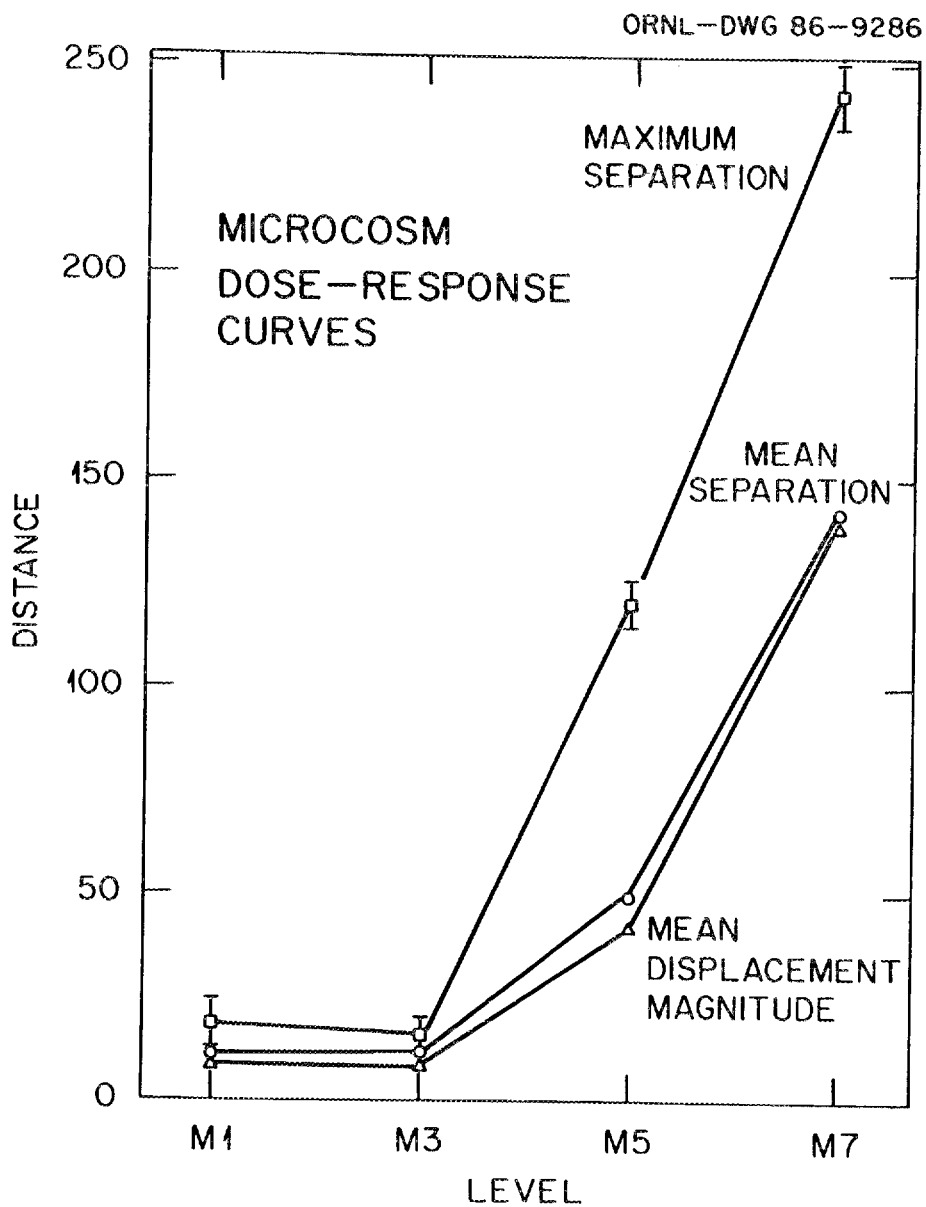


Figure 3.13 Dose-response curves for aquarium microcosms exposed to synthetic oil. Squares represent maximum separation, diamonds mean separation, triangles mean displacement magnitude. Bars represent range of maximum separation values observed.

initially similar systems in response to different levels of toxicant exposure. In contrast, a comparison of mean separation and mean displacement magnitude indicates that the direction of the displacement vectors was relatively uniform, especially at the higher doses. This indicates that there was relatively little change over time in the contribution of each of the state variables to the total response. It is possible that changes in direction, due to delayed responses and differential recovery rates, would have been observed if the analysis had extended beyond the dosing period.

The description of ecosystem response provided by state space analysis is consistent with that provided by previous analyses based on univariate statistical methods (Franco et al. 1985, Giddings et al. 1985). Moreover, while those authors provided only a verbal and qualitative description of the overall multivariate response, state space analysis provides a statistically valid quantitative description. It is frequently possible for a statistically significant effect in a multivariate quantity to not be observable as a statistically significant effect in any of its univariate components. Therefore, the lack of an appreciable response at low doses as quantified by the state space analysis provides important additional support for conclusions previously predicated on univariate analyses alone.

### 3.2.2 Correlation with Original State Variables

The relationship of the calculated state space separation to the original variables was assessed by calculating correlation coefficients from the data pooled over the 56 day treatment period. In the ponds, separation was most highly correlated with conductivity, alkalinity, and cladoceran abundance ( $r = 0.84$ ,  $0.82$ , and  $-0.74$ , respectively). Phytoplankton chlorophyll a, rotifer abundance, and ammonium concentration were least correlated with separation ( $|r| < 0.2$ ). All other variables were moderately correlated ( $0.5 < |r| < 0.7$ ). Correlations were generally higher for the microcosms than for the ponds. All variables except for phytoplankton chlorophyll a had  $|r|$  values  $> 0.7$ . The highest correlations were found for conductivity ( $r = 0.99$ ), pH ( $r = -0.93$ ), ammonium concentration ( $r = 0.88$ ), and cladoceran abundance ( $r = -0.84$ ). For most variables, the relationship to separation appeared similar in both ponds and microcosms, with the exceptions of ammonium concentration and rotifer abundance. Because a correlation coefficient is a measure of the linear association between variables, values of  $r$  can be misleading if the true relationship is significantly nonlinear. This may be the case for rotifer abundance, which increased at moderate doses but decreased at higher doses.

### 3.2.3 Changes in Covariance Structure

A large number of state variables were measured in a small number of replicate systems. Therefore, it was not possible to

obtain reliable estimates of the covariance matrix without pooling the data over time. Consequently, the variations in covariance structure over time were not analyzed, but changes in the correlation of state variables induced by toxicant exposure can be evaluated from the pooled data.

The state variables showed stronger overall correlations in those ponds subjected to toxicant stress. This is clearly demonstrated in Fig. 3.14, where the percentage of correlations greater than 0.7 in absolute value is seen to increase steadily as a function of treatment level. Although somewhat arbitrary, the value of 0.7 was chosen because a correlation coefficient of 0.7 implies that the given variable explains approximately half of the measured variance in its correlate. The trend exhibited in Fig. 3.14 would seem to indicate a situation in which most of the state variables were relatively independent of one another in the controls, but which came to covary under toxicant exposure, either due to direct interaction between state variables, or due to their separate but simultaneous reactions to a common stress.

The toxicant-induced changes in the covariance structure of the ponds is further elucidated by the use of principal components analysis. Geometrically, principal components correspond to the principal axes of a concentration ellipse (or higher dimensional analog) of a cloud of multivariate data (Fig. 3.15). Principal components are numbered such that the first principal component explains the greatest amount of the total variance. If no

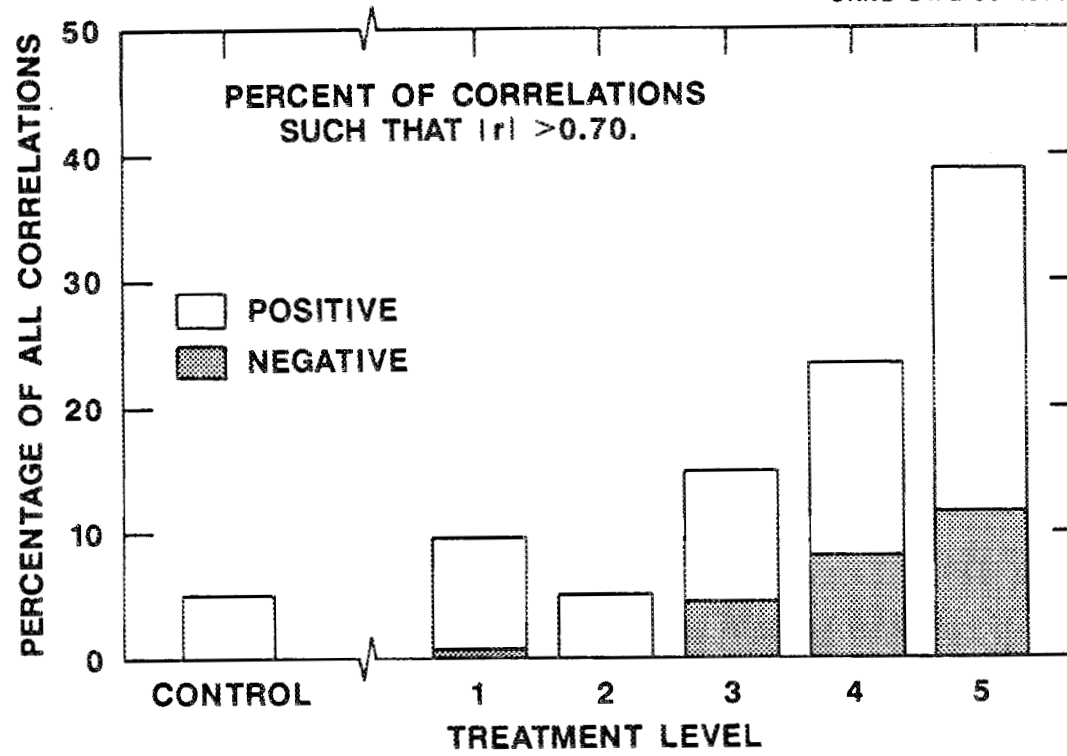


Figure 3.14 Percentage of state variable correlations greater than 0.7 in absolute value as a function of treatment level.

ORNL-DWG 86-15719

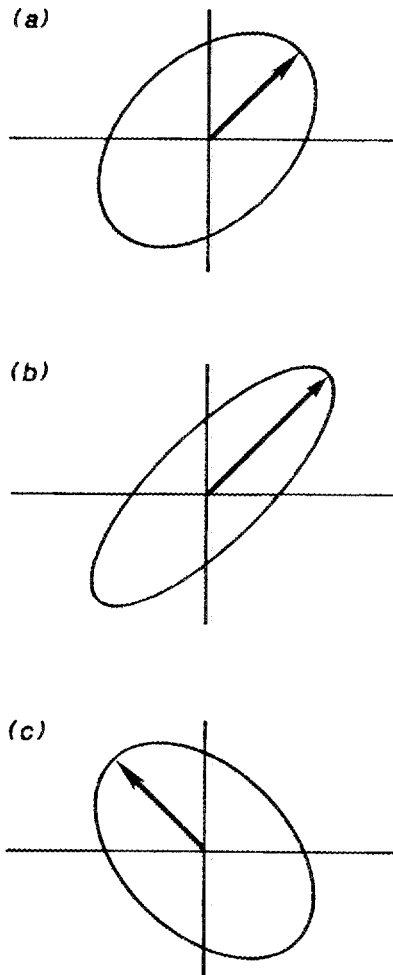
**FIRST PRINCIPAL COMPONENT  
FOR CORRELATED DATA**

Figure 3.15 Eigenvectors associated with first principal component of correlated data. (a) Eigenvector aligned along major axis of concentration ellipse for moderately correlated data. (b) Eigenvector of greater magnitude associated with more strongly correlated data. (c) Rotated eigenvector associated with change in the nature of the correlation.

correlations are present in the data, then (except for sampling error) all principal components should explain an equal fraction of the total variance. As the strength of the correlations increases, fewer principal components are required to explain most of the variance, and the proportional variance explained by the first principal component increases. Also, as the nature of the correlations change, the orientation of the multivariate data cloud shifts, and the first principal component is rotated in space. Changes in the variance explained and in the orientation of the first principal component resulting from toxicant exposure are shown in Fig. 3.16. The explained variance increases, especially at the three higher doses, confirming the overall increasing degree of correlation. Also, the nature of the correlations changes, as indicated by the large angle of rotation of the major axis of the concentration ellipsoid relative to the controls.

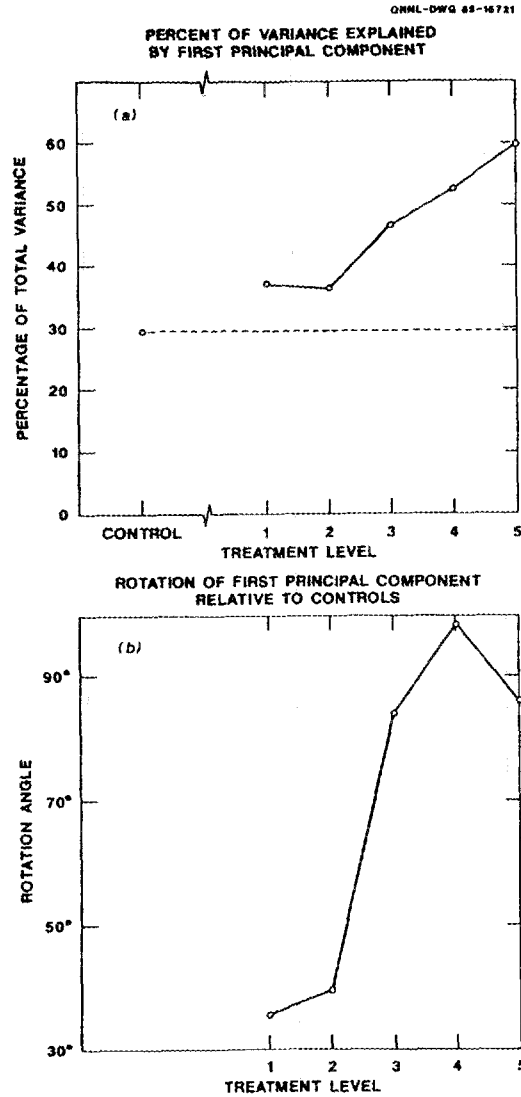


Figure 3.16 Changes in covariance structure of state variables as a function of treatment level in pond experiment. (a) Percentage of total variance explained by the first principal component. (b) Rotation of first principal component relative to controls.

## SIMULATION RESULTS

This chapter presents results of the analysis of output from an ecosystem simulation model. The model used is intended to simulate a small littoral ecosystem analogous to the experimental ponds. Results of deterministic runs of this model, both with and without the effects of the toxicant, are presented in section 4.1, along with comparisons to observations from the experimental studies whenever possible. In section 4.2, the influence of natural variability and measurement error on the model output is described. Section 4.3 summarizes the results of applying state space displacement analysis to the model output. Furthermore, by varying the number of simulations used in the state space analysis, the sample size requirements of the method are investigated. Section 4.4 explores changes in the covariance structure of the simulated state space trajectories, both over time and in response to the toxicant. Finally, section 4.5 considers the problem of monitoring the state of an ecosystem within a decision-oriented, management context, and introduces the concept of diagnostic variables.

## 4.1 RESULTS OF DETERMINISTIC SIMULATIONS

### 4.1.1 Model Dynamics in the Absence of Toxicant

In the absence of toxicant exposure, the phytoplankton exhibit a bloom peaking at approximately the midpoint of the 56 day simulation period. This bloom is dominated by phytoplankton species 9, with species 8 as an important subdominant. This accords with previous experience with SWACOM, where species 8 and 9 are typically late-summer species with temperature optima near 25 °C, high light saturation constants, and low Michaelis-Menten nutrient uptake half-saturation constants. Accompanying the phytoplankton bloom, there is a sigmoidal increase in zooplankton biomass, leveling off near the end of the simulation period. Lagging several days behind the zooplankton is a nearly exponential rise in fish biomass. The dynamics of the three trophic levels of the pelagic food web are summarized in Fig 4.1a.

Macrophyte biomass increases rapidly to a maximum of nearly 1200 g dry wt m<sup>-2</sup> on day 8 of the simulation, followed by a period of slow, but steady, decrease (Fig 4.2). The mass of detritus decreases continually throughout the 56 day interval, although the rate of loss is more rapid at first. The change in the rate of decomposition is primarily a reflection of changes in detrital composition, which initially is 60% labile, but which is only approximately 10% labile at the end of the simulation period (Fig. 4.3). Primary production in the system is dominated by the

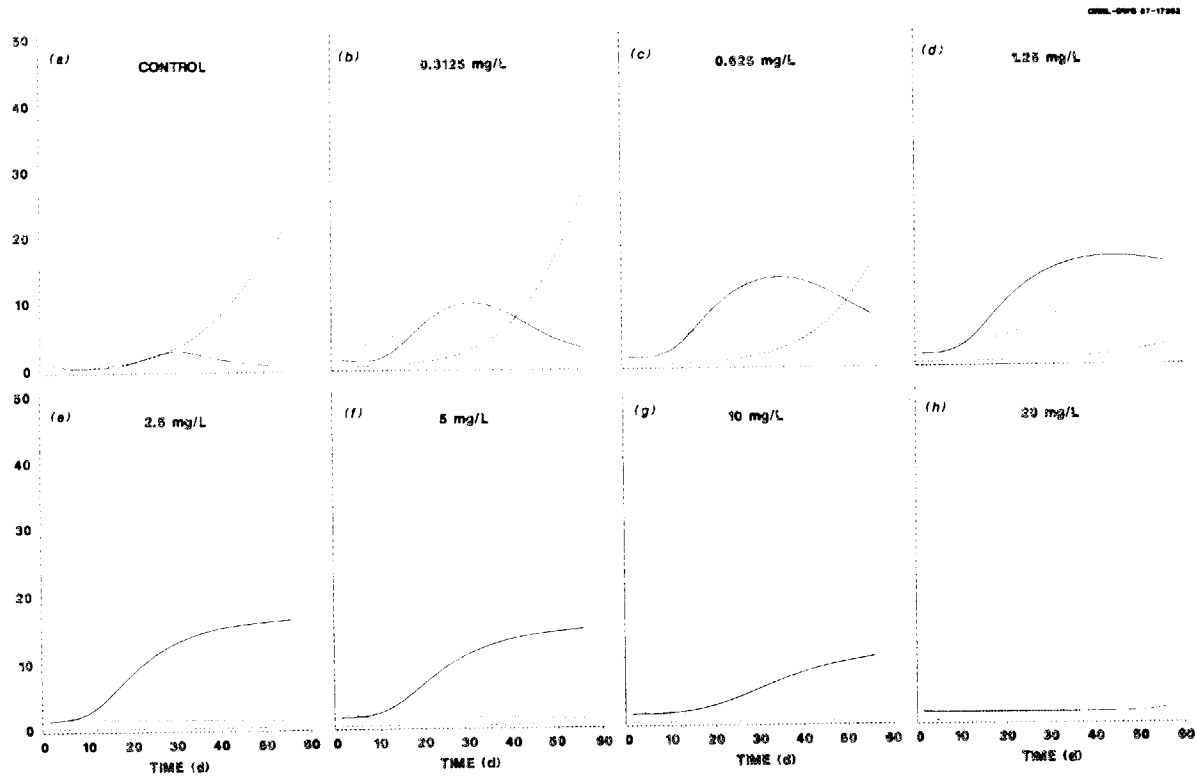


Figure 4.1 Biomasses of pelagic trophic levels in deterministic simulations at various toxicant concentrations. phytoplankton, ..... zooplankton, — fish, - - - -.

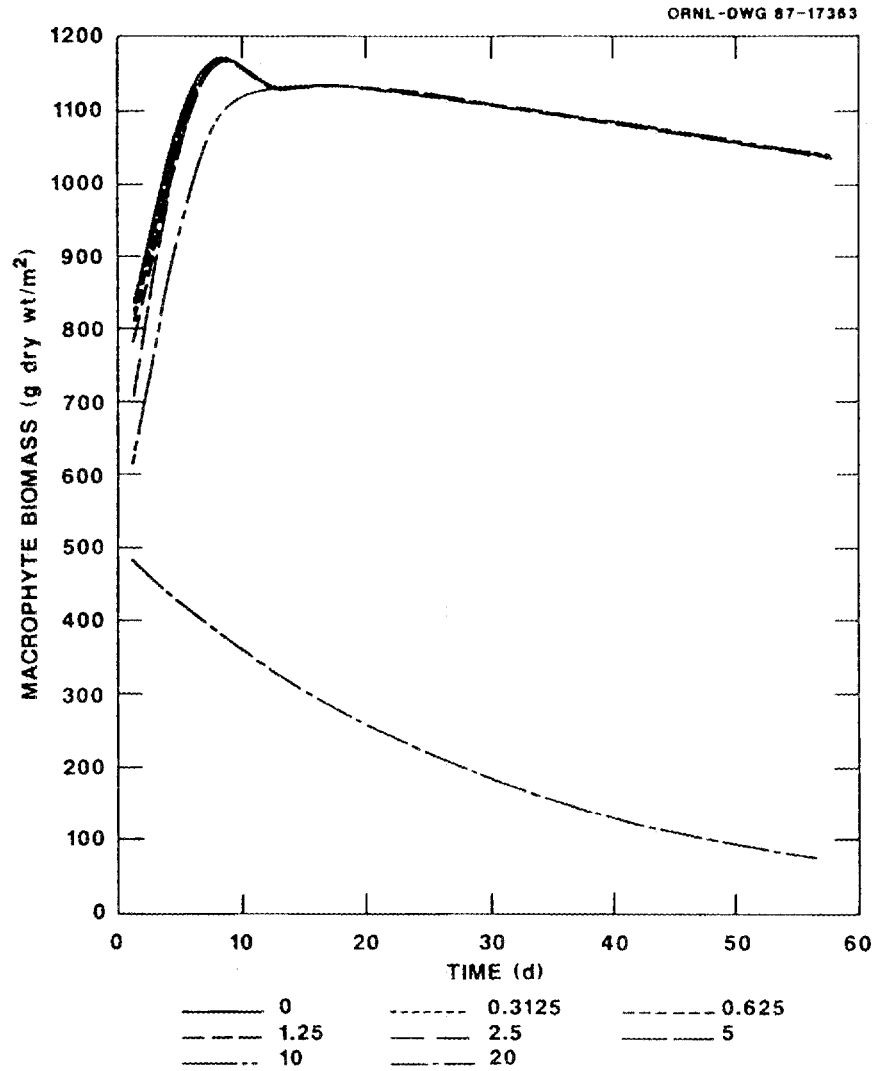


Figure 4.2 Macrophyte biomass dynamics in deterministic simulations at various toxicant concentrations.

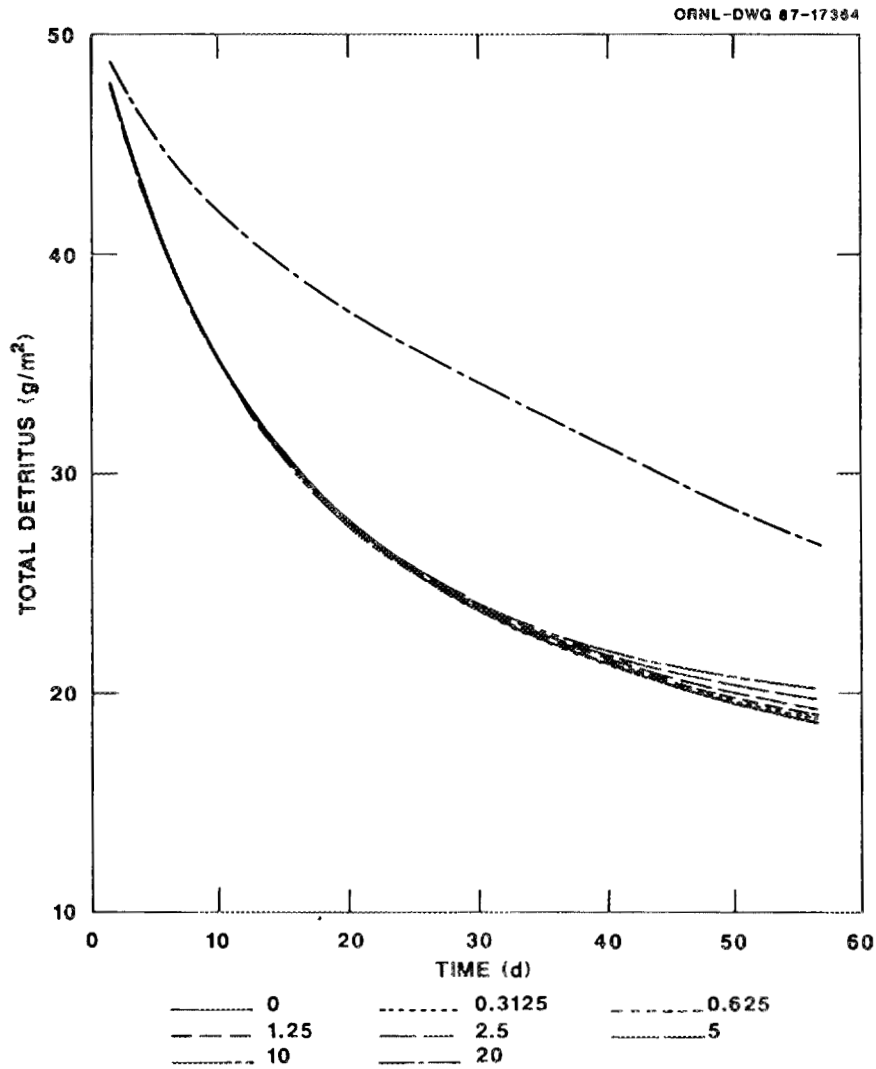


Figure 4.3 Detritus dynamics in deterministic simulations at various toxicant concentrations.

contribution of macrophytes. Macrophyte net photosynthesis shows an initial increase corresponding to the initial growth of the macrophyte bed, followed by a slight depression as summer temperatures exceed the plant's physiological optimum, and finally an increase as environmental conditions once again become more favorable (Fig. 4.4). The phytoplankton exhibit a somewhat different temporal pattern of productivity, and are always at least an order of magnitude less important than macrophytes in terms of total photosynthetic production (Fig. 4.5).

Dissolved oxygen displays a temporal pattern qualitatively similar to the macrophyte productivity curve (Fig. 4.6). The dissolved oxygen concentrations predicted by the model were consistently above saturation (oxygen solubility is 7.64 ppm at 29°C, the approximate average temperature). Such oxygen supersaturation was frequently observed in the experimental ponds, including concentrations as high as 14.00 ppm. The other physicochemical parameter in the model, dissolved nutrient concentration, generally decreased over the period of the simulation, with the greatest rate of decrease occurring during the phytoplankton bloom (Fig. 4.7).

#### 4.1.2 Model Dynamics with Toxicant Effects

At low concentrations, the introduction of the toxicant has an apparently stimulatory effect at all trophic levels. For instance, at a simulated phenol concentration of 0.3125 mg/L, the initial direct toxic effects on the consumer populations allow for a substantially

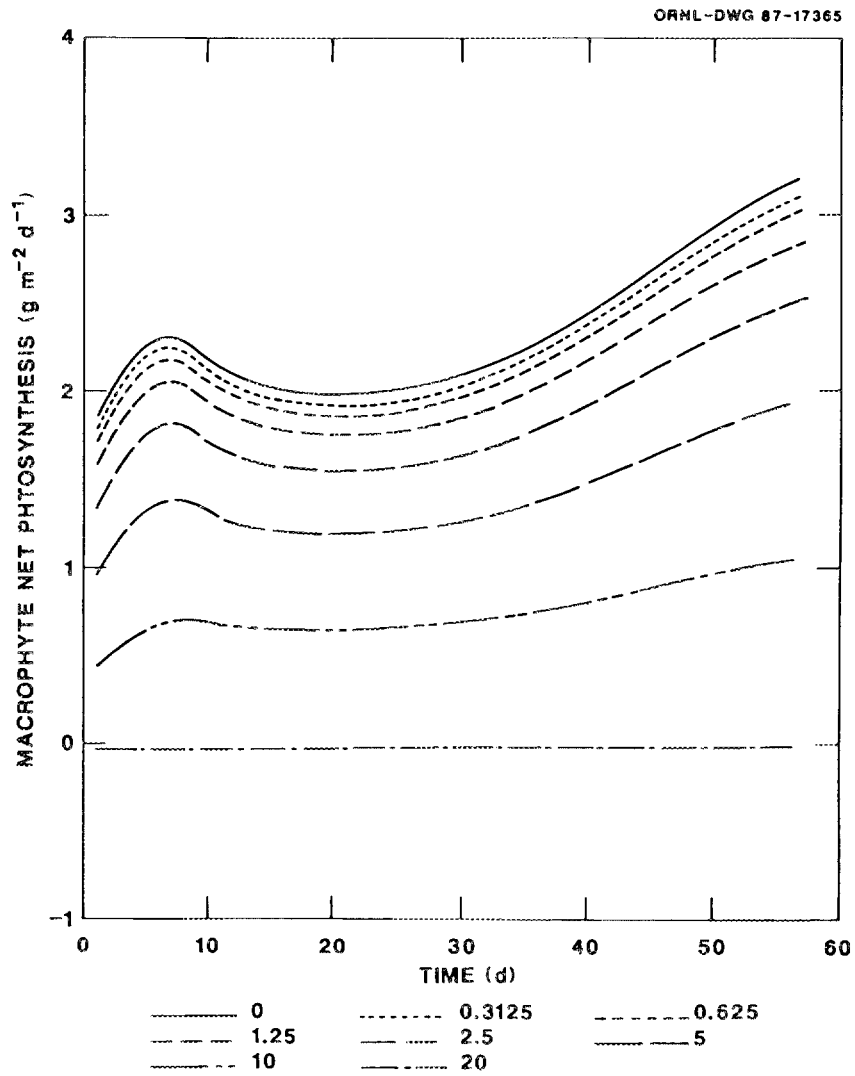


Figure 4.4 Dynamics of macrophyte net photosynthesis in deterministic simulations at various toxicant concentrations.

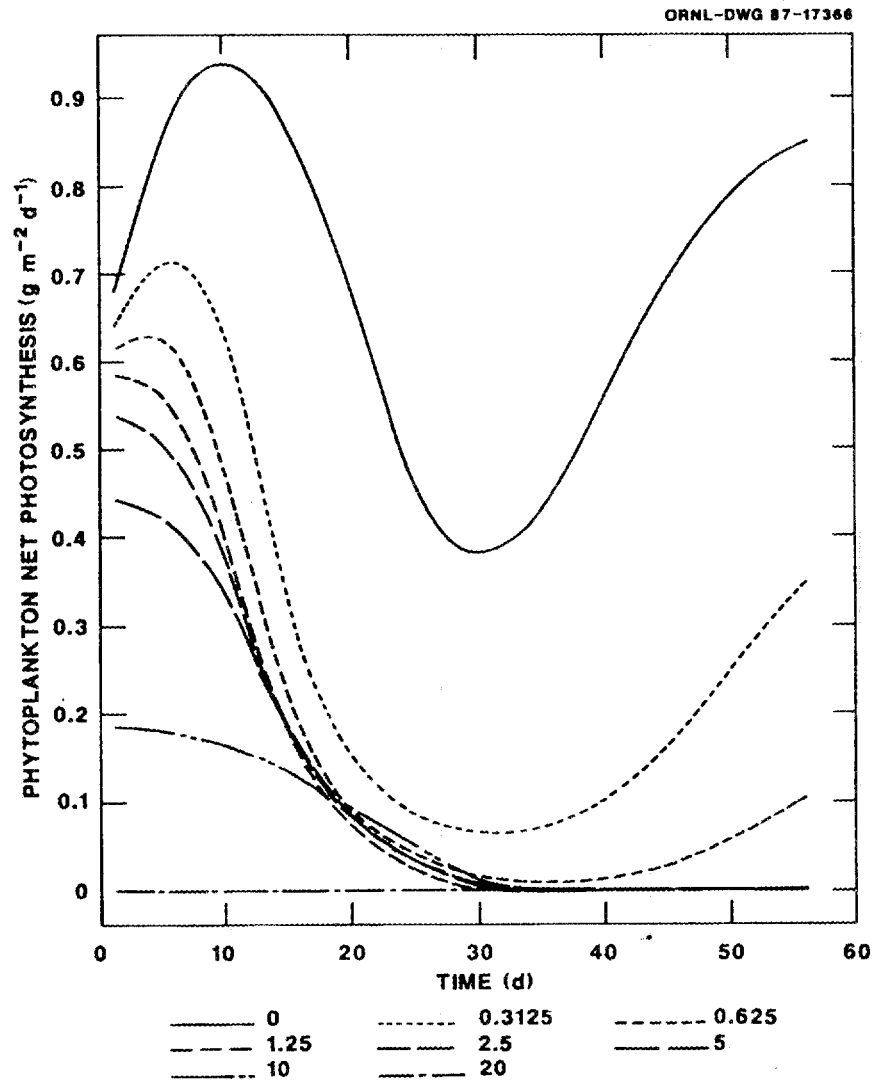


Figure 4.5 Dynamics of phytoplankton net photosynthesis in deterministic simulations at various toxicant concentrations.

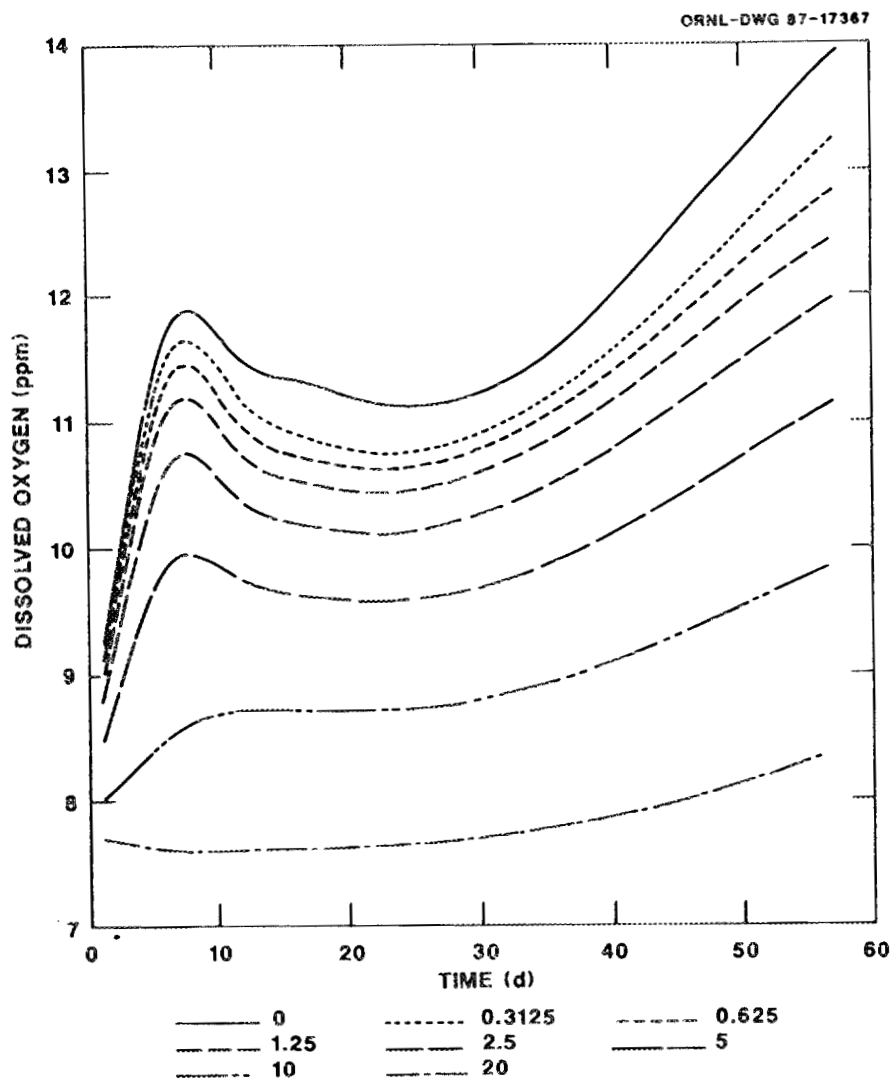


Figure 4.6 Dissolved oxygen dynamics in deterministic simulations at various toxicant concentrations.

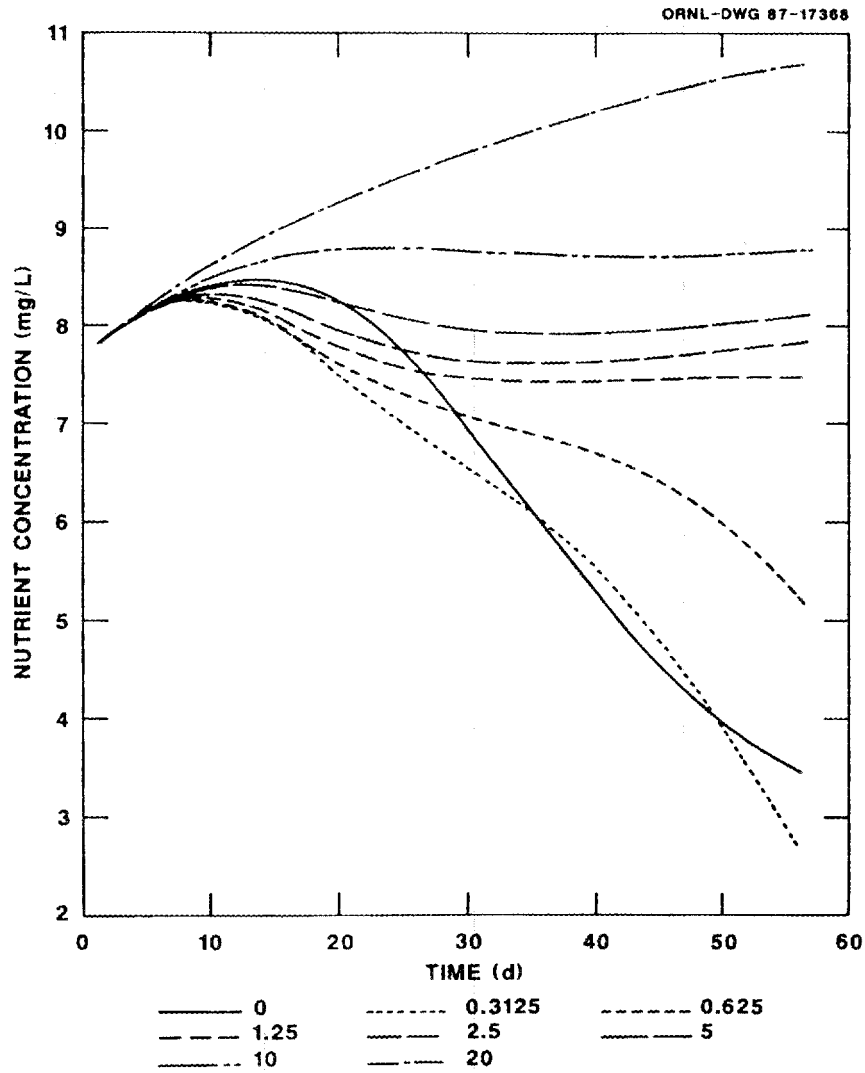


Figure 4.7 Nutrient dynamics in deterministic simulations at various toxicant concentrations.

larger phytoplankton bloom. In response to increased food availability, all zooplankton except for species 5 eventually attain a higher biomass than in the absence of toxicant (Fig. 4.1b). Similarly, fish biomass, although initially depressed, is eventually increased above control levels due to greater availability of prey.

The phenomenon of stimulatory effects arising from exposure to low toxicant concentrations is called hormesis. It has been repeatedly observed at the organismal level and may be a general feature of physiological response to inhibitors (Stebbing 1982). In attempting to provide a theoretical basis for understanding hormesis, Stebbing (1982) hypothesizes that hormetic effects can be explained as "a consequence of the adaptive behavior of rate sensitive control mechanisms". Stebbing's explanation of hormetic effects at the organismal level is based upon the properties of biosynthetic networks with feedback control. The same properties are apparent in ecological systems, so it seems appropriate to extend the concept of hormesis to include ecosystem-level phenomena. In these terms, it can be said that the model predicts a hormetic effect on plankton and fish populations in response to phenolics. This prediction is partially confirmed by the the pond, and more dramatically, by the aquarium microcosm studies, where increases in water column chlorophyll a were observed at low to moderate treatment levels. Also in the microcosms, there is a clear increase in cladoceran biomass concurrent with the increase in chlorophyll a. Copepod biomass and rotifer biomass did not show a clear increase, but these

groups contain many carnivorous or bacteriovorous species which are not represented by the model structure.

If the toxicant concentration is doubled to 0.625 mg/L, the phytoplankton bloom becomes even larger. Total zooplankton biomass is also increased, but now both species 4 and 5 show lower standing crops than in the controls. Fish biomass is also reduced below control levels (Fig. 4.1c). At 1.25 mg/L the phytoplankton bloom is longer in duration, total zooplankton biomass attains higher levels than in the control, but not as high as at 0.625 mg/L, and the production of fish biomass is very slight (Fig. 4.1d).

Another doubling of toxicant concentration to 2.5 mg/L causes the virtual elimination of both fish and zooplankton (Fig. 4.1e). As concentrations increase to 5 and to 10 mg/L, the magnitude of the phytoplankton bloom progressively decreases due to direct toxic effects (Fig. 4.1f and g). A minor shift in community composition is also observed, with phytoplankton species 8 becoming relatively more important until it is a codominant with species 9. Finally, at a concentration of 20 mg/L, all phytoplankton species are negatively affected by the toxicant, and phytoplankton biomass remains essentially constant except for a small increase in species 5 occurring near the end of the simulation (Fig. 4.1h).

Macrophyte biomass is relatively unaffected at phenol concentrations up to 10 mg/L. However, a concentration of 20 mg/L is directly toxic to Elodea, and the predicted biomass of the macrophyte bed decreases exponentially with time (Fig. 4.2). Similarly, the

dynamics of the detritus pool is relatively unperturbed except at the highest toxicant concentration, where a large influx of dying macrophytes occurs (Fig. 4.3). Macrophytes were observed to be relatively resistant in the pond and aquarium systems, although not quite as resistant as predicted by the model. A substantial reduction in growth was observed at a toxicant concentration of approximately 1 mg/L, and at 10 mg/L the macrophyte bed was nearly destroyed.

The model predicts a decline in net photosynthesis with increasing toxicant exposure for both phytoplankton and macrophytes (Fig. 4.4 and 4.5). In the experimental ponds, phytoplankton photosynthesis, as measured by  $^{14}\text{C}$ -incorporation, tended to be lower in levels P3 through P5 (where average phenol concentration ranged from 0.5 to 8 mg/L) immediately following the oiling period, while ponds exposed to lower doses of synthetic oil had elevated photosynthesis corresponding to a phytoplankton bloom. However, due to the very high variability in the photosynthesis data, these differences were not found to be statistically significant using Dunnett's two-sided test ( $\alpha = 0.05$ ). Total ecosystem net production, as computed from diurnal changes in dissolved oxygen, was significantly reduced in the highest exposure (P5) ponds.

Dissolved oxygen concentrations predicted by the model decline with increasing toxicant exposure, falling to approximately 7.6 ppm (near saturation) at the highest dose (Fig. 4.6). In the experimental systems, effects on dissolved oxygen were in the same

direction, but of greater magnitude. The high dose microcosms became essentially anaerobic for the last 5 weeks of the oiling period, and in the outdoor ponds, dissolved oxygen dropped to below 2.0 ppm. There are several possible explanations for this discrepancy. One factor may be that microbial respiration is inadequately accounted for within the model. Currently, the model includes a microbial respiration term proportional to the pools of detrital material, but no account is taken of respiration associated with biodegradation of the phenols themselves or of catabolism of dissolved organic substances which may be secreted by the macrophytes under conditions of sublethal stress.

Additionally, oxygen exchange with the atmosphere may not be accurately predicted by the model. The rate of oxygen exchange between the aqueous and gaseous phases depends upon the extent of mixing. The model currently assumes an effective mixing depth of 1.0 m, the depth of the entire water column. However, the available dissolved oxygen profile data suggests that although the ponds were usually well mixed in the mornings, they could become stratified later in the day. Unfortunately, such profile data were obtained too sporadically to provide a clear picture of the diurnal changes in mixing regime. If, somewhat arbitrarily, a time-weighted effective mixing depth of 0.5 m is assumed, the model predicts dissolved oxygen concentrations ranging from 6.1 to 9.8 ppm in the controls, and from 4.3 to 3.8 ppm at the highest toxicant dose.

The general trend in simulated nutrient dynamics is toward increased dissolved nutrient concentrations in response to toxicant exposure (Fig 4.7). This trend is supported by measurements of increased water column ammonium concentrations in the highest dose ponds and microcosms.

## 4.2 RESULTS OF STOCHASTIC SIMULATIONS

### 4.2.1 Natural Variability

Natural variability encompasses various factors that preclude the possibility of attaining exactly uniform behavior in complex experimental systems. Individual ponds or microcosms differ in their ecological dynamics due to dissimilarities in composition and differences in environmental influences. Differences in composition were simulated by selecting random initial conditions for replicate model runs. Variability in environmental driving variables was introduced by using stochastic functions for ambient light and temperature. The effects of including these these sources of natural variability on the behavior of the model, both separately and in concert, are discussed below.

#### 4.2.1.1 Random initial conditions

Initial values of state variables were chosen from a multivariate normal distribution with centroid equal to the deterministic initial state and a coefficient of variation of 10% in

each dimension (as described in section 2.3.3). The resulting dynamics are illustrated for six representative state variables in Fig. 4.8.

#### 4.2.1.2 Stochastic forcing functions

Light and temperature forcing functions were modeled as one dimensional random walks superimposed on a deterministic, sinusoidal trend (see section 2.3.3). Typical realizations of this stochastic process are illustrated in Fig. 2.3. It should be noted that the variability among Monte Carlo replicates in temperature and light conditions increased with time during over the simulation period. The resulting variability in the dynamic behavior of six state variables is illustrated in Fig. 4.9.

#### 4.2.2 Measurement Error

Measurement errors were added to the simulation results as independent normal deviates as described in section 2.3.3. Examples of simulation output from ten typical runs with measurement error as the sole source of variability are shown in Fig. 4.10.

#### 4.2.3 Combined Sources of Variation

The effects of random initial conditions, stochastic forcing functions, and superimposed measurement error on the output of the model have been illustrated. In most, if not all, experimental

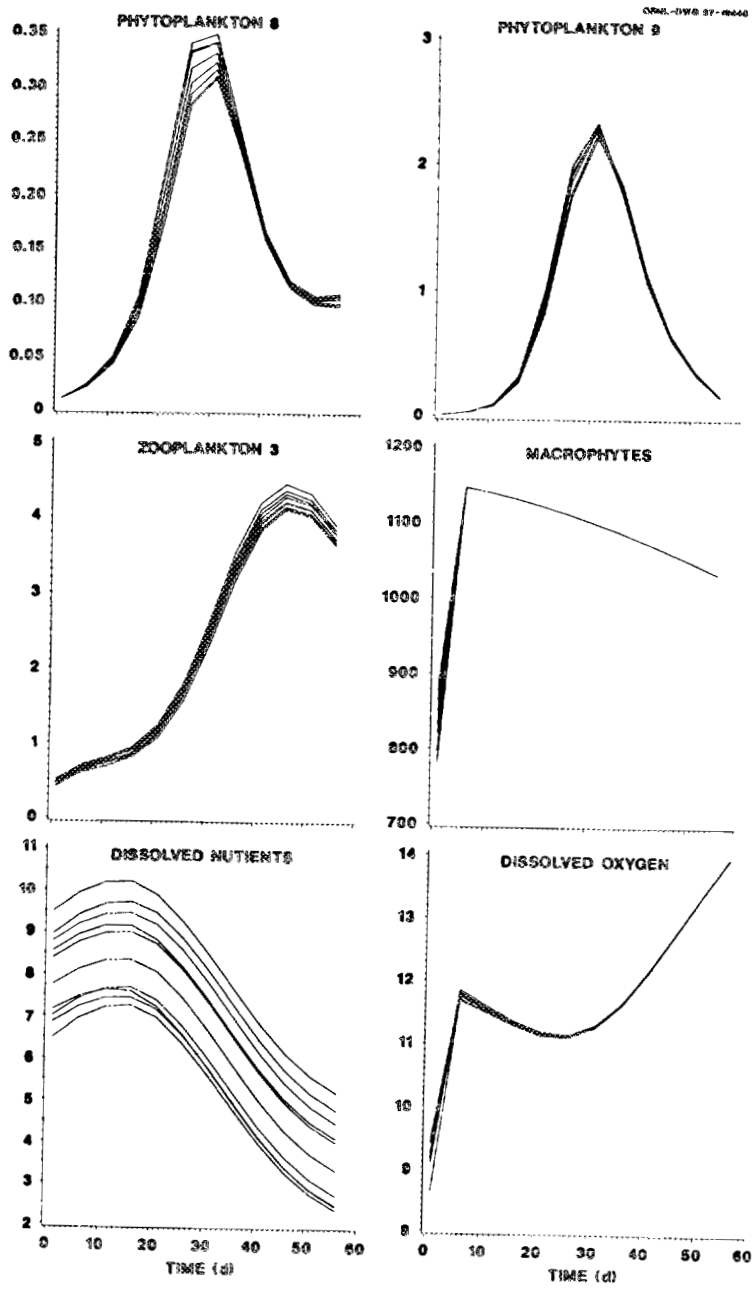


Figure 4.8 Dynamics of representative state variables in Monte Carlo simulations with random initial conditions.

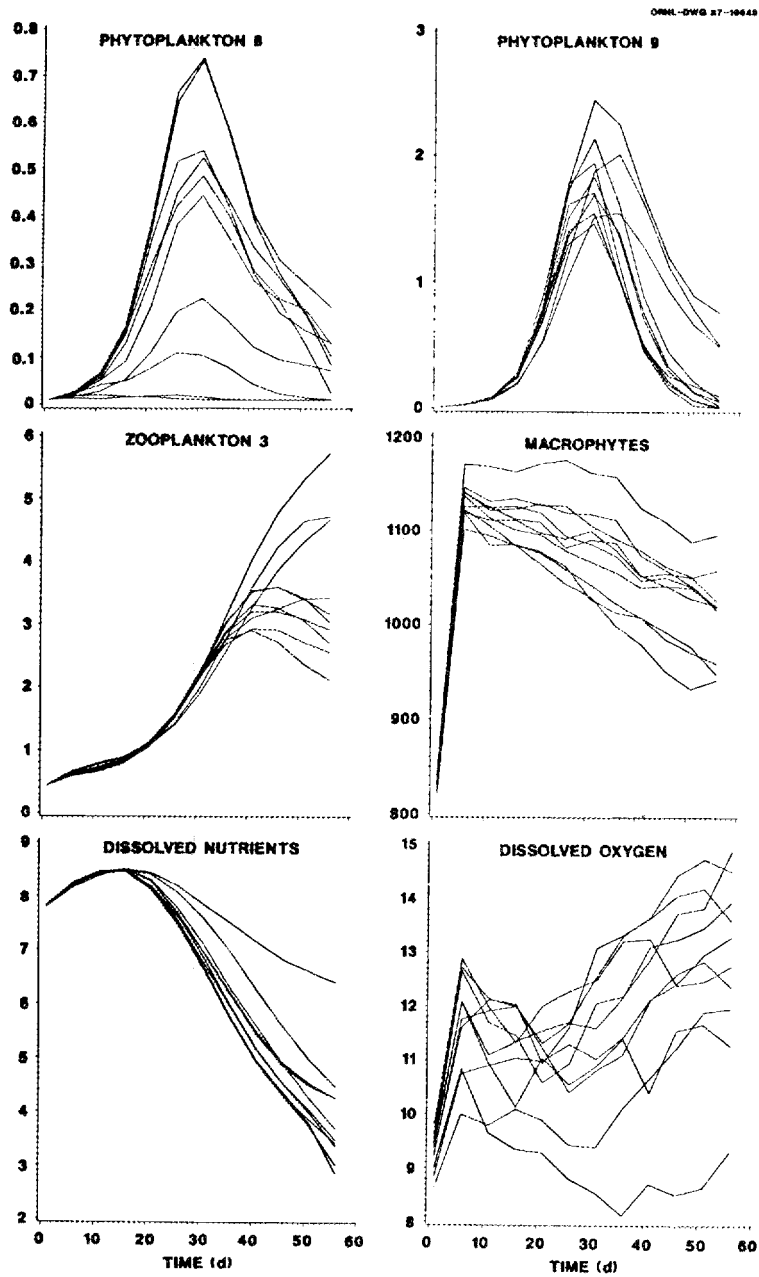


Figure 4.9 Dynamics of representative state variables in Monte Carlo simulations with stochastic forcing functions.

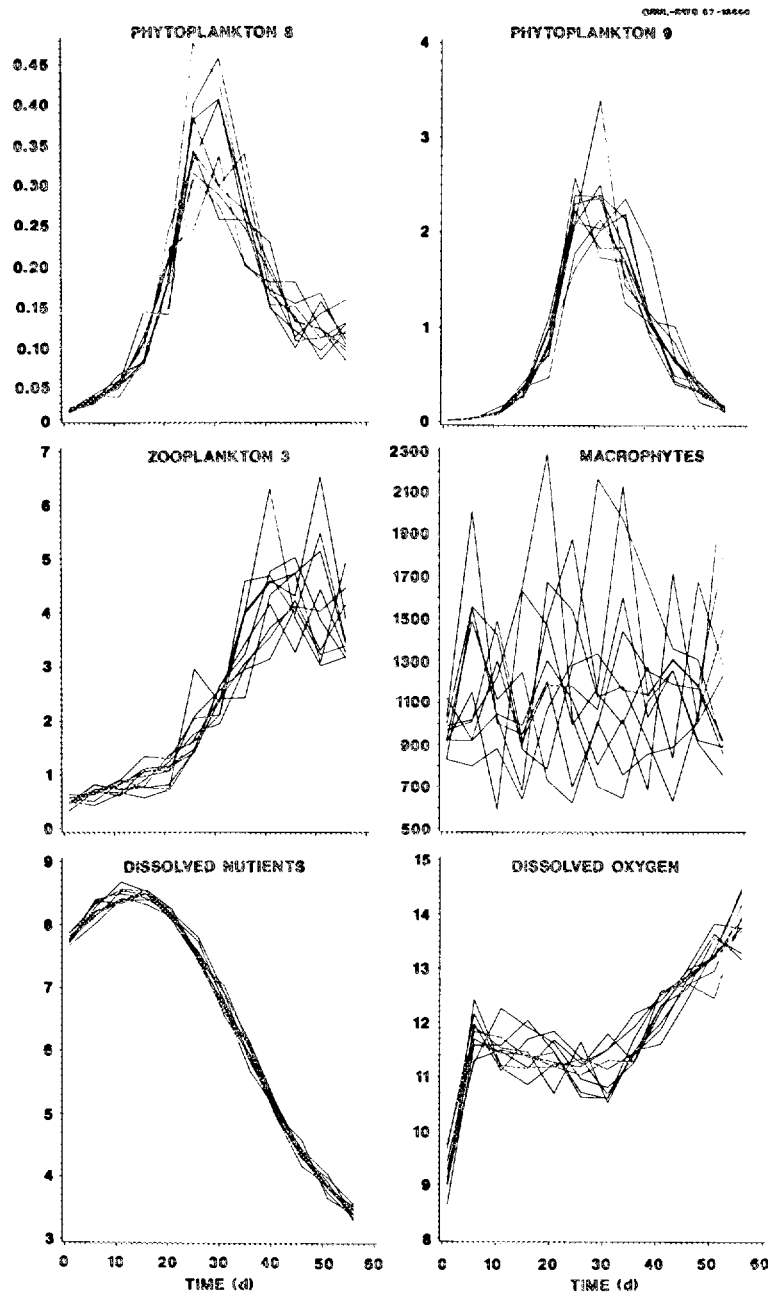


Figure 4.10 Dynamics of representative state variables in Monte Carlo simulations with measurement error.

situations, all of these sources of variation must be taken into account. The simulation results shown in Fig. 4.11 were obtained by simultaneously including all these sources of variation.

### 4.3 STATE SPACE ANALYSIS

#### 4.3.1 Summary of State Space Dose-Response Relationships

Simulation results were summarized by a state vector in a space defined by the following dimensions: log-transformed biomasses of each of the biotic components of the model, log-transformed masses of labile and refractory detritus, dissolved oxygen, nutrient concentration, and net photosynthesis rates for phytoplankton and macrophytes. The results is a 23-dimensional state vector. State space displacements were computed every five days, beginning on day 1, resulting in twelve comparisons during the 56 day simulation period. The stochastic simulations were run to provide 200 replicates at each of the treatment levels. For each treatment level on each sampling day, 4000 different pairwise comparisons between control and perturbed state vectors are possible. The state space analysis presented here is based on comparisons from 100 randomly matched pairs of trajectories.

##### 4.3.1.1 Calculations based on natural variability

Figure 4.12 shows the response surface for state space separation calculated as a function of time and dose from 100

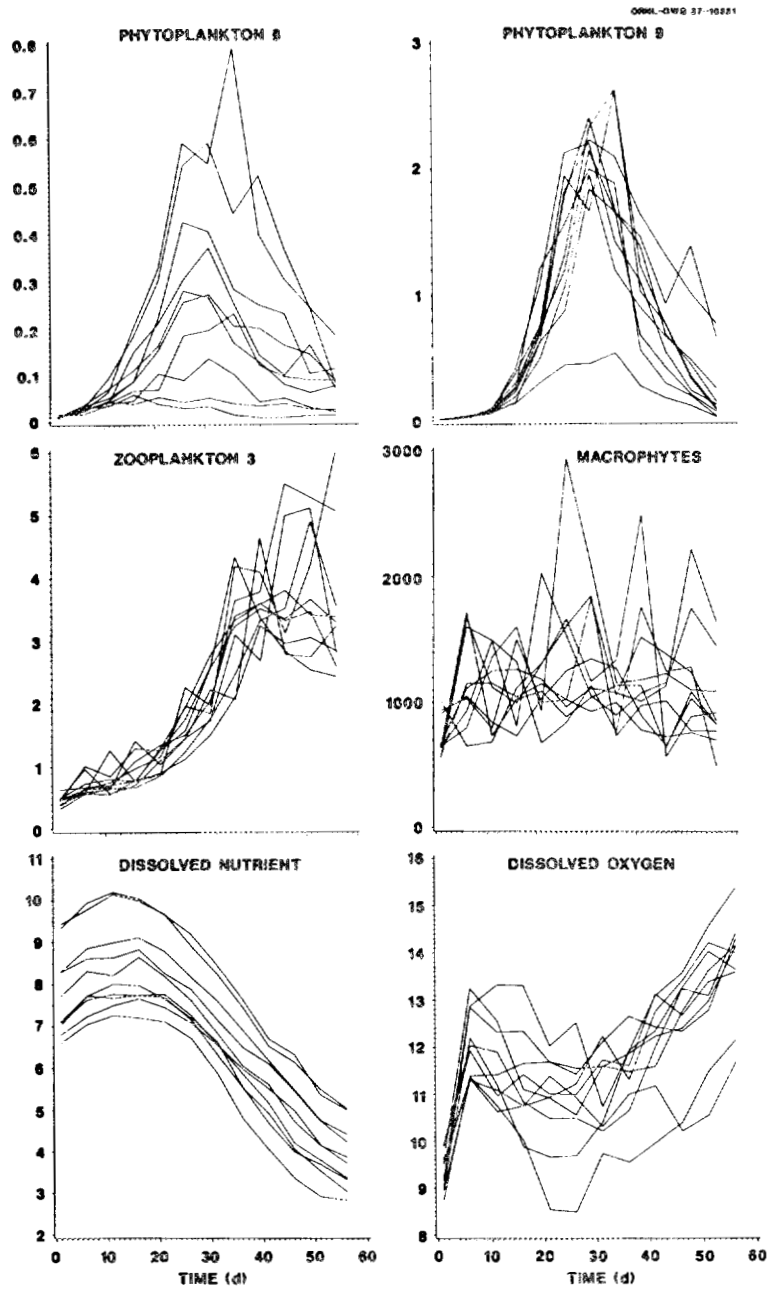


Figure 4.11 Dynamics of representative state variables in Monte Carlo simulations with combined sources of variability.

ORNL-DWG 87-9707

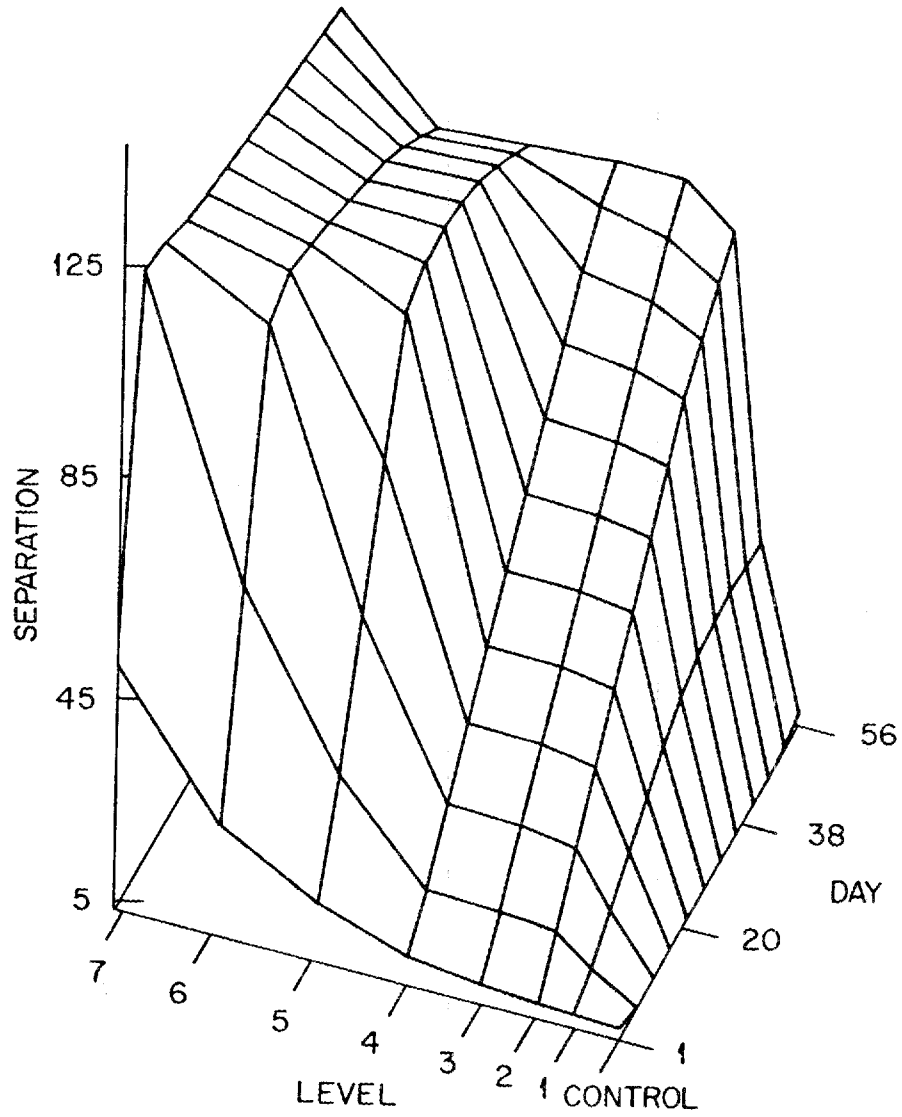


Figure 4.12 State space separation as a function of time and treatment level for ecosystem simulation model with natural variability alone.

stochastic simulations with natural variability incorporated but without measurement error. The resulting surface displays a monotonic increase in separation with increasing dose or length of exposure. The increase is not always smooth, however. There appears to be a sharp jump in response between the treatment concentrations of 2.5 and 5.0 mg/L, especially during the middle of the simulation period.

Dose-response curves based on the three state space summary measures defined in section 2.4.3 are shown in Fig. 4.13. Maximum separation increases rapidly at the two lowest treatment levels, and steadily but more slowly thereafter. Both mean separation and mean displacement magnitude increase rapidly at first, then exhibit a plateau followed by the sharp jump at 5.0 mg/L, and further steady increase. The closeness of the numerical values for these two quantities implies a relatively constant directional orientation for the displacement vector over the simulation period.

#### 4.3.1.2 Calculations based on measurement error

The surface in Fig. 4.14 shows the response as a function of time and toxicant concentration in simulations where measurement error is the sole source of variability. State space separation generally increases with increasing dose or length of exposure, but with the peak response actually occurring under intermediate conditions. More dramatic than the changes in the pattern of response, however, is the change in numerical scaling of the

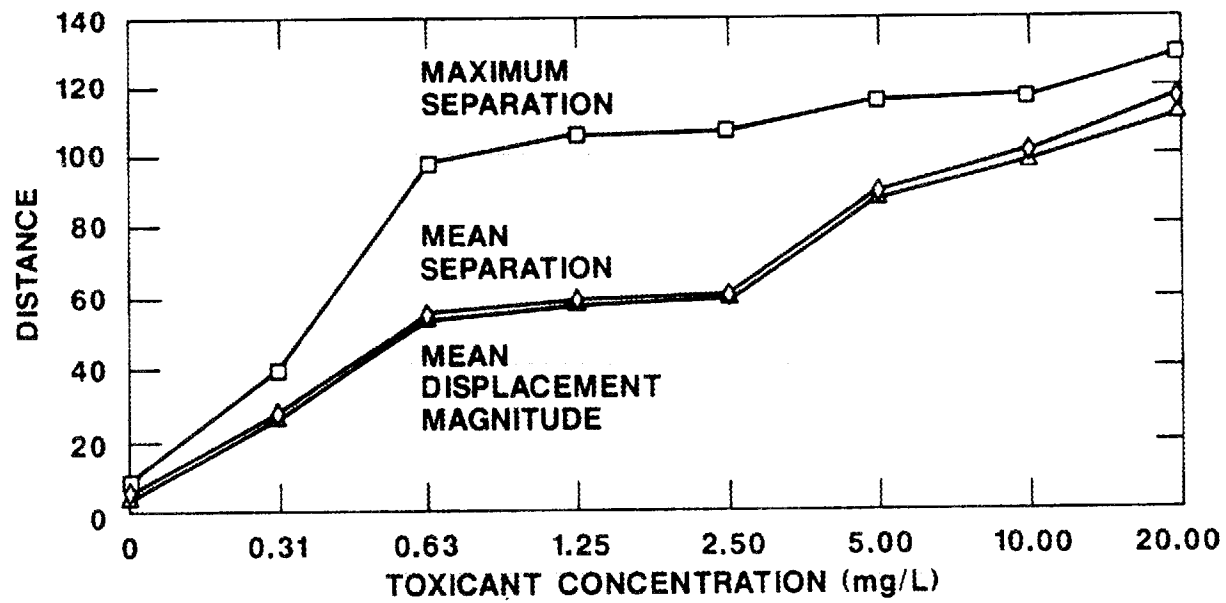


Figure 4.13 Dose-response curves for ecosystem simulation model with natural variability alone. Squares represent maximum separation, diamonds mean separation, triangles mean displacement magnitude.

ORNL-DWG 87-9706

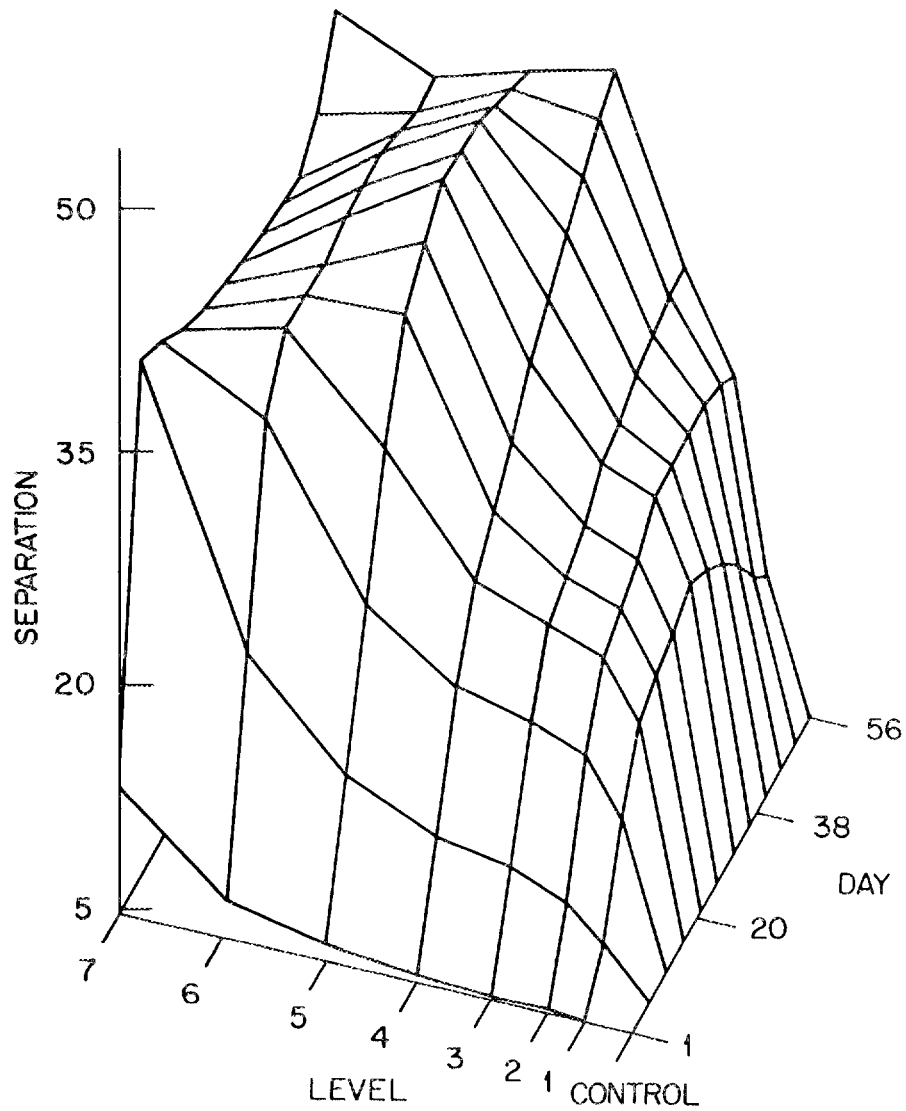


Figure 4.14 State space separation as a function of time and treatment level for ecosystem simulation model with measurement error alone.

separation values as compared to Fig. 4.12. As will be argued in subsequent sections, this is a typical consequence of the use of a Mahalanobis distance metric. Mahalanobis distances can be relatively sensitive to changes in the covariance matrix used in the calculations. Since, in this case, the measurement errors were uncorrelated, whereas the simulations under natural variability had a correlation structure imposed by the system dynamics, the distances calculated for these two scenarios cannot be directly compared. They are, in effect, measured in different units.

The dose-response curves for the three summary indices are shown in Fig. 4.15. Again, the close similarity of the mean separation and the mean displacement magnitude curves suggests a nearly unidirectional displacement over time.

#### 4.3.1.3 Calculations based on combined sources of variation.

The response surface of state space separations calculated from simulations which included both natural variability and measurement error is shown in Fig. 4.16. Again, the numerical scaling of the vertical axis reflects the different covariance matrix used in calculating the Mahalanobis distances. The general pattern of response, as reflected in the qualitative features of the surface, appears intermediate between that observed in Figs. 4.12 and 4.14. The same is true for the dose-response curves, shown in Fig. 4.17.

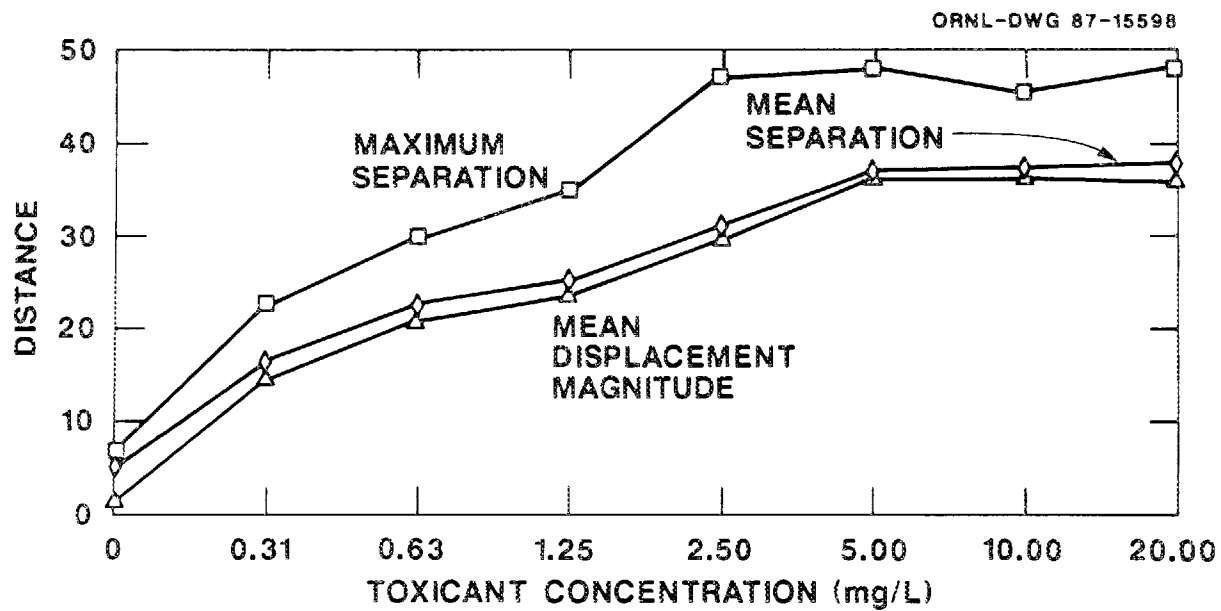


Figure 4.15 Dose-response curves for ecosystem simulation model with measurement error alone. Squares represent maximum separation, diamonds mean separation, triangles mean displacement magnitude.

ORNL-DWG 87-9708

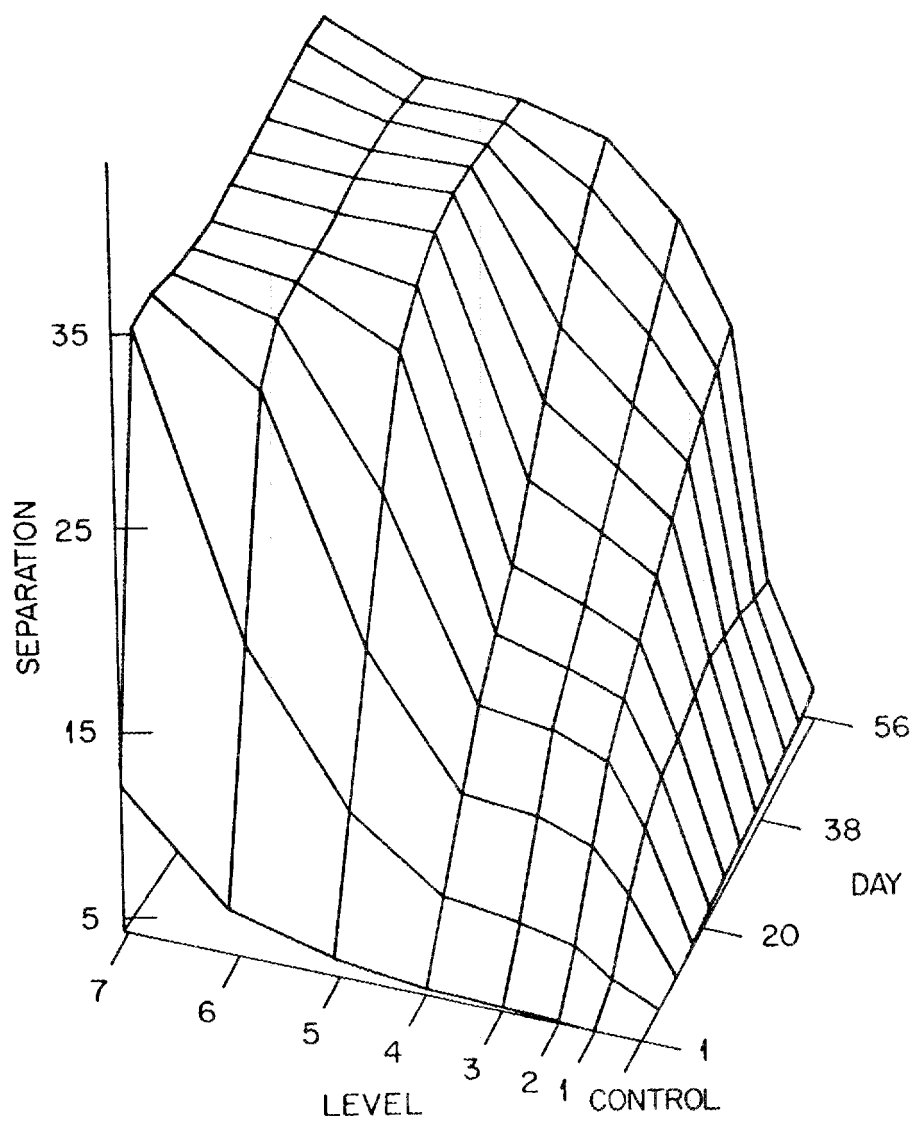


Figure 4.16 State space separation as a function of time and treatment level for ecosystem simulation model with combined sources of variability.

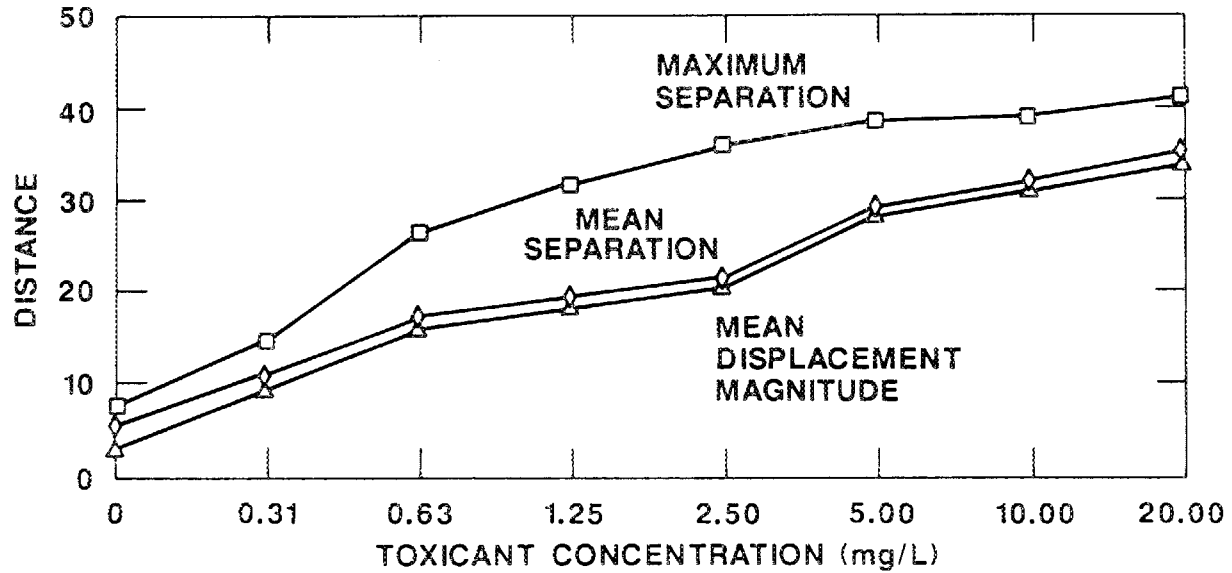


Figure 4.17 Dose-response curves for ecosystem simulation model with combined sources of variability. Squares represent maximum separation, diamonds mean separation, triangles mean displacement magnitude.

#### 4.3.2 Statistical Power and Sample Size Requirements

The simulation results presented thus far have been based upon sample sizes of 100 Monte Carlo replicates at each treatment level. In experimental situations such large sample sizes are seldom attainable. The experimental studies described in the preceding chapter included only two or three replicates at each level of toxicant exposure, and this degree of replication is representative of ecotoxicological studies. It is important, therefore, to investigate the effect of sample size on the results derived from a state space displacement analysis. Specifically, two questions need to be addressed: (1) How does the statistical accuracy of the method vary with sample size; and (2) Is the method powerful enough to detect ecologically significant effects on the basis of reasonable sample sizes?

To investigate the effects of sample size on statistical accuracy, attention was directed toward the estimation of mean separation. The sampling distribution for the mean separation estimator was approximated, for each sample size, by repeatedly resampling from a universe of 200 trajectories produced by the Monte Carlo runs at a given treatment level. In other words, for each treatment level and each sample size  $N$ , a sample of  $N$  trajectories was drawn from the 200 trajectories previously generated by the model, and the mean separation was estimated on the basis of that sample. Then a new sample of  $N$  trajectories was drawn, again from the entire set of 200 possible trajectories, and a new calculation of

the mean separation was made. This process continued until 20 samples of size  $N$  had been drawn at each treatment level for values of  $N = 1, 2, 4, 8, 16, 32,$  and  $64$ .

The results of this resampling exercise are shown in Fig. 4.18. The sampling error clearly decreases monotonically with increasing sample size. Yet, even for small sample sizes, the sampling error is not large enough to obscure the basic dose-response pattern observed from large sample calculations. This is shown in Fig. 4.19, where the range between the 5th and 95th percentiles of the sampling distribution for a sample size of one is plotted as a function of toxicant concentration. Another convenient descriptor of the statistical accuracy of an estimator is its standard error, which is the standard deviation of the sampling distribution. Estimated standard errors for mean separation, as a function of exposure concentration and of sample size, are given in Table 4.1. A decrease in the standard error with sample size is observed at all toxicant concentrations. Changes in standard error as a function of concentration for a fixed sample size are not as consistent, but often the largest standard errors occur at intermediate toxicant exposures. This suggests that the model dynamics are more tightly constrained at very high or very low toxicant concentrations, and that the greatest potential for dynamic variability exists at intermediate levels of toxicant stress.

On the basis of the information on the statistical accuracy of the mean separation estimator, it is possible to assess the ability

Table 4.1. Standard error of the mean separation as calculated from the empirical sampling distribution.

---

Concentration (mg/L)	Sample Size						
	<u>1</u>	<u>2</u>	<u>4</u>	<u>8</u>	<u>16</u>	<u>32</u>	<u>64</u>
0.0	0.59	0.49	0.27	0.16	0.12	0.06	0.04
0.3125	0.64	0.44	0.34	0.24	0.15	0.10	0.06
0.625	0.66	0.50	0.34	0.15	0.13	0.09	0.05
1.25	1.40	0.68	0.48	0.36	0.29	0.15	0.11
2.5	1.49	0.91	0.58	0.54	0.41	0.26	0.11
5.0	0.80	0.71	0.40	0.43	0.30	0.13	0.06
10.0	1.11	0.94	0.43	0.27	0.19	0.12	0.06
20.0	1.16	0.97	0.74	0.46	0.30	0.17	0.08

---

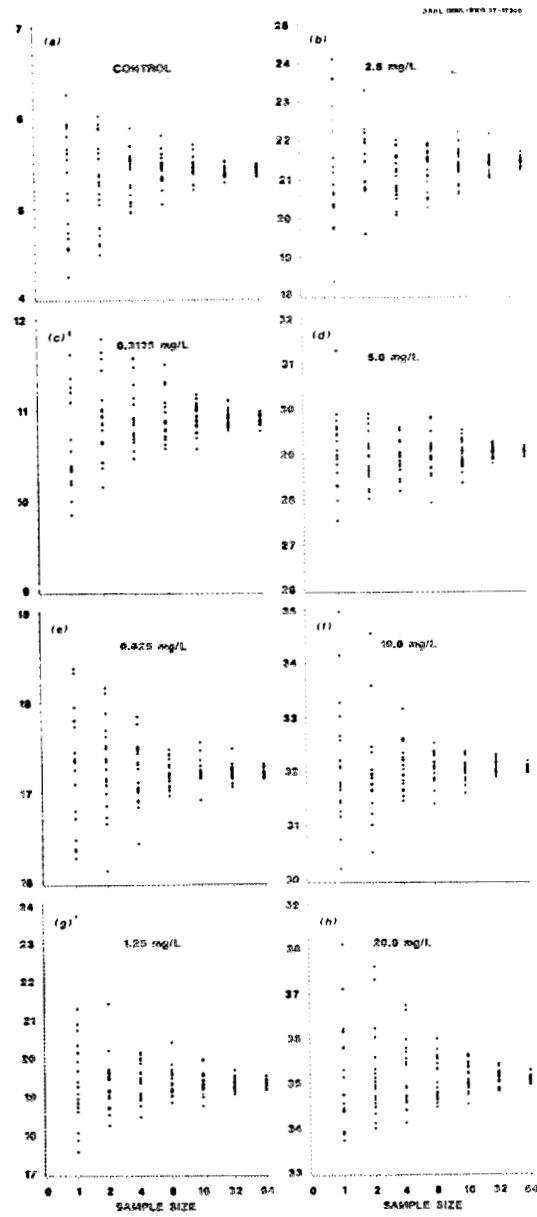


Figure 4.18 Mean separation for 20 independent samples of size N (N=1,2,4,8,16,32,64) at various toxicant concentrations.

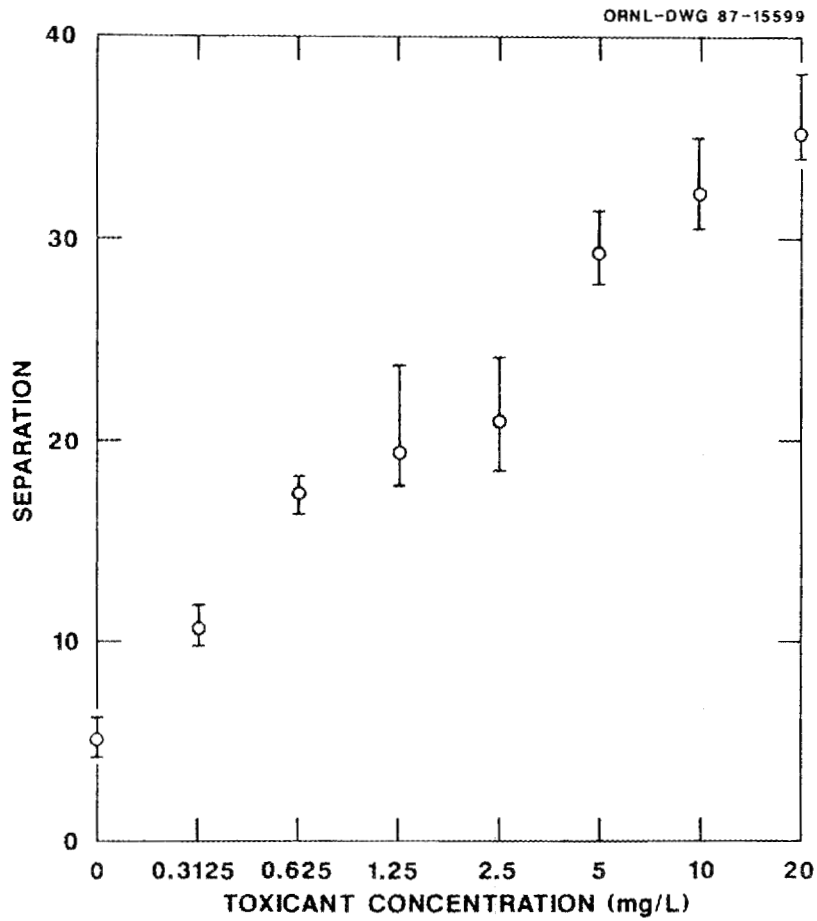


Figure 4.19 Mean separation as a function of toxicant concentration for a sample size of  $N=1$ . Circles represent estimated median of the sampling distribution. Bars represent an estimated 90% confidence interval.

of the method to detect ecologically significant perturbations from small samples. This is best described in terms of statistical hypothesis testing. Take as a null hypothesis ( $H_0$ ) that there is no effect. This implies that  $\mu_c = \mu_p$ , or equivalently, that  $d_M(\mu_c, \mu_p) = 0$ . This can be contrasted to the one-sided alternative hypothesis ( $H_1$ ) that  $d_M(\mu_c, \mu_p) > 0$ . The mean separation will be used as an estimator of the Mahalanobis distance between population centroids. The null hypothesis will be rejected if and only if the the mean separation calculated for the "perturbed" trajectories is significantly greater than for the control trajectories. Statistical significance can be established on the basis of what is known about the sampling distribution of the estimator. Examination of the empirical sampling distributions showed that they tended to be at least approximately normal. In particular, all four of the empirical sampling distributions for  $N = 1, 2$  and toxicant concentrations of 0.0 and 0.3125 mg/L could not be distinguished from normality using a Shapiro-Wilk test with  $\alpha = 0.05$  (Shapiro and Wilk 1965). Therefore, for low toxicant exposures ( $\leq 0.3125$  mg/L), it was assumed that the sampling distribution was normal, with a variance equal to the pooled variance of the control and 0.3125 mg/L distributions.

Given these assumptions, the power of the statistical test can be derived. Statistical power is defined as the probability that an effect, in this case a difference between population centroids, will be detected when such an effect truly exists. The power of a test

depends upon three factors: (1) the actual magnitude of the effect, (2) the significance level of the test, and (3) sample size. The significance level, denoted by  $\alpha$ , is the probability of rejecting the null hypothesis when in fact the null hypothesis is true. Such an incorrect inference is referred to as a type I error. In contrast, a type II error is the acceptance of a null hypothesis which is false, and the probability of a type II error is represented as  $\beta$ . It follows from the above definitions that the statistical power of a test is  $1-\beta$ .

Fig. 4.20 shows plots of the probability of accepting the null hypothesis as a function of the true separation between population centroids in Mahalanobis distance units. Such plots are traditionally referred to as operating characteristic curves (see, for example, Hines and Montgomery 1980, p.270ff). Operating characteristic curves can be thought of as inverted plots of statistical power. Two graphs are shown, one for a sample size of 1, and one for a sample size of 2. Each graph contains several curves, corresponding to different significance levels ( $\alpha = 0.10, 0.05, 0.01, 0.005, 0.001$ ). It can be seen that even with a sample size of 1 and a significance level of 0.001, a true separation of 5 Mahalanobis distance units is almost certain to be detected. This is approximately the magnitude of effect observed at the lowest toxicant concentration used in the simulation. These operating characteristic curves illustrate the power of the state space analysis to detect changes in trajectories under realistic conditions of natural

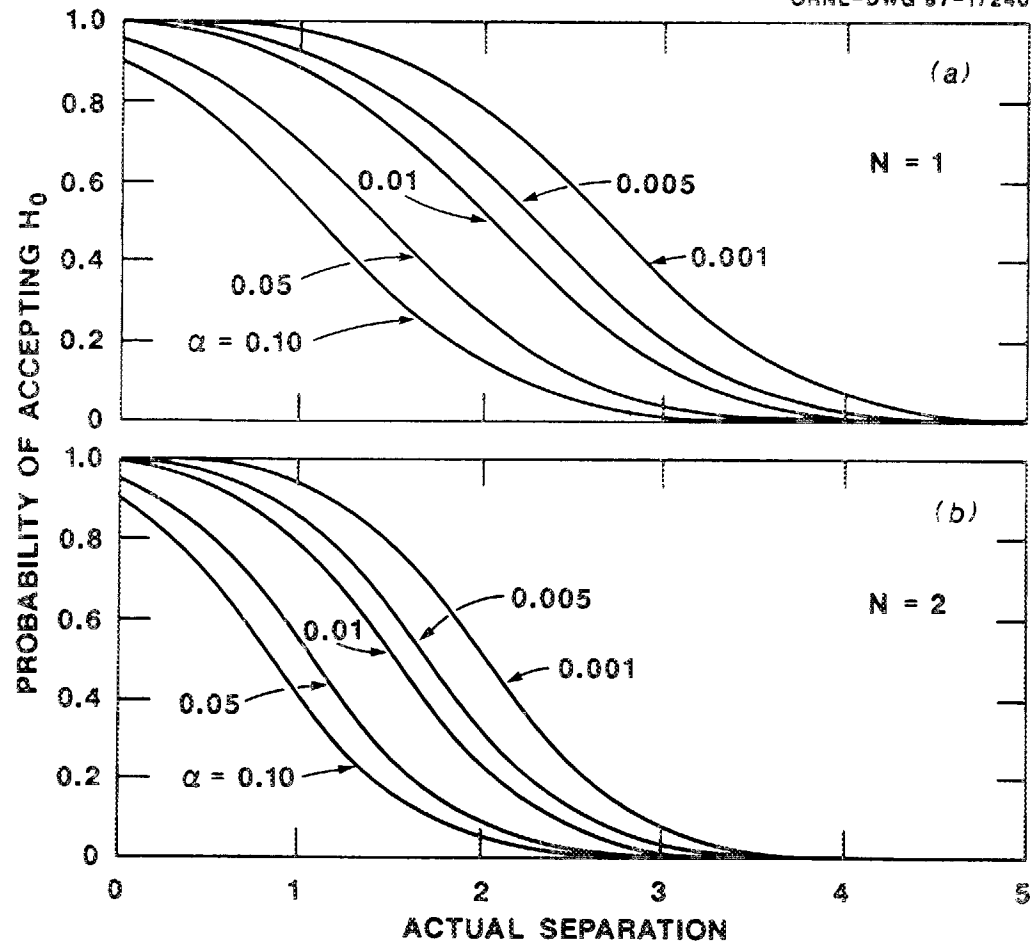


Figure 4.20 Operating characteristic curves for mean separation for samples of size  $N=1$  and  $N=2$ .

variability, measurement error, and small sample sizes. It would appear, on the basis of this analysis, that the state space methodology developed in this study is quite sensitive, and that, if properly applied, ecologically significant effects should rarely go undetected.

#### 4.4 CHANGES IN COVARIANCE STRUCTURE

##### 4.4.1 Changes in Covariance Structure with Time

Since initial values for the state variables were chosen independently by latin hypercube sampling, the initial correlations between state variables were negligible. This rapidly changed, however. Within five days, the model dynamics had imposed a definite correlation structure upon the simulation results. This is clearly observable in Fig. 4.21, which summarizes the results of a principal components analysis of the control trajectories. The increasing degree of state variable intercorrelation is demonstrated by the monotonic increase in the variance explained by the first principal component (Fig 4.21a). The rotation angle of the first principal component relative to its orientation on day 1 was calculated as  $\cos^{-1}(e_1'e_d)$ , where  $e_1$  and  $e_d$  are standardized eigenvectors oriented in the directions of the first principal component on day 1 and day d, respectively. These rotation angles are shown in Fig. 2.41b. Inspection of the rotation angles confirms that there is a rapid convergence toward a relatively constant

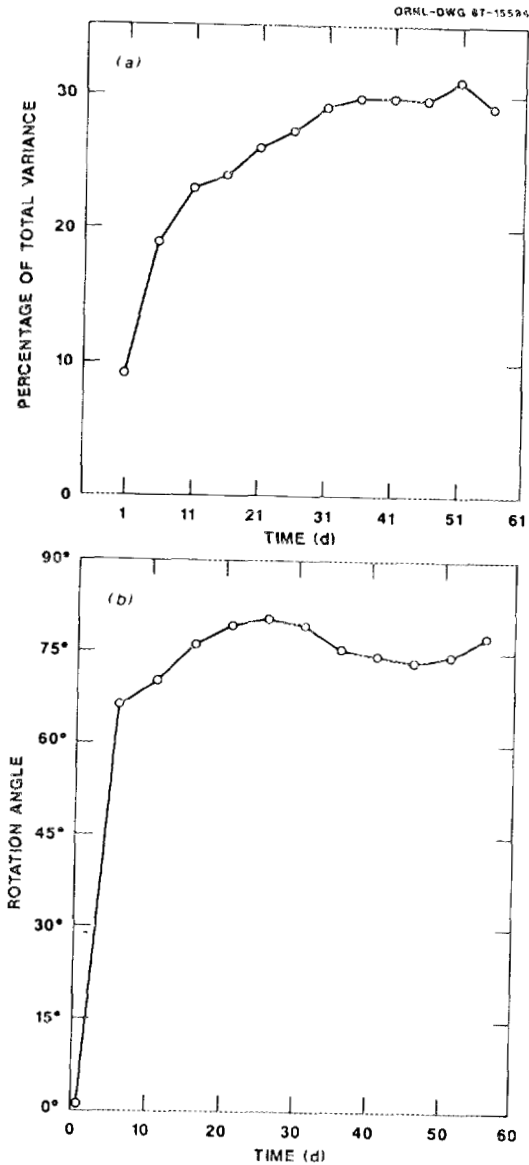


Figure 4.21 Changes in covariance structure of state variables over time in the simulation model. (a) Percentage of total variance explained by the first principal component. (b) Rotation of first principal component relative to controls.

orientation (after day 11 all rotation angles are within 20° of each other). Subsequent evolution of the correlation structure may be taking place, but at a slower rate than in the initial transient phase.

The nature of the correlation structure that arises from the dynamics of the model is best characterized by inspection of some of the individual correlations between state variables. Specifically, the two strongest correlations present in later part of the simulation period are the negative correlation between phytoplankton species 7 and 9, and the positive correlation between dissolved oxygen and the net photosynthetic rate of the macrophytes. The strength of these two correlations as a function of time is shown in Fig. 4.22. A number of other variables consistently exhibited moderate to strong correlations ( $|r| > 0.6$ ). For example, zooplankton species 3 became negatively correlated with phytoplankton species 7 and positively correlated with phytoplankton species 9.

#### 4.4.2 Toxicant-Induced Changes in Covariance Structure

The alterations in model dynamics resulting from toxicant exposure were reflected in altered correlations between state variables. Again, this is conveniently summarized in terms of the behavior of the first principal component, as illustrated in Fig. 4.23 for an analysis of the simulation results pooled over the entire 56-day exposure period. The overall strength of correlations increases at low to moderate toxicant exposures, but declines

ORNL-DWG 87-17239

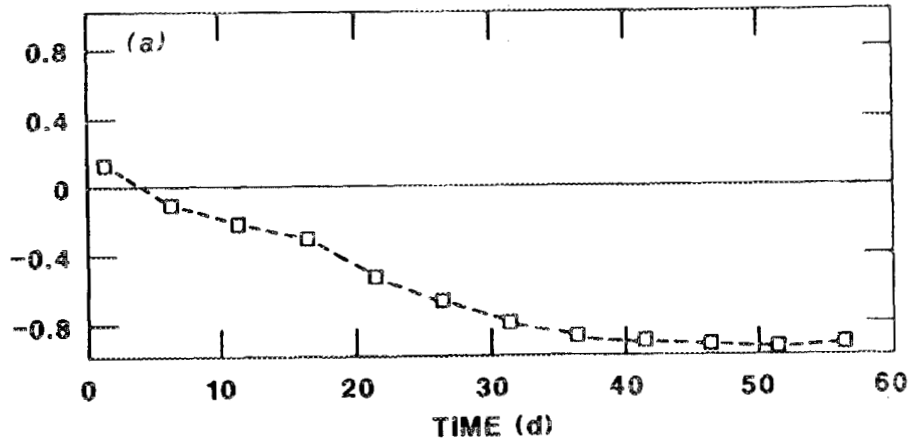
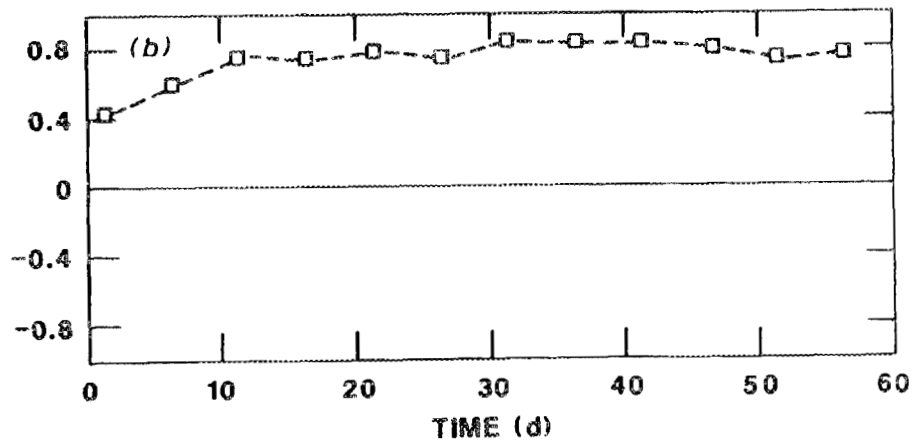
**PHYTOPLANKTON 7 - PHYTOPLANKTON 9****DISSOLVED OXYGEN - MACROPHYTE  
NET PHOTOSYNTHESIS**

Figure 4.22 Changes in selected state variable correlations over time in the simulation model.

dramatically at the highest concentration (Fig. 4.23a). The orientation of the first principal component changes progressively for toxicant exposures up to 1.25 mg/L, then remains relatively constant for exposures ranging from 2.5 to 10 mg/L, and shifts once again at the highest dose of 20 mg/L (Fig. 4.23b). A progressive change in the nature of the correlations is also evident, as illustrated by the change in orientation of the first principal component.

A more detailed inspection of the correlations between state variables reveals some interesting patterns. When the data are pooled over time, the strongest correlations evident in the control simulations are those between the consumer biomasses. As a matter of fact, given five zooplankton species and one fish species, there are 15 nonidentical consumer correlations, and these turn out to be the 15 strongest correlations in the entire correlation matrix, all having positive values exceeding 0.90.

The introduction of the toxicant causes changes in this pattern. At an exposure concentration of 0.625 mg/L, zooplankton species 5 becomes strongly negatively, rather than positively, correlated with the other consumer populations. This is a result of the negative impact of the toxicant on the success of zooplankton species 5, which is the most sensitive of the consumers to direct effects of the toxicant. At a concentration of 1.25 mg/L, the correlations among consumer biomasses are similar, and strong positive correlations among phytoplankton species 7 through 10 become

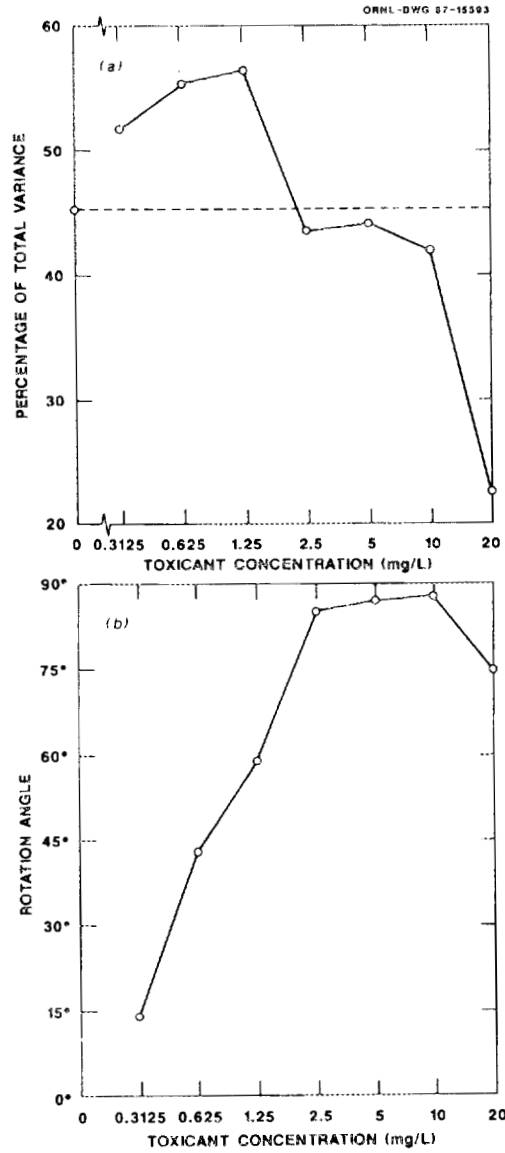


Figure 4.23 Changes in covariance structure of state variables as a function of treatment level in the simulation model. (a) Percentage of total variance explained by the first principal component. (b) Rotation of first principal component relative to controls.

apparent. These phytoplankters also generally exhibit strong negative correlations with phytoplankton net photosynthetic rate. Similar correlations are observable at concentrations of 2.5 and 5.0 mg/L, with additional positive correlations of phytoplankters 7 through 10 with zooplankton species 5, and accompanying negative correlations with all other consumers. Finally, at the two highest toxicant exposures, zooplankton species 3 and 4 are also impacted by the toxicant, exhibiting a negative correlation with phytoplankton species 7 through 10.

#### 4.5 DIAGNOSTIC VARIABLES

The number of variables required to provide a comprehensive description of ecosystem state is usually large. This introduces difficulties from the standpoint of ecosystem protection or management. Routine monitoring of such a large suite of ecological state variables can be a formidable task. Practical constraints on the expenditure of time, effort, or monetary resources may dictate a sampling scheme which allows routine monitoring of only a portion of the relevant variables. Perturbations, once detected in this subset of routinely monitored variables, can then be further characterized by measurement of ancillary state variables, and remedial actions taken as appropriate.

Routinely monitored variables which can be used as indicators of ecosystem state will be referred to as diagnostic variables,

following the terminology of Patten (1984). Ideally, a small set of easily measured diagnostic variables which accurately predict actual ecosystem state is sought. In the context of ecosystem management, it is usually desired that the ecosystem remain within some bounded region of the state space. Let this set of acceptable ecosystem states be denoted by  $X$ . The objective is then to find a set  $\Omega$  of states in the space of diagnostic variables corresponding to the set  $X$  in the state space. This correspondence is achieved if two conditions are met: (1) a measured vector of diagnostic variables,  $\omega$ , which is contained within  $\Omega$  insures that the state vector  $x$  is within  $X$  (sufficiency), and (2) the state vector  $x$  is found within  $X$  only if  $\omega$  is within  $\Omega$  (necessity).

In the real world, insistence on absolute sufficiency and necessity is too stringent of a requirement. The problem is more fruitfully addressed within the framework of statistical hypothesis testing. Take as a null hypothesis that the state vector  $x$  is within the acceptable domain  $X$ . This hypothesis is tested using the measured diagnostic vector  $\omega$ . If  $\omega$  is within  $\Omega$ , the null hypothesis is accepted; if not, it is rejected. As with any statistical test of a hypothesis, two types of incorrect inference are possible. If  $\omega$  falls outside of  $\Omega$  when in fact  $x$  is within  $X$ , the null hypothesis will be mistakenly rejected when it is true, and a type I statistical error is made. Alternatively, a type II error occurs if the diagnostic vector remains within  $\Omega$  when in fact the state vector is outside of  $X$ .

Type I errors can be thought of as false positives. Actions taken in response to such a false positive will in fact be unnecessary, leading to an unacceptable waste of time, effort, and money if they occur too frequently. On the other hand, type II errors can be thought of as false negatives, the occurrence of which can lead to unacceptable environmental damage that might have been avoided if mitigating steps had been taken. Clearly, it is desirable to minimize the occurrence of both types of error. Diagnostic criteria may be designed so as to yield an appropriate balance between the rates of type I and type II errors. Determining acceptable error rates and the balance between types of error must be done on a case by case basis, and may entail consideration of numerous social, political, economic, aesthetic, or ethical factors.

The scientific task is to devise procedures for identifying possible diagnostic variables and for estimating the error rates associated with specific diagnostic criteria so that their acceptability can be evaluated. The simulation results presented here provide a context for examining various procedures which may prove useful.

To illustrate the selection and use of diagnostic variables, variables were sought which would be good predictors of ecosystem state on day 21 of the simulation. Furthermore, it was decided that any state space separation of 15 or less Mahalanobis distance units would be considered acceptable. Day 21 was chosen as being late enough for responses to be evident, but early enough to exclude an

undue influence of state variables with very slow response time. Definition of an acceptable state space domain as a hypersphere with Mahalanobis radius=15 allows for a statistically significant, but not severe, deviation from the control trajectory (see Fig. 4.16 and 4.17). This is probably representative of most ecosystem management situations, where maintenance of completely pristine conditions is impractical, but limits are set at some low level of allowable impact.

There are many possible diagnostic variables. Each of the state variables is a candidate, as are aggregate variables such as the sum of phytoplankton biomasses, or other functions of state variables, such as the ratio of consumer biomass to producer biomass. Several procedures were used to identify promising diagnostic variables from the pool of candidates. First, simple correlations of the state space separation with the candidate variables was considered. Second, various linear regressions of state space separation against candidate variables were examined. This included a set of stepwise multiple regressions performed using the maximum  $R^2$  improvement method in the STEPWISE procedure available in SAS (SAS 1985c). Finally, the observations in the data set of simulation results were partitioned into two groups based on whether or not the state space separation exceeded 15 Mahalanobis distance units, and a stepwise discriminant analysis was performed on the classified data using the STEPDISC procedure (SAS 1985c).

As a result of these analyses, the best single diagnostic variable identified was the total zooplankton biomass. Linear regression yielded the relationship

$$S = 25.8784 + 3.2608 \ln Z \quad (4.1)$$

where  $S$  is the predicted separation, and  $Z$  is the sum of the biomasses of the five zooplankton species. This regression had an adjusted  $R^2$  value of 0.731. The result is a one dimensional diagnostic space defined by a single aggregate variable. It remains to define the set  $\Omega$  in this diagnostic space which will best corresponds to the set  $X$  in the state space. Since  $X$  is taken to be the set of all states such that  $S \leq 15$ , where  $S$  is the separation calculated in the full state space, an obvious choice of diagnostic criterion would be  $S \leq 15$ , which is equivalent to  $\ln Z \leq -3.3361$ . The statistical error rates associated with this diagnostic criterion can be estimated on the basis of the simulation results. Out of 800 Monte Carlo simulations, spanning the range of toxicant concentrations from 0.0 to 20 mg/L, the rate of occurrence of type I and type II errors is 3.13% and 15.6%, respectively.

The frequency of type II errors is higher than one might like. Since a type II error implies that actual environmental degradation occurs but is undetected, this is a potentially serious flaw. One alternative is to retain the same diagnostic space, but to define the set  $\Omega$  differently. A more conservative diagnostic criterion would

be  $S \leq Q$  where  $Q < 15$ . Such a strategy will reduce the probability of type II errors, but at the cost of an increased frequency of type I errors. Fig. 4.24 illustrates the trade-off between type I and type II error probabilities for values of  $Q$  between 12 and 15. Although it is possible to achieve a low rate of type II errors (say less than 5%), the result is a much higher rate of type I errors (greater than 20%). Since money and effort may be unnecessarily expended in responding to such false alarms, a high type I error probability may also be unacceptable.

If the error rates associated with the use of total zooplankton biomass as a diagnostic variable are deemed unacceptable, another diagnostic space must be sought. Several other one dimensional diagnostic spaces were examined, but none were found to be superior to total zooplankton in overall predictive power. Therefore, consideration is now given to possible two dimensional state spaces.

One method of searching for possible two dimensional diagnostic spaces is with stepwise multiple regression analysis. Using the STEPWISE procedure in SAS with a maximum  $R^2$  criterion for variable selection, the best two variable model found was

$$S = 31.8689 + 2.1648 \ln Z - 11.2891 \ln P_4 \quad (4.2)$$

where the new variable,  $P_4$ , is the biomass of the fourth phytoplankton species. This regression has an adjusted  $R^2$  of 0.822. Using this regression with a diagnostic criterion of  $S \leq 15$

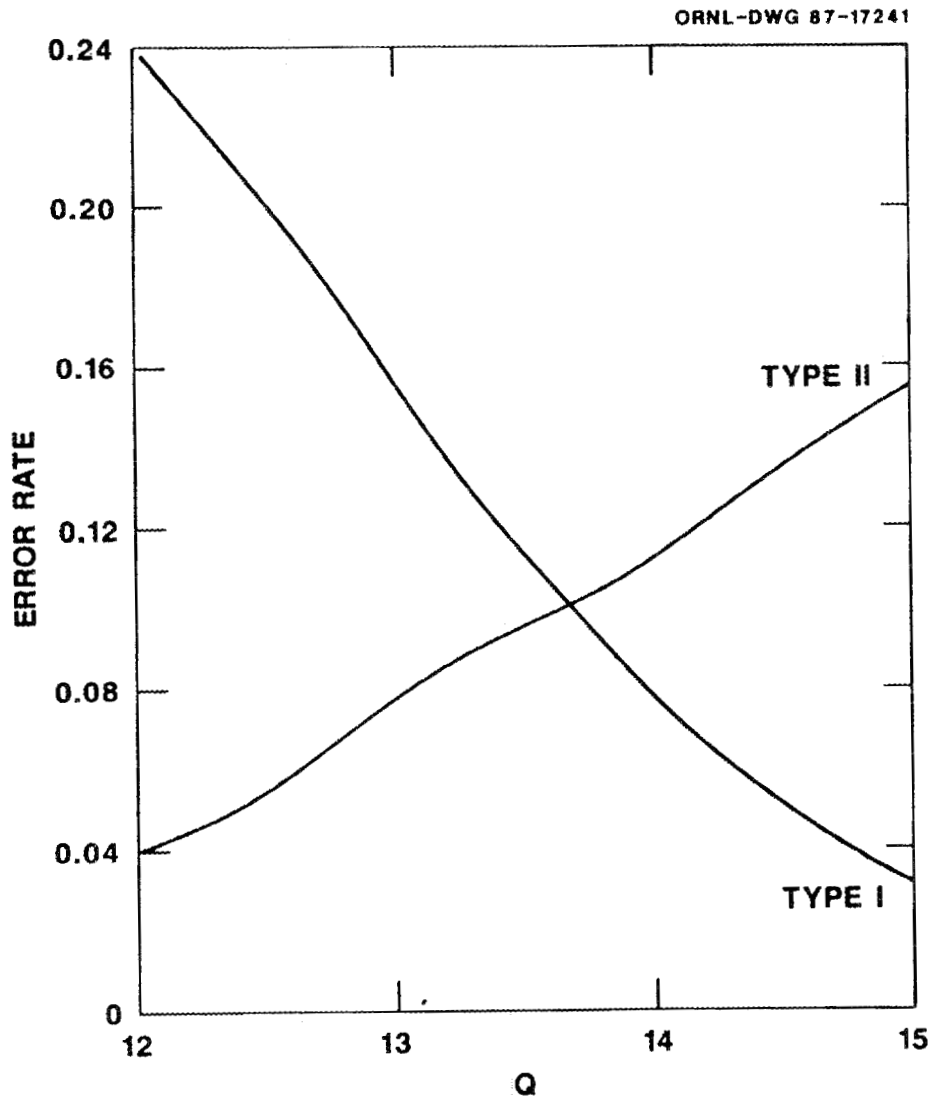


Figure 4.24 Rates of occurrence of type I and type II errors as a function of numerical criterion using total zooplankton as a diagnostic variable.

yields type I and type II error rates of 5.88% and 14.13%, respectively. Compared to the regression with Z alone, use of this relationship only slightly improves the type II error rate, and in fact leads to a higher total (type I + type II) error rate. Inspection of a scatterplot of ecosystem states projected into the two dimensional  $Z-P_4$  space, and coded to indicate whether or not  $S \leq 15$ , indicated that it was unlikely that any other diagnostic criterion within this space would be substantially better than one based on Z alone.

Alternatively, stepwise discriminant analysis can be used to search for sets of diagnostic variables. Using the STEPDISC procedure in SAS, with groups classified according to whether or not  $S \leq 15$ , the best two variable discrimination achieved was in a space defined by Z and  $P_{\text{blugrn}}$ , where  $P_{\text{blugrn}}$  is the sum of the biomasses of phytoplankton species 8 through 10, which occupy an ecological niche within the model similar to typical blue-green algal species. Having identified Z and  $P_{\text{blugrn}}$  as a candidate pair of diagnostic variables, it remains to specify a numerical diagnostic criterion within this two dimensional space. This is easily accomplished using the DISCRIM procedure within SAS. For each observation in the data set, the DISCRIM procedure calculates a probability of membership in X, the set of acceptable states, based upon the values of the diagnostic variables. The set  $\Omega$  is then defined as the collection of states such that the calculated probability of membership in X exceeds some specified threshold

referred to as a prior probability. In the absence of relevant information on which to base selection of a prior probability, a value of 0.5 is usually chosen. On the basis of this criterion, the estimated type I and type II error rates are 3.25% and 15.88%, respectively. Unfortunately, this set of diagnostic variables also fails to provide a substantial improvement over the previously considered candidates.

The failure of stepwise regression and stepwise discriminant analysis to find an adequate two dimensional diagnostic criterion does not prove its nonexistence. A suitable criterion may have been missed for two reasons: (1) stepwise procedures which do not consider all possible models may fail find the best model due to a convergence of the optimization criterion to a local, rather than a global, extremum; and (2) both stepwise procedures seek linear relationships between ecosystem state and sets of diagnostic variables, although nonlinear relationships may exist and prove to be more useful. With this in mind, several candidate two dimensional diagnostic spaces were examined which had been suggested primarily on the basis of intuitive appeal.

One such diagnostic space is that defined by the variables  $P_{\text{blugrn}}$  and  $P_{\text{spring}}$ , where  $P_{\text{spring}}$  is the sum of the biomasses of phytoplankton species 3 through 5, the dominant species of the spring bloom. If a diagnostic criterion is derived in this space on the basis of linear regression with  $S \leq 15$ , the resulting error rates are 9.50% and 6.25% for type I and type II errors, respectively.

This can be improved by using discriminant analysis to arrive at the numerical criterion. Assuming a prior probability of membership in set X of 0.5, error rates of 4.38% (type I) and 6.38% (type II) result. This is a clear improvement over the diagnostic criteria considered so far, but an even better criterion can be derived within this diagnostic space. This becomes evident upon inspection of the data as plotted in Fig. 4.25. It is apparent that a nonlinear criterion, such as curve C, provides a better prediction of ecosystem state than either of the criteria based on regression analysis (line A) or discriminant analysis (line B). In fact, the calculated type I and type II error rates associated with such a nonlinear diagnostic criterion are 7.63% and 0.00%, respectively.

Finally, a note must be made about the interpretation of the probabilities of type I and type II errors as presented in this section. These probabilities are not equivalent to  $\alpha$  and  $\beta$  error rates as traditionally defined for statistical hypothesis testing. Although  $\alpha$  ( $\beta$ ) is sometimes loosely referred to as the probability of making a type I (type II) error, in fact,  $\alpha$  ( $\beta$ ) is the conditional probability of a type I (type II) error given that the null hypothesis is true (false). The occurrence rates discussed above, on the other hand, are estimates of the probability of a type I or type II error without regard to the truth or falsity of the null hypothesis. The relationship between the two quantities can be seen by applying the definition of conditional probability:

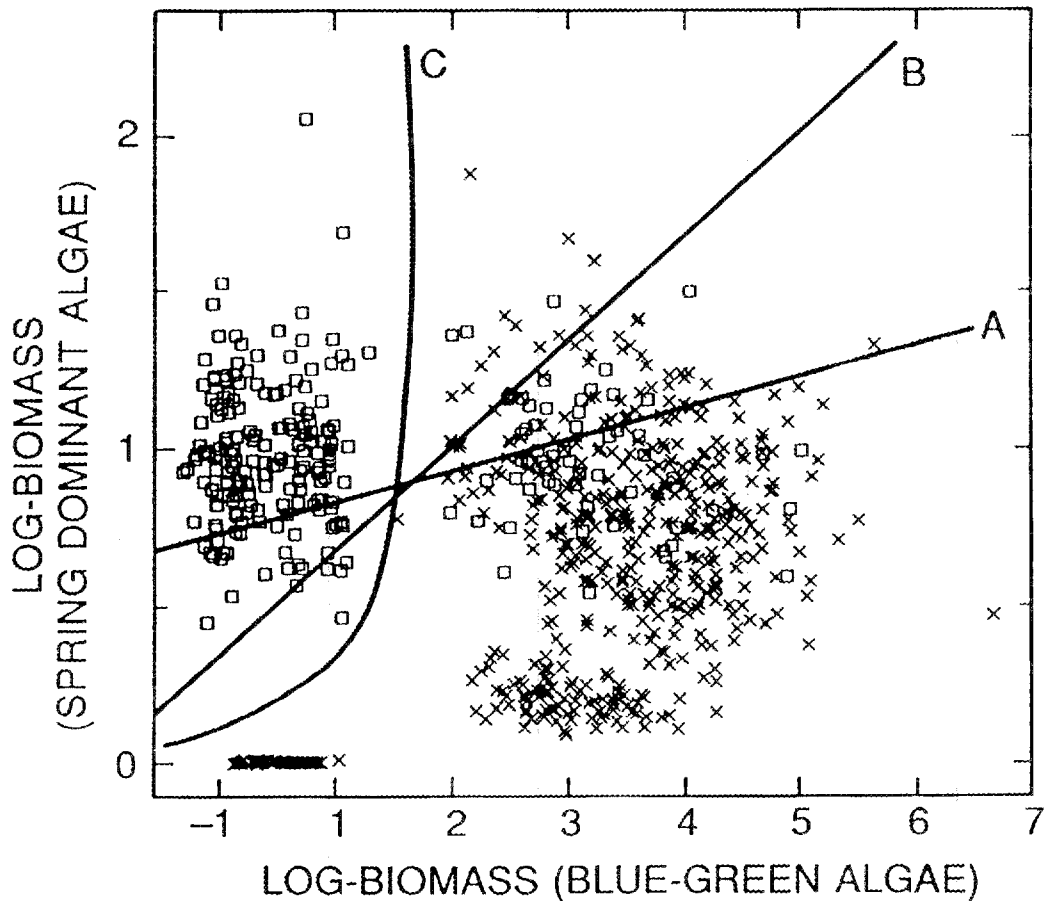


Figure 4.25 Simulation results projected into two-dimensional diagnostic space defined by  $P_{bluegrn}$  and  $P_{spring}$ . Squares represent simulations within the acceptable domain. X's represent simulations outside the acceptable domain. Three possible diagnostic criteria are shown: A - based on linear regression, B - based on discriminant analysis, and C - an ad-hoc nonlinear criterion.

$$\alpha = P(\omega \notin \Omega | x \in X) = P(\omega \notin \Omega \cap x \in X / P(x \in X)) \quad (4.3)$$

$$\beta = P(\omega \in \Omega | x \notin X) = P(\omega \in \Omega \cap x \notin X / P(x \notin X)) \quad (4.4)$$

A lucid discussion of the logic of statistical inference, with relevant remarks on error probabilities, is contained in Oakes (1986, see especially Chapter 1).

The numerators in equations 4.3 and 4.4 are joint probabilities, expressing the rates of simultaneous occurrence of two events, one in the diagnostic space and one in the full state space. It is these joint probabilities which have been reported in the discussion of possible diagnostic variables. The choice between reporting conditional probabilities or joint probabilities is partially a matter of personal taste, but in this application, the latter seem more readily interpretable. For instance, if the conditions of toxicant exposure are such that it is improbable that the state vector will in fact be within the acceptable domain (i.e.,  $P(x \in X)$  is near zero), then even if the conditional probability of a type I error is high, the expected frequency of type I errors will be low. The joint probability, on the other hand, is always proportional to the expected error frequency.

It should be noted that both the conditional and the joint error probabilities depend upon the exposure conditions. Strictly speaking therefore, the error rates presented are only valid for the particular exposure scenario used in the simulation. The relationship between error probabilities and exposure conditions is

examined in greater detail in section 5.4, where the use of diagnostic variables is linked to the theory of risk analysis.

## DISCUSSION AND CONCLUSIONS

## 5.1 SUMMARY AND EVALUATION OF RESULTS

The method of using state space displacements to summarize ecosystem response to a toxicant has been applied in three relatively independent situations: (1) to investigate the response of flask microcosms to 2,4-dimethylphenol, (2) to investigate the response of aquarium microcosms and of experimental ponds to a coal-derived synthetic oil, and (3) to investigate the dynamics of an aquatic ecosystem model under simulated conditions of exposure to a mixture of phenols. The results of these investigations have been presented in preceding chapters. Now, attention will be directed toward summarizing the important features of these results, and toward evaluating the strengths and weaknesses of the state space displacement methodology employed in this study.

In all three applications of the method, the primary product of the analysis was a description of the dose-response characteristics of the system to the toxicant under consideration. Dose-response relationships were derived using state space displacements, or scalar quantities derived from displacements, as indicators of ecosystem response. Inevitably, reducing ecosystem response to one or a few quantities involves the suppression of certain detailed aspects of the original multivariate data. However, the complexity of a large multivariate data set can obscure general trends or patterns which

can be clearly shown by the use of appropriate summary statistics. The most successful strategy is to develop statistical measures which effectively capture the trends or patterns of interest, but which can be readily related to the original variables to aid in the interpretation of the results.

The state space measures used in this study have demonstrated their heuristic value. Calculation of a state space displacement vector recasts the original data in a different mathematical framework, discarding information on the absolute values of state variables, but preserving information on the differences between control and perturbed systems. The contribution of individual state variables can be reconstructed from the directionality of the displacement vector. The displacement vector will be close to (at a small angle from) the axes corresponding to the state variables contributing most heavily to the response. Thus state space displacements are readily interpretable in terms of the original variables.

Summarizing response in terms of the magnitude of the displacement vector means suppressing the directional information, but provides a measure of the distance between control and perturbed ecosystem states. It has proved convenient to use a Mahalanobis metric to measure this distance, since Mahalanobis distances can be regarded as an inverse measure of the probability of such a displacement being realized in the absence of toxicant stress. The response surfaces shown in Figs. 3.4, 3.11, 4.12, 4.14, and 4.16 are

plots of the Mahalanobis distances separating control and perturbed trajectories as a function time and toxicant input.

Occasionally it is useful to further summarize the data by suppressing the temporal dynamics of ecosystem response. Three measures were proposed for this purpose: maximum separation, mean separation, and mean displacement magnitude. Maximum separation is primarily of interest as a possible index of ecosystem resistance (see discussion in sections 1.3 and 1.4). Mean separation and mean displacement magnitude are both measures of response averaged over a time period. In the case of mean separation, the distances are averaged, whereas mean displacement magnitude, as the name implies, is based on an averaging of displacement vectors. The distinction was discussed more fully in section 2.4.4. It was suggested that a comparison of the mean separation with the mean displacement magnitude could be used to assess the extent of changes in the directional nature of the displacements over the time period. Such comparisons, however, were not especially informative with respect to the data analyzed in this study. Perhaps information on directionality would be better conveyed by direct calculation of angular rotation between successive displacement vectors, as was done to indicate changes in the orientation of the first principal component (see Figs. 3.16, 4.21 and 4.23).

As a multivariate statistical technique, state space analysis can frequently provide greater statistical power than univariate analysis of individual state variables. This results simply from the

geometric fact that the length of a displacement vector (separation) cannot be less than the length of its projection onto any axis. This is true whether an Euclidean or a Mahalanobis metric is used, although, to be consistent, the projection must, in the latter case, be defined to be orthogonal in terms of Mahalanobis angles (Mardia 1977). The power of a linear function of state variables to detect changes in state is a function of both the length of the displacement vector projected onto that axis and of the covariance structure of the data. In practical applications the length considerations frequently dominate, meaning that separation is usually nearly the most powerful statistic. (The strictly most powerful statistic is that provided by discriminant analysis, see section 5.2.2).

The statistical power obtained by the use of state space separation can be compared to that obtained with individual state variables using the simulation results. The type II error rates, based on the use of separation or of several of the individual state variables, are shown in Table 5.1. In most cases these were calculated from the number of simulations at the lowest treatment level (0.3125 mg/L) that fell within the the interval defined by the 1st and the 99th percentiles of the control simulations (all on day 21). This analysis estimates the probability of a type II error under a two-sided test of the hypothesis of no effect with a significance probability  $\alpha = 0.02$ . In those cases where the type II error rate was low, it was estimated by assuming that the statistic followed a normal sampling distribution. In the case of

Table 5.1 Type II error rates associated with the use of separation and of individual state variables to test the hypothesis of no effect on day 21 of the ecosystem simulation.

---

<u>Test Statistic</u>	<u>Type II Error Rate (<math>\beta</math>)</u>
separation	0.0060
phytoplankton 4 biomass	0.0014
phytoplankton 8 biomass	0.20
phytoplankton 9 biomass	0.0075
zooplankton 1 biomass	0.36
zooplankton 2 biomass	0.24
zooplankton 3 biomass	0.21
zooplankton 4 biomass	0.76
zooplankton 5 biomass	0.76
fish biomass	0.80
macrophyte biomass	0.98
refractory detritus mass	0.99
phytoplankton net photosynthesis	0.025
macrophyte net photosynthesis	0.99
nutrient concentration	0.94
dissolved oxygen	0.98

---

separation this proved to be a good approximation. The phytoplankton biomasses, however, deviated significantly from a normal distribution (as determined by a Kolmogorov-Smirnov test,  $\alpha = 0.05$ ), but the approximation was probably good enough for an order-of-magnitude estimate of the error rate. The null hypothesis (no effect) was in fact false; therefore, these error rates are estimates of  $\beta$  as traditionally defined. The statistical power associated with each statistic is  $1-\beta$ . Note that the state space separation is typically an order of magnitude more powerful than individual state variables. The only state variables of comparable power were the biomasses of phytoplankton species 4 and 9, which are representatives of the two phytoplankton groups identified as diagnostic variables in section 4.5.

In applications of state space displacement analysis, especially if few replicates are available, consideration must be given to the sensitivity of Mahalanobis distances to errors in the estimated covariance matrix. Although qualitative patterns of response appear relatively robust to variations in the estimated covariance structure, the numerical values of calculated separations can depend quite strongly on the covariance matrix. This implies that for quantitative studies in which emphasis is placed on the absolute, and not just the relative, magnitude of response, the covariance structure must be well characterized. Extensive sampling may be required to reliably estimate even a stationary covariance matrix, and if the covariance structure changes with time, the sampling

requirements are likely to be formidable. Fortunately, many ecotoxicological questions can be answered on the basis of relative, rather than absolute, separations. Nevertheless, derivation of methods that reduce the sensitivity to covariance structure would be a major improvement to the method. Two possible improvements, based on robust estimation of the covariance matrix and on an alternative distance metric, are outlined in section 5.3.

The emphasis on estimating the covariance structure of ecological variables necessitated by the methods employed in this study has had a positive aspect also. On the basis of the experimental data and simulations results presented here, it can be seen that the covariance structure of ecological state variables may change significantly over time, either due to internal system dynamics or in response to a toxicant. If the state variables are selected appropriately, changes in covariance structure should provide valuable information on the underlying changes in ecosystem function. Exploring the use of measures based on covariance structure to monitor ecosystem dynamics along both perturbed and unperturbed trajectories appears to one of the more fruitful avenues of research suggested by this study. Analysis of covariance structure may provide a useful means for comparing the dynamics of systems, whether the comparison is between different experimental ecosystems, simulation models, or both.

The state space methodology presented in this study also provides a convenient framework for practical application of Patten's

(1984) concept of diagnostic variables. This concept has broad applicability to a range of problems encountered in the management of ecological systems. The statistical framework developed in section 4.5, allowing the estimation of the error rates associated with the use of any particular diagnostic criterion, seems particularly relevant as a guide to rational decision making. The usefulness of this approach is enhanced by its compatibility with established theory in risk analysis. A first step in linking the concept of diagnostic variables with the theory of risk analysis is taken in section 5.4.

## 5.2 RELATIONSHIP WITH OTHER MULTIVARIATE TECHNIQUES

The state space methodology developed in this study can be regarded as primarily a multivariate statistical technique. Further insight can be gained, therefore, by comparing it with other well established multivariate techniques, both to point out the similarities in the underlying theoretical basis, and the differences that influence the choice of an appropriate method for a particular problem. State space displacement analysis will be compared with two commonly used multivariate techniques: principal components analysis and discriminant analysis.

### 5.2.1 Principal Components Analysis

One technique frequently applied to the analysis of state space trajectories is the projection of the data into a lower dimensional space defined by principal components. This technique has been used to elucidate qualitative features of the trajectories (e.g., Allen et al. 1977, Bartell et al. 1978, Allen and Shugart 1983, Allen et al. 1984), and in quantitative assessments of perturbation-induced displacements (Bloom 1980). It is worth considering the relative merits of this approach.

Fig. 5.1 shows the results of an analysis of hypothetical data designed to illustrate the potential shortcomings of an analysis in principal component space. The hypothetical data consist of repeated observations of two bivariate normal populations. Both populations have a constant, and identical, covariance structure, with a positive correlation of 0.78 between the two state variables. The distance between the two population centroids, however, varies with time. The largest displacement occurs on day 4, with an increase in one state variable and a concomitant decrease in the other, followed by a period of recovery. The true Mahalanobis distance between population centroids is shown in Fig. 5.1a. The state space separation estimated by the methods developed in this study is shown in Fig. 5.1b for a particular random sample of 14 replicate trajectories. Some of the details of the population response are obscured by random error, but the existence of the peak at day 4 is clearly indicated.

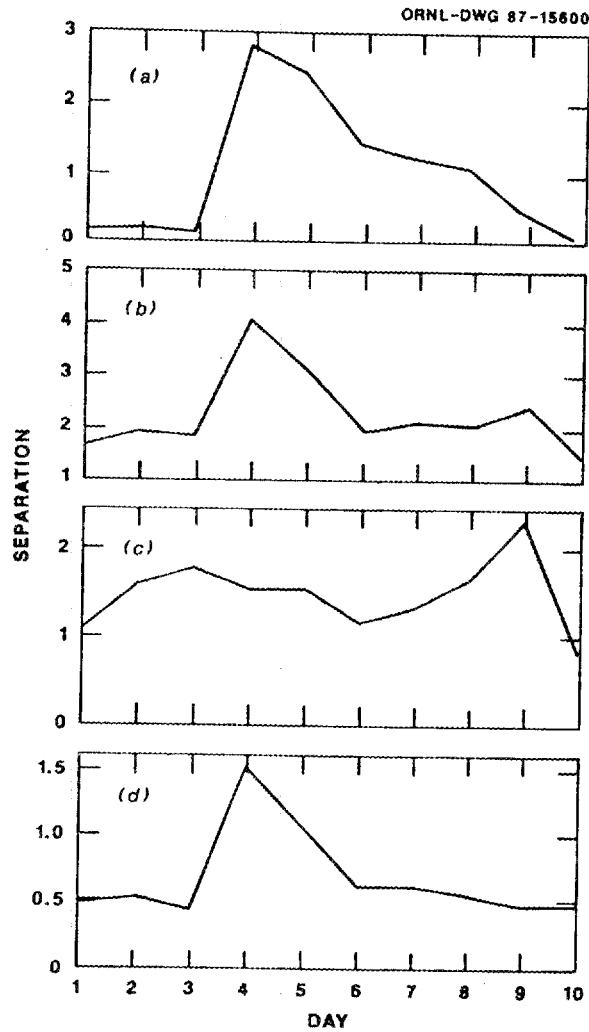


Figure 5.1 Results of analysis of hypothetical data set. (a) True state space separation between population centroids. (b) State space separation estimated from sample. (c) Separation estimated in reduced space defined by first principal component. (d) Separation estimated in reduced space defined by second principal component.

In practice, principal components analysis would rarely be applied to a two dimensional data set. However, this hypothetical data set serves to illustrate a phenomenon which can also easily arise in data sets of higher dimensionality. It is found that 82% of the variance in the data is explained by the first principal component, so one might suppose that this one dimensional principal component space would adequately reflect behaviors in the full state space. Such is not the case, as can be seen from Fig. 5.1c which shows the separation calculated in the first principal component space. The separation of trajectories projected into the first principal component space shows no hint of the actual perturbation on day 4, and misleadingly suggests a perturbation on day 9. Surprisingly, most of the displacement information is contained in the second principal component, which, though it only explains 18% of the total variance (Fig. 5.1d), shows the perturbation on day 4 as clearly as the full state space separation.

The data analyzed in this example are admittedly contrived to illustrate a point. The displacements were deliberately chosen to be in a direction nearly perpendicular to the reduced principal component space, insuring the inadequacy of the principal component representation. In general, however, the direction of displacement is not known a priori, so trajectories in spaces of reduced dimensionality must be interpreted cautiously. Such spaces may be useful for graphical presentation of the data, or to explore certain

qualitative features of the trajectories, but for quantitative analysis, calculations based on the full state space are preferable.

Although the methodology developed in this study does not rely on a principal components analysis to reduce the dimensionality of the state space, the method is closely related to principal components analysis in another sense. This connection arises in the use of the Cholesky decomposition of the inverted covariance matrix to transform the data prior to analysis. Under this transformation, a random vector  $x$  from a population with covariance matrix  $\Sigma$  is transformed into a vector  $y$  ( $= Ax$ , where  $A = \Sigma^{-1/2}$ ) with an identity covariance matrix. Under principal components analysis, if all the principal components are retained, a random vector  $x$  with covariance matrix  $\Sigma$  is transformed into a vector  $z$  ( $= Bx$ ) with a diagonal covariance matrix  $\Lambda$  (Tatsuoka 1971, pp. 127-130). The elements of  $\Lambda$  are the eigenvalues of the original covariance matrix  $\Sigma$ , and can be interpreted as the amount of variance explained by each of the principal components. Standardizing the principal component scores results in a transformation to a vector with an identity covariance matrix, and the resulting vectors are identical to those resulting from the transformation used in calculating the state space measures. Effectively, the transformation is equivalent to that which results from plotting the data in a space of standardized principal components calculated from the covariance matrix of the control

ecosystems. The relationship is summarized in the equality  $A = \Lambda^{-1/2} B$ .

### 5.2.2 Discriminant Analysis

Discriminant analysis is a multivariate statistical technique designed to identify a subspace of reduced dimensionality which maximizes the distinction between groups selected prior to the analysis. The technique has been used to quantify the response of microbial communities to toxicant exposure (Sayler et al. 1982, 1983). State space displacement analysis is also aimed at the quantification of differences between control and perturbed state trajectories. Hence, it is worth investigating the relationship between the two techniques. A description based on the geometric interpretation of a discriminant function is presented here; a more rigorous treatment of discriminant analysis is available in standard texts (e.g., Tatsuoka 1971, pp. 157-177).

Imagine two clusters of points in a multidimensional space corresponding to the two groups (e.g., control and perturbed system states). Consistent with the focus of this study, these clusters can represent measured states along control and perturbed state trajectories. Discriminant analysis techniques construct a discriminant function which is a linear combination of state variables, or equivalently an axis in the state space, such that the overlap between groups is minimized when the data are projected onto

that axis. The axis which satisfies this requirement is determined by a compromise between maximizing the distance between the projected centroids and minimizing the projected within-group variance.

This compromise is illustrated for the case of a two dimensional state space in Fig. 5.2. In Fig. 5.2, centroids and concentration ellipses are shown for two groups of data. In Fig. 5.2a, the results of projecting the data onto an axis which maximizes the (Euclidean) distance between centroids is shown. The difference between the means of the resulting distributions is large, but so is the within-group variance, so there is a noticeable overlap in the tails. Fig. 5.2b shows the data projected onto an axis which minimizes the within-group variance. Although the spread of the distributions is much smaller than in Fig. 5.2a, the distance between the means is also much reduced, and a noticeable overlap still exists. Finally, Fig. 5.2c shows the data projected onto the axis which serves as the best discriminant function. This axis is oriented in a direction between the other two axes considered. With this compromise it is possible to separate the two groups such that there is no significant overlap between the projected distributions.

Unlike discriminant analysis, state space displacement analysis is not aimed solely at maximizing the ability to distinguish between groups, but rather attempts to provide an objective quantification of the differences in control and perturbed systems relative to normal variation. For this purpose, it is the displacement between group centroids which conveys the most useful information. Thus, the

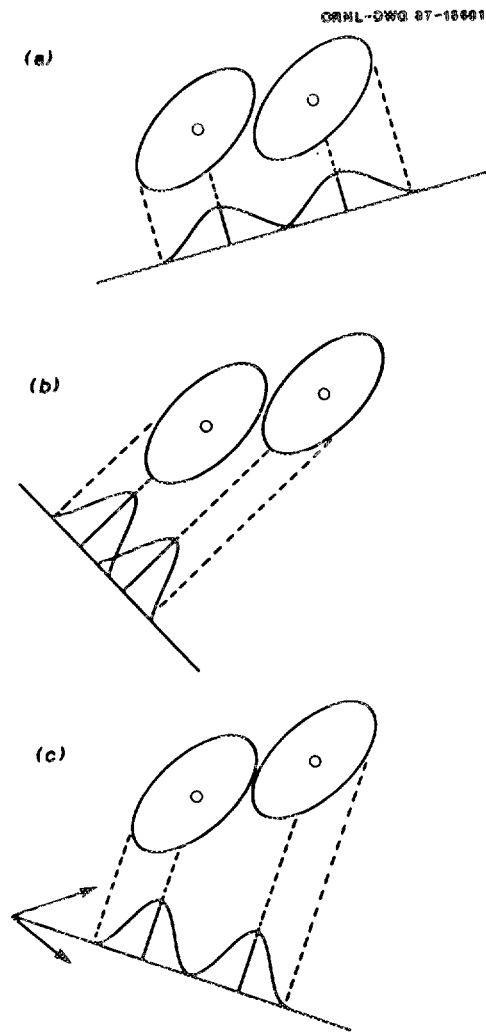


Figure 5.2 Illustration of geometric interpretation of discriminant analysis. (a) Axis maximizing the distance between centroids. (b) Axis minimizing the within-group variance. (c) Compromise axis yielding best discrimination.

expected orientation of the displacement vector is parallel to the axis in Fig. 5.2a. As this is one ingredient in determining the discriminant function, there is relationship between the two, but they are not equivalent, the degree of difference being determined by the variance-covariance structure of the data. The Mahalanobis transformation used in this study is designed to convert the control data to a spherically symmetrical distribution, in which case it is only the covariance structure of the perturbed state vectors which influences the discriminant function. In the special case of a perturbation which does not affect the covariance structure, the discriminant function and the displacement vector are equivalent when both are described in the transformed space.

### 5.3 DIRECTIONS FOR FUTURE RESEARCH

#### 5.3.1 Use of Alternative Distance Metrics

The applications of state space analysis explored in the course of this study have all relied upon the use a Mahalanobis metric to measure distances. This metric was used in preference to the traditional Euclidean metric to compensate for the differences in scaling of the various measured state variables, and for their intercorrelations. For the cases examined in this study the Mahalanobis metric appears to have served its intended purpose, but it is not the only non-Euclidean metric available, and others may be of use in some situations. The choice of a metric will largely

depend upon the nature of the problem to which state space analysis is being applied.

One distance metric which, because it does not require estimation of the entire covariance matrix, may be useful is the Karl Pearson distance (originally called the coefficient of racial likeness, Pearson 1926; for a recent treatment see Mardia 1977). Given two random vectors,  $v$  and  $w$ , drawn from a population with covariance matrix  $\Sigma$ , the Karl Pearson distance between them is

$$d_K(v-w) = [(v-w)' \text{diag}(\Sigma)^{-1}(v-w)]^{1/2} \quad (5.1)$$

where  $\text{diag}(\Sigma)$  represents a matrix which contains the diagonal elements of the covariance matrix (i.e., the variances) and zeroes elsewhere. It can be demonstrated that the Karl Pearson distance is equivalent to the Euclidean distance between vectors with standardized state variables. Unlike the Mahalanobis metric, the Karl Pearson metric does not account for correlations between the state variables. However, empirical studies have shown that Karl Pearson distances are highly correlated with Mahalanobis distances, and the former can be used as a substitute for the latter in many cases (Penrose 1954). The relationship between the two breaks down as the intercorrelations among state variables becomes strong.

Within the context of the state space analyses conducted in this study, the primary advantage to using the Karl Pearson distance is the elimination of the need to estimate the entire covariance structure for the control ecosystems. In an  $n$ -dimensional state

space, only the  $n$  variances are needed to calculate Karl Pearson distances, as opposed to the  $n(n-1)/2$  variance-covariance elements needed to calculate Mahalanobis distances. Estimates of this smaller number of statistics should be more reliable, which is an important consideration in the case of small sample sizes frequently encountered in ecotoxicological data. In particular, time-varying estimates of the variances may show less sampling variation than time-varying estimates of the entire covariance structure.

Another important family of distance metrics are the Minkowski  $p$ -metrics (Gatrell 1983, pp. 27-33). The Minkowski distance between two vectors,  $v = (v_1, v_2, \dots, v_n)'$  and  $w = (w_1, w_2, \dots, w_n)'$ , is calculated as

$$d_p(v, w) = \left[ \sum_{i=1}^n |v_i - w_i|^p \right]^{1/p} \quad (5.2)$$

where  $p$  can be any real number from 1 to infinity. If  $p = 2$ , this formula reduces to the Euclidean metric. The metric obtained by setting  $p = 1$  is referred to as the taxicab or city-block metric, since it can be viewed as a measure of distance in a space where travel is restricted to a rectangular grid, such as city streets. At the other extreme, as  $p$  approaches infinity, the Minkowski metric possesses a well defined limit which can be written as

$$\lim_{p \rightarrow \infty} d_p(v, w) = d_D(v, w) = \max_j |v_j - w_j| \quad (5.3)$$

and is simply the largest difference between pairs of vector components. Thus, it is referred to as a dominance metric.

The geometric interpretation of Minkowski metrics can be illustrated by considering sets of points which are equidistant from some center as measured by a Minkowski metric. A set of such Minkowski "circles" is shown in Fig. 5.3. At  $p = 2$ , the result is, of course, the traditional Euclidean circle. At  $p = 1$ , the result is a diamond inscribed within the traditional Euclidean circle, whereas at  $p = \infty$ , the result is a square circumscribing the Euclidean circle.

The dominance metric ( $p = \infty$ ) may be applicable in some cases where state space analysis is used in a regulatory framework. Within this context, an acceptable state space domain is frequently defined in terms of acceptable ranges for each of the state variables. This describes a rectangular region in state space which can be made square by an appropriate scaling of the axes, and which therefore is a circle as measured by the dominance metric. This reduces the problem of determining whether an ecosystem is within the acceptable domain to that of determining if its distance from the centroid, as measured by the dominance metric, is less than the radius of the Minkowski circle. Application of the dominance metric would probably have facilitated Bloom's (1980) analysis of the recovery of perturbed communities, which was based on distance from a rectangular "rejection envelope" (see discussion in section 1.3).

The Minkowski  $p$ -metrics are independent of the covariance structure of the data. It is possible to devise a metric which combines the geometric properties of the Minkowski metrics and the

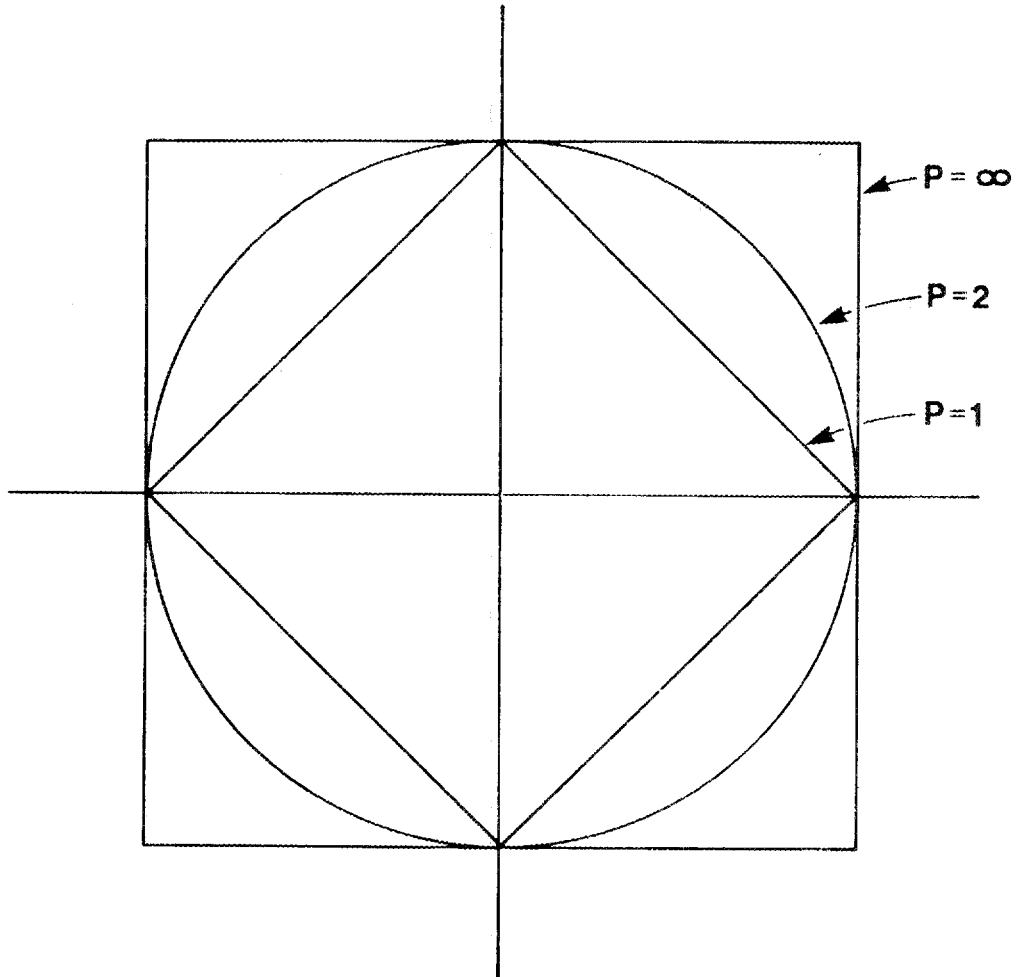


Figure 5.3 Minkowski circles for  $p = 1, 2,$  and  $\infty$ .

covariance correction of the Mahalanobis metric. The following is such a hybrid metric:

$$d_H(v,w) = [((v-w)^{p/2})' \Sigma^{-1} (v-w)^{p/2}] \quad (5.4)$$

If  $p = 2$ , this is equivalent to the Mahalanobis metric, and the set of points equidistant from a centroid describe an ellipse. For other values of  $p$ , the shape of the set of equidistant points changes in the same fashion as for a Minkowski metric. For example, if  $p = \infty$  the metric results in a set of equidistant points which form a rectangle circumscribing the  $p = 2$  ellipse.

### 5.3.2. Robust Estimation of the Covariance Matrix

In many cases, the number of degrees of freedom available to estimate a covariance matrix from experimental data is not much greater than the number of state variables. In such cases, the estimated covariance matrix can be strongly influenced by one or two anomalous observations, or outliers. Recently, considerable effort has been directed toward the development of robust statistical methods which are relatively insensitive to the presence of small numbers of outliers. One class of robust statistics encompasses the M-estimators, where the influence of an observation on the statistic varies gradually with its distance from the sample centroid. To make the estimator robust, the influence function is bounded such that the effect of an outlier is limited.

Robust M-estimators for the covariance matrix have been discussed by Huber (1977) and by Hampel et al. (1986). Unfortunately, the equations for such an estimate of the covariance matrix have no analytical solution, and must be solved by iterative methods. This can be computationally expensive, requires that an initial estimate of the covariance matrix be derived by non-robust means, and is not guaranteed to converge to the optimal robust estimate. In general these problems become more acute in higher dimensions. Research into better and more efficient computational schemes is underway. It can be concluded that robust estimators of covariance matrices are not yet practical for routine application, but that further research into their potential usefulness in state space displacement analysis is warranted.

#### 5.4. DIAGNOSTIC VARIABLES AND RISK ANALYSIS

Risk can be defined as the probability of occurrence of a specified undesirable event. This definition can be applied to the scenario presented in section 4.5. There it was assumed that on day 21 of the simulation a set of acceptable ecosystem states could be defined as those less than 15 Mahalanobis distance units from a matched control trajectory. This set was denoted by  $X$ . Lower dimensional diagnostic spaces were sought which could be used to predict the acceptability or unacceptability of an ecosystem state on the basis of restricted monitoring data. This goal is achieved if a

set of states,  $\Omega$ , can be found in the diagnostic space such that knowing whether or not the vector of diagnostic variables,  $\omega$ , is in  $\Omega$  can be used to predict (with sufficient accuracy) whether the state vector,  $x$ , is in  $X$ .

For the situation outlined above, risk can be defined as the probability that an ecosystem state vector will be found outside of the acceptable domain (i.e., greater than 15 Mahalanobis distance units from the control centroid). This probability will, of course, depend upon the toxicant exposure regime imposed on the ecosystem, as well as other factors. Assuming that for a specified system all other factors are either constant or are predictable (at least in a statistical sense), then risk can be examined as a function of toxicant concentration. Taking the ecological simulation model as the system to be considered, risk can be estimated by the fraction of Monte Carlo results which fall outside the acceptable domain at a given toxicant concentration. As the number of Monte Carlo iterations becomes large, this estimate converges toward a constant value which, within the context of this modeling exercise, is regarded as the true risk. Whether or not this is an accurate estimate of the true risk for any particular real-world ecosystem depends upon the adequacy of the model as a representation of that ecosystem. For a discussion of that aspect of risk evaluation, see Suter et al. (1987).

Since the acceptable domain is defined in terms of the full (23-dimensional) state space, estimates of the actual risk must be

made in the full state space to avoid bias. However, in practice, risk estimates are often required on the basis of incomplete knowledge of some of the state variables. Diagnostic variables, which were introduced in section 4.5 as predictors of ecosystem state, can now be used to predict ecological risk. Within the modeling context, the risk predicted by various sets of possible diagnostic variables can be estimated and compared with the estimates of actual risk calculated in the full state space.

The relationship between the accuracy of risk predictions and the rates of type I and type II errors can be derived as follows. There are four distinct events which can occur with the use of diagnostic variables.

$E_1: x \subset X \text{ and } \omega \subset \Omega$  (correct inference of no damage)

$E_2: x \subset X \text{ and } \omega \not\subset \Omega$  (type I error)

$E_3: x \not\subset X \text{ and } \omega \subset \Omega$  (type II error)

$E_4: x \not\subset X \text{ and } \omega \not\subset \Omega$  (correct inference of damage)

Denoting the risk at a specified toxicant concentration  $C$  as  $R_C$ , we have

$$R_C = P(x \not\subset X | C) \quad (5.5)$$

Since events  $E_3$  and  $E_4$  mutually exhaust the possibilities for  $x$  to fall outside of  $X$ , this becomes

$$R_C = P(E_3 \cup E_4 | C) \quad (5.6)$$

Furthermore, since  $E_3$  and  $E_4$  are mutually exclusive, the probability of their union is simply the sum of their separate probabilities:

$$R_C = P(E_3 | C) + P(E_4 | C) \quad (5.7)$$

The risk predicted on the basis of the diagnostic variables, denoted  $R_C$ , is

$$R_C = P(\omega \notin \Omega | C) \quad (5.8)$$

By reasoning analogous to that used above, we find

$$R_C = P(E_2 \cup E_4 | C) = P(E_2 | C) + P(E_4 | C) \quad (5.9)$$

Combining 5.7 and 5.9 yields

$$R_C - P(E_3 | C) = (R_C - P(E_2 | C)) \quad (5.10)$$

or, by rearranging terms,

$$R_C = R_C + P(E_2 | C) - P(E_3 | C) \quad (5.11)$$

The last two terms in equation 5.11 are analogous to the joint probabilities of type I and type II error reported in section 4.5. The only difference is that these probabilities are conditional upon a specified toxicant concentration, whereas the probabilities reported in section 4.5 were calculated from the entire set of toxicant concentrations used in the simulations. It is

straightforward to obtain the error rates conditional upon toxicant concentration by performing the same analysis as in section 4.5 for each simulated toxicant concentration.

The results of such an analysis using total zooplankton biomass ( $Z$ ) is shown in Fig. 5.4. A shortcoming of this diagnostic variable is readily apparent from inspection of Fig. 5.4a: the risk function is seriously underestimated for a range of intermediate toxicant concentrations. This is due to a high probability of making a type II error at these concentrations (Fig. 5.16b). Although the joint probability of a type II error averaged over the range of exposure conditions is 15.6% (as reported in section 4.5), at the intermediate concentration of 1.25 mg/L the type II error rate is 68%. In contrast, the type I error rate is always relatively low (less than 10%), although type I errors are likely over a wider range of exposure conditions than type II errors.

Risk functions and toxicant-specific error rates for diagnostic criteria defined on the variables  $P_{\text{spring}}$  and  $P_{\text{blugrn}}$  (summed biomasses of phytoplankton species 3-5 and 8-10, respectively) are shown in Figs. 5.5, 5.6 and 5.7. These three functions differ in the way the boundaries of the  $\Omega$  region are defined (see Fig. 4.25). The first function (Fig. 5.5) uses predicted values from a multiple linear regression to define the  $\Omega$  region. The resulting predicted risk function approximates the true risk function fairly well, but the error rates are in fact moderately high. At a toxicant concentration of 0.625 mg/L, the predicted risk equals the true risk,

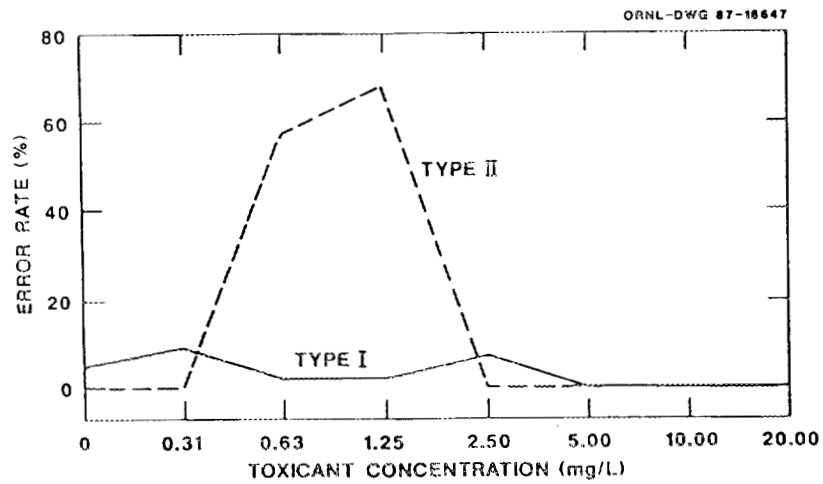
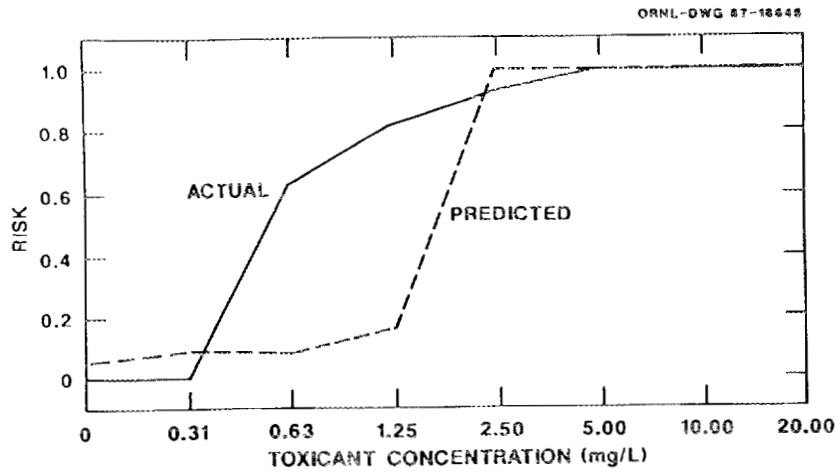


Figure 5.4 Total zooplankton as a diagnostic variable. (a) solid line, actual risk; dashed line, predicted risk. (b) Solid line, type I error rate, dashed line, type II error rate.

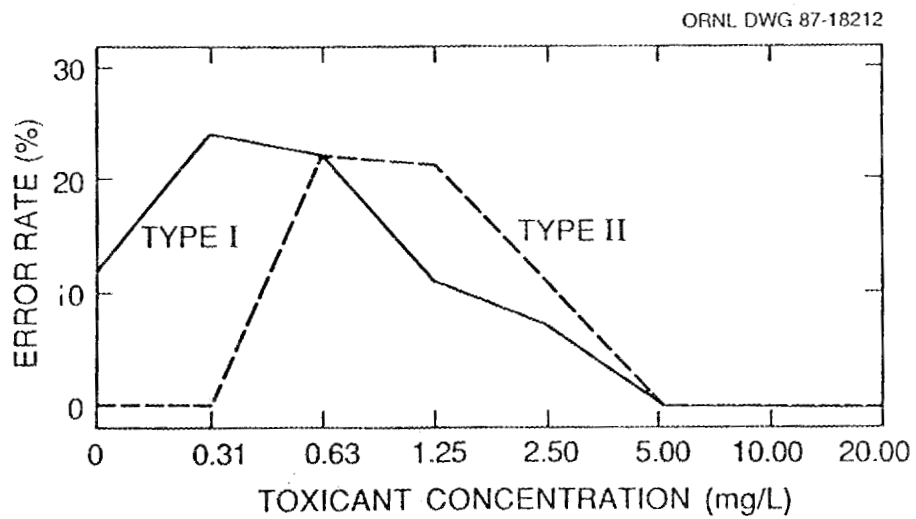
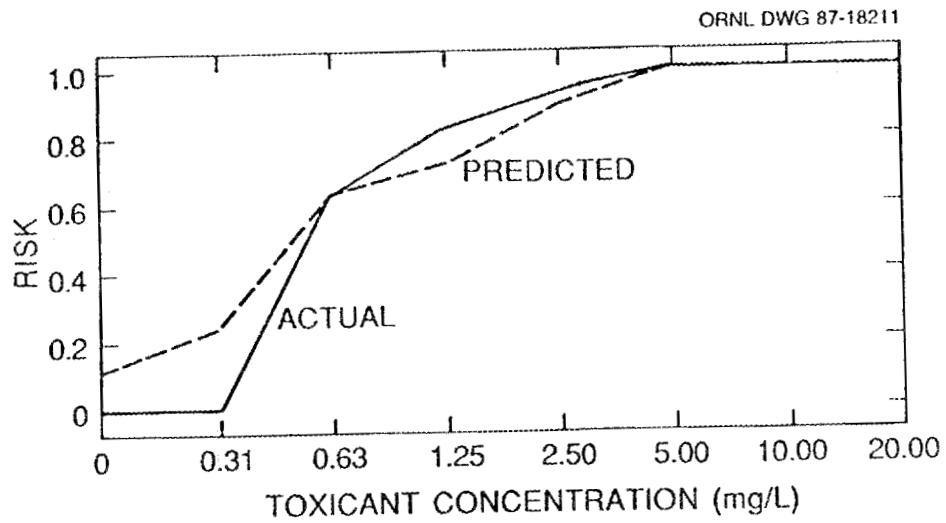


Figure 5.5 Blue-green and spring dominant phytoplankton as diagnostic variables based on linear regression. (a) solid line, actual risk; dashed line, predicted risk. (b) Solid line, type I error rate, dashed line, type II error rate.

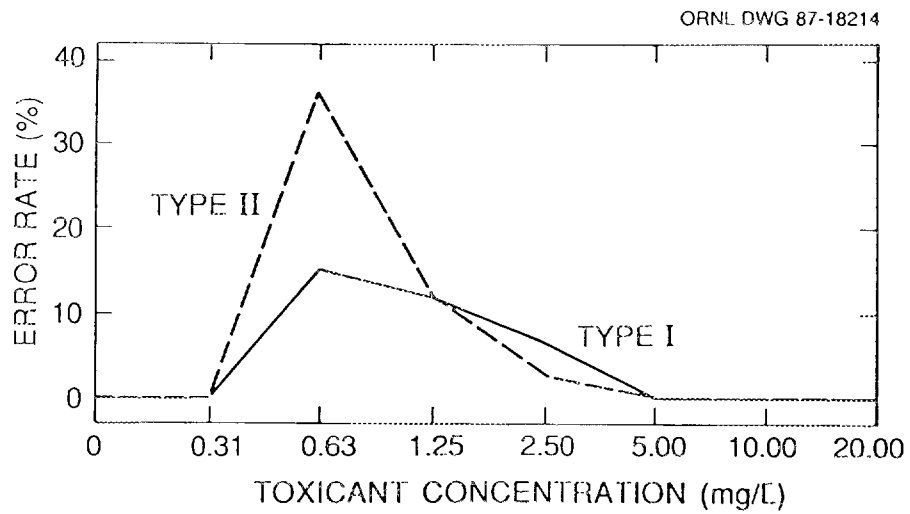
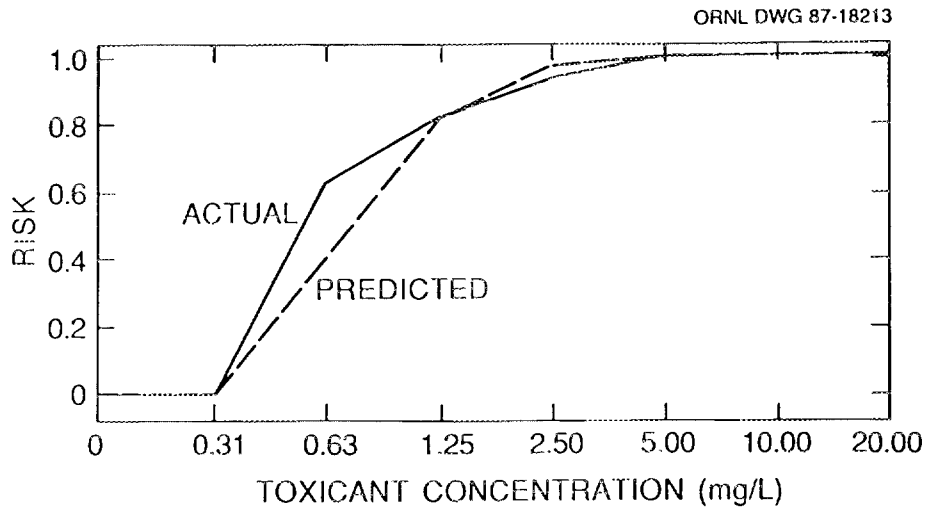


Figure 5.6 Blue-green and spring dominant phytoplankton as diagnostic variables based on discriminant analysis. (a) solid line, actual risk; dashed line, predicted risk. (b) Solid line, type I error rate, dashed line, type II error rate.

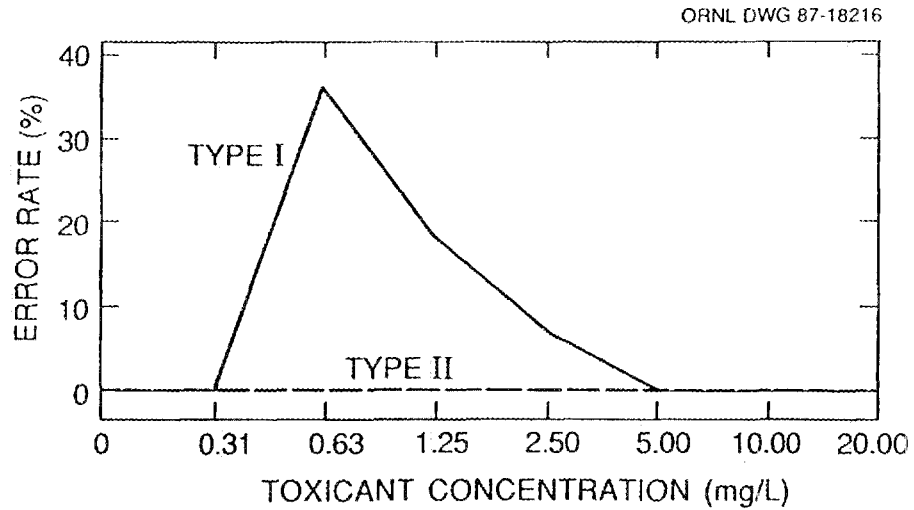
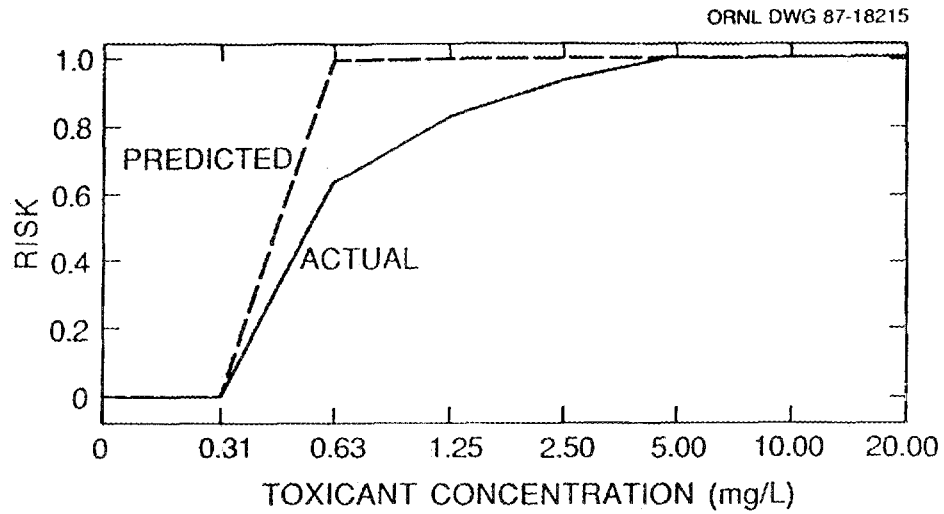


Figure 5.7 Blue-green and spring dominant phytoplankton as diagnostic variables based on ad-hoc nonlinear criterion. (a) solid line, actual risk; dashed line, predicted risk. (b) Solid line, type I error rate, dashed line, type II error rate.

but this is simply because the type I and type II error rates, being equal, cancel each other out. In fact, there is only a 56% chance of any particular prediction of the ecosystem state acceptability being correct at this concentration. If the  $\Omega$  region is defined on the basis of discriminant analysis, the predicted risk function more closely approximates the true risk, but again the error rates are substantial at intermediate exposures (Fig. 5.6). Finally, results based on a region with an ad-hoc nonlinear boundary are shown in Fig. 5.7. This diagnostic criterion is conservative in the sense that the predicted risk is always greater than or equal to the actual risk. Accordingly, the type II error rate is zero over the entire range of concentrations. The type I error rate, however, reaches a maximum of 36% at a toxicant concentration of 0.625 mg/L.

In section 4.5, selection of a diagnostic criterion was seen to involve making a compromise between type I and type II error rates. Although these error rates were quantified, choosing an appropriate trade-off was left as a matter of subjective judgment. It is possible, however, to arrive at more objective means of determining an optimal balance in the rates of occurrence of type I and type II errors. In particular, if costs can be associated with each of the various possible outcomes of management decisions, it is possible to select a diagnostic criterion to minimize the overall expected cost. Such a cost-minimizing strategy will now be considered, following the approach outlined by Page and Ricci (1985).

Reconsider the four mutually exclusive events which may occur with the use of diagnostic criteria in ecosystem management. We can associate costs with these events as follows:

$E_1$ : no damage, cost=0

$E_2$ : unnecessary management activity, cost= $\xi$

$E_3$ : undetected damage, cost= $\delta$

$E_4$ : management activity (cost= $\xi$ ) resulting in lessened damage (cost= $\delta^*$ , where  $0 \leq \delta^* \leq \delta$ )

In the long run, the expected total cost will be determined by the costs of these individual events, and by their relative likelihood. Specifically, the expected cost,  $E(\text{cost})$ , is:

$$E(\text{cost}) = 0 \cdot P(E_1) + \xi P(E_2) + \delta P(E_3) + (\xi + \delta^*) P(E_4) \quad (5.12)$$

In general, these probabilities, and perhaps also the costs, are conditional upon the toxicant concentration, but this dependence is not explicitly shown for the sake of notational simplicity. Equation 5.12 can be simplified to yield

$$E(\text{cost}) = \xi [P(E_2) + P(E_4)] + \delta P(E_3) + \delta^* P(E_4) \quad (5.13)$$

and then, substituting on the basis of 5.9,

$$E(\text{cost}) = \xi R + \delta P(E_3) + \delta^* P(E_4) \quad (5.14)$$

If, following Page and Ricci (1985), we assume that mitigatory strategies are possible which prevent significant damage to the ecosystem ( $\delta^*$  near zero), the last term can be dropped. Then, substituting on the basis of equation 5.11,

$$\begin{aligned} E(\text{cost}) &= \xi [R + P(E_2) - P(E_3)] + \delta P(E_3) \\ &= R + \xi P(E_2) + (\xi - \delta) P(E_3) \end{aligned} \quad (5.15)$$

The first term in equation 5.15, the actual risk, will not vary with the choice of diagnostic criteria. Therefore, the task simplifies to minimizing the sum of the last two terms, which is solely a function of the probabilities of occurrence of type I and type II errors.

Once the costs associated with the four basic events are determined, the expected cost associated with any particular diagnostic criterion is seen to a function of quantities previously determined. Greater flexibility in the model may be achieved by assuming that management and damage costs, rather than being described by constants, are themselves a function of ecosystem state. Again, the state space approach elaborated in this study, coupled with Monte Carlo simulation modeling, are useful tools which would be well-suited for such analysis.

## 5.5. CONCLUSION

This study has focused on the problem of quantitative and qualitative description of the dynamic response of ecosystems to toxicant stress. Due to the multifaceted aspects of ecosystem behavior required to characterize such response, it was argued that a multidimensional state space description is most appropriate. Specifically, the response can be characterized by the trajectory of a displacement vector, which is calculated as the vector difference between a perturbed system state trajectory and an unperturbed (control) trajectory.

State space analysis is readily applied to deterministic models of ecosystem dynamics, but extrapolation to the case of systems sampled discretely in the presence of noise is not trivial. Traditional multivariate techniques, such as principal components or discriminant analysis, are useful for elucidating certain aspects of ecosystem dynamics, but do not necessarily yield information on the displacement of perturbed trajectories. Therefore, I opted for direct estimation of the state space displacements as measured by a Mahalanobis distance metric. Since Mahalanobis distances are a function of the covariance structure of the data, it became important to consider changes in the covariance structure of ecological variables as a function of time and of toxicant exposure.

State space displacement analysis was applied to study the responses of aquatic ecosystems to phenolic toxicants. Data from

experimental systems encompassing 1.2 L flask microcosms, 72 L aquarium microcosms, and 15 m<sup>3</sup> outdoor ponds, were analyzed. Also analyzed were Monte Carlo computer simulations produced by a littoral ecosystem model incorporating the effects of natural variability and measurement error. The results of these analyses demonstrated the feasibility and utility of using state space measures as indicators of ecosystem response. The Monte Carlo simulation results were also used to demonstrate the high degree of statistical power provided by state space displacement analysis even with realistically noisy data. The ability of analysis to detect simulated effects of low toxicant concentrations even with little or no replication strongly supports its application to experimental data. It is likely that the state space approach will uncover effects not detected by conventional univariate approaches.

Additionally, analyses of both experimental data and simulation output reveals that the covariance structure of ecological systems is not constant. Rather, the covariance structure displays both temporal dynamics and changes in response to toxicant exposure. This emphasizes the importance of careful and adequate characterization of the covariance matrix used in the calculation of Mahalanobis distances. In situations where accurate estimation of the covariance matrix is a problem, the use of robust estimation techniques, or of Karl Pearson distances, may be desirable.

Although the best descriptions of ecosystem dynamics may require a state space of high dimensionality, practical considerations often

preclude the routine monitoring of large numbers of ecological variables. In this situation, a space of reduced dimensionality is desired which can be used to predict the position of the state vector in its higher dimensional space. The variables defining the lower dimensional space are referred to as diagnostic variables. Using the simulation output, it was possible to explore several possible sets of diagnostic variables, and to estimate their associated type I and type II statistical error rates.

The emphasis of this research has been on the description of ecosystem dynamics in response to toxicant stress. Such a description may not translate directly into an understanding of the underlying mechanisms or causal relationships generating the dynamics. However, any experiments aimed at elucidating mechanisms will require adequate measures of response, such as provided by state space analysis. Moreover, the covariance structure can be used as a tool to investigate underlying mechanisms. While it is true that the existence of a correlation does not logically imply a causal relationship, certain causal relationships do have logical implications regarding the correlation structure. Thus, the existence of an incompatible correlation structure may be used to rule out otherwise plausible mechanisms. It is hoped that the use of the methods developed in this study will lead to an increased understanding of ecosystem dynamics, and to more effective protection and management of ecosystems subject to toxicant stress.

## REFERENCES

- Allen, T.F.H., S.M. Bartell, and J.F. Koonce. (1977) Multiple stable configurations of phytoplankton community change rates. *Ecology* 58:1076-1084.
- Allen, T.F.H., D.A. Sadowsky, and the late N. Woodhead. (1984) Data transformation as a scaling operation in ordination of plankton. *Vegetatio* 56:147-160.
- Allen, T.F.H., and H.H. Shugart. (1983) Ordination of simulated complex forest succession: a new test of ordination methods. *Vegetatio* 51:141-155.
- Bartell, S.M., T.F.H. Allen, and J.F. Koonce. (1978) An assessment of principal components analysis for description of phytoplankton periodicity in Lake Wingra. *Phycologia* 17:1-11.
- Best, E.P.H. (1981) A preliminary model for growth of Ceratophyllum demersum L. *Verh. Internat. Verein. Limnol.* 21:1484-1491.
- Bloom, S.A. (1980) Multivariate quantification of community recovery. In J. Cairns, Jr. (ed.), *The Recovery Process in Damaged Ecosystems*. Ann Arbor Science Publishers, Ann Arbor, pp. 141-151.
- Bloomfield, J.A. (1975) Modeling the dynamics of microbial decomposition and carbon cycling in the pelagic zone of Lake George, New York. Ph.D. dissertation, Rensselaer Polytechnic Institute.
- Bowmer, K.H., D.S. Mitchell, and D.L. Short. (1984) Biology of Elodea canadensis Mich. and its management in Australian irrigation systems. *Aquat. Bot.* 18:231-238.
- Cairns, J. Jr., and K.L. Dickson. (1977) Recovery of streams and spills of hazardous materials. In Cairns, J. Jr., K.L. Dickson, and E.E. Herricks (eds.), *Recovery and Restoration of Damaged Ecosystems*, Univ. Virginia Press, Charlottesville, pp. 24-44.
- Carpenter, S.R. (1982) Comparison of equations for decay of leaf litter in tree-hole ecosystems. *Dikos* 39:17-22.
- Dale, H.M., and T.J. Gillespie. (1977) The influence of submersed aquatic plants on temperature gradients in shallow water bodies. *Can. J. Bot.* 55:2216-2225.
- Efron, B., and R. Tibshirani. (1986) Bootstrap methods for standard errors, confidence intervals, and other measures of statistical accuracy. *Statistical Science* 1:54-77.

- Allen, T.F.H., S.M. Bartell, and J.F. Koonce. (1977) Multiple stable configurations of phytoplankton community change rates. *Ecology* 58:1076-1084.
- Allen, T.F.H., D.A. Sadowsky, and the late N. Woodhead. (1984) Data transformation as a scaling operation in ordination of plankton. *Vegetatio* 56:147-160.
- Allen, T.F.H., and H.H. Shugart. (1983) Ordination of simulated complex forest succession: a new test of ordination methods. *Vegetatio* 51:141-155.
- Bartell, S.M., T.F.H. Allen, and J.F. Koonce. (1978) An assessment of principal components analysis for description of phytoplankton periodicity in Lake Wingra. *Phycologia* 17:1-11.
- Best, E.P.H. (1981) A preliminary model for growth of Ceratophyllum demersum L. *Verh. Internat. Verein. Limnol.* 21:1484-1491.
- Bloom, S.A. (1980) Multivariate quantification of community recovery. In J. Cairns, Jr. (ed.), *The Recovery Process in Damaged Ecosystems*. Ann Arbor Science Publishers, Ann Arbor, pp. 141-151.
- Bloomfield, J.A. (1975) Modeling the dynamics of microbial decomposition and carbon cycling in the pelagic zone of Lake George, New York. Ph.D. dissertation, Rensselaer Polytechnic Institute.
- Bowmer, K.H., D.S. Mitchell, and D.L. Short. (1984) Biology of Elodea canadensis Mich. and its management in Australian irrigation systems. *Aquat. Bot.* 18:231-238.
- Cairns, J. Jr., and K.L. Dickson. (1977) Recovery of streams and spills of hazardous materials. In Cairns, J. Jr., K.L. Dickson, and E.E. Herricks (eds.), *Recovery and Restoration of Damaged Ecosystems*, Univ. Virginia Press, Charlottesville, pp. 24-44.
- Carpenter, S.R. (1982) Comparison of equations for decay of leaf litter in tree-hole ecosystems. *Oikos* 39:17-22.
- Dale, H.M., and T.J. Gillespie. (1977) The influence of submersed aquatic plants on temperature gradients in shallow water bodies. *Can. J. Bot.* 55:2216-2225.
- Efron, B., and R. Tibshirani. (1986) Bootstrap methods for standard errors, confidence intervals, and other measures of statistical accuracy. *Statistical Science* 1:54-77.

- Flury, B.K., and H. Riedwyl. (1986) Standard distance in univariate and multivariate analysis. *Amer. Statis.* 40:249-251.
- Franco, P.J., J.M. Giddings, S.E. Herbes, L.A. Hook, J.D. Newbold, W.K. Roy, G.R. Southworth, and A.J. Stewart. (1984) Effects of chronic exposure to coal-derived oil on freshwater ecosystems: I. Microcosms. *Environ. Toxicol. Chem.* 3:447-463.
- Gardner, R.H., B. Rödger, and U. Bergström. (1983) PRISM: A Systematic Method for Determining the Effect of Parameter Uncertainties on Model Predictions. STUDSVIK/NW-83/555, Studsvik Energiteknik AB, Nyköping, Sweden.
- Gates, M.A. (1983) Trajectories of cell volume distribution during the growth cycle of Tetrahymena. *J. Gen. Microb.* 129:895-900.
- Gates, M.A., A.P. Zimmerman, W.G. Sprules, and R. Knoechel. (1983) Planktonic biomass trajectories in lake ecosystems. *Can. J. Fish. Aquat. Sci.* 40:1752-1760.
- Gatrell, A.C. (1983) Distance and Space: A Geographical Perspective. Clarendon Press, Oxford.
- Giddings, J.M., P.J. Franco, R.M. Cushman, L.A. Hook, G.R. Southworth, and A.J. Stewart. (1984) Effects of chronic exposure to coal-derived oil on freshwater ecosystems: II. Experimental ponds. *Environ. Toxicol. Chem.* 3:465-488.
- Giddings, J.M., P.J. Franco, S.M. Bartell, R.M. Cushman, S.E. Herbes, L.A. Hook, J.D. Newbold, G.R. Southworth, and A.J. Stewart. (1985) Effects of Contaminants on Aquatic Ecosystems: Experiments with Microcosms and Outdoor Ponds. ORNL/TM-9536, Oak Ridge National Laboratory, Oak Ridge, Tennessee.
- Godshalk, G.L. and R.G. Wetzel. (1978) Decomposition of aquatic angiosperms. II. Particulate components. *Aquat. Bot.* 5:301-327.
- Hampel, F.R., E.M. Ronchetti, P.J. Rousseeuw and W.A. Stahel. 1986. Robust Statistics: The Approach Based on Influence Functions. John Wiley and Sons, New York.
- Harrison, G.W. (1979) Stability under environmental stress: resistance, resilience, persistence and variability. *Am. Nat.* 113:659-669.
- Heath, R.T. (1980) Are microcosms useful for ecosystem analysis? In J.P. Giesy (ed.), *Microcosms in Ecological Research*, DOE Symposium Series 52, pp. 333-347.

- Hines, W.W., and D.C. Montgomery. (1980) Probability and Statistics in Engineering and Management Science, 2nd edition. John Wiley and Sons, New York.
- Holling, C.S. (1973) Resilience and stability of ecological systems. *Ann. Rev. Ecol. Syst.* 4:1-23.
- Huber, P.J. 1977 Robust Statistical Procedures. Society for Industrial and Applied Mathematics, Philadelphia.
- Ikusima, I. (1970) Ecological studies on the productivity of aquatic plant communities. IV. Light condition and community photosynthetic production. *Bot. Mag. Tokyo* 83:330-341.
- Iman, R.L., and W.J. Conover. (1982) A distribution-free approach to inducing rank correlation among input variables. *Commun. Statis.-Simula. Computa.* 11:311-334.
- Innis, G. (1975) Stability, sensitivity, resilience, persistence. What is of interest? In S.A. Levin (ed.) *Ecosystems: Analysis and Prediction*. SIAM-SIMS Research Application Conference on Ecosystems. Society for Industrial and Applied Mathematics, Philadelphia. pp. 131-139.
- Jewell, W.J. (1971) Aquatic weed decay: dissolved oxygen utilization and nitrogen and phosphorus regeneration. *J. Wat. Poll. Control Fed.* 43:1457-1467.
- Kunii, H. (1984) Seasonal growth and profile structure of Elodea nuttallii (Planch.) St. John in Pond Ojaga-Ike, Japan. *Aquat. Bot.* 18:239-247.
- Leffler, J.W. (1978) Ecosystem responses to stress in aquatic microcosms. In J.H. Thorp and J.W. Gibbons (eds.), *Energy and Environmental Stress in Aquatic Systems*, DOE Symp. Ser., pp. 102-119.
- Leffler, J.W. (1980) Microcosmology: theoretical applications of biological models. In J.P. Giesy (ed.), *Microcosms in Ecological Research*, DOE Symposium Series 52, pp. 14-29.
- Mahalanobis, P.C. (1936) On the generalized distance in statistics. *Proc. Nat. Inst. Sci. India* 2:49-55.
- Mardia, K.V. (1977) Mahalanobis distances and angles. In P.R. Krishnaiah (ed.), *Multivariate Analysis IV*. North-Holland Publishing Co., pp. 495-511.

- Marmorek, D.R. (1984) Changes in the temporal behavior and size structure of plankton systems in acid lakes. In G.R. Hendrey (ed.), *Early Biotic Responses to Advancing Lake Acidification*, Butterworth Publishers, Boston, pp. 23-41.
- Miller, Jr., R.G. (1966) *Simultaneous Statistical Inference*. McGraw-Hill, New York.
- May, R.M. (1975) Stability in ecosystems: some comments. In W.H. van Dobben, and R.H. Lowe-McConnell (eds.), *Unifying Concepts in Ecology, First International Congress of Ecology*, Dr W. Junk B. V. Publishers, The Hague, pp. 161-168.
- McKay, M.D., Conover, W.J., and R.J. Beckman. (1979) A comparison of three methods for selecting values of input variables in the analysis of output from a computer code. *Technometrics* 21:239-245.
- Moore, M.T. (1985) *The Effect of Phenolics on Photosynthesis and Respiration by Elodea canadensis*. M.S. thesis, Environmental Biology Program, Ohio State University.
- Morkoc, F., J.W. Biggar, D.R. Neilsen, and D.E. Rolston. (1985) Analysis of soil water content and temperature using state-space approach. *Soil. Sci. Soc. Am. J.* 49:798-803.
- Oakes, M. (1986) *Statistical Inference: A Commentary for the Social and Behavioral Sciences*. John Wiley and Sons, New York.
- Ondok, J.P., J. Porkorný, and J. Květ. (1984) Model of diurnal changes in oxygen, carbon dioxide and bicarbonate concentrations in a stand of Elodea canadensis Michx. *Aquat. Bot.* 19:293-305.
- Ollason, J.G. (1977) Freshwater microcosms in fluctuating environments. *Oikos* 28:262-269.
- O'Neill, R.V. (1976). Ecosystem persistence and heterotrophic regulation. *Ecology* 57:1244-1253.
- O'Neill, R.V., S.M. Bartell, and R.H. Gardner. (1983) Patterns of toxicological effects in ecosystems: a modeling study. *Environ. Toxicol. Chem.* 2:451-461.
- O'Neill, R.V., R.H. Gardner, L.W. Barnthouse, G.W. Suter, S.G. Hildebrand, and C.W. Gehrs. (1982) Ecosystem risk assessment: a new methodology. *Environ. Toxicol. Chem.* 1:167-177.

- O'Neill, R.V., W.F. Harris, B.S. Ausmus, and D.E. Reichle. (1975) A theoretical basis for ecosystem analysis with particular reference to element cycling. In F.G. Howell, J.B. Gentry and M.H. Smith (eds.), Mineral Cycling in Southeastern Ecosystems ERDA Symposium Series, CONF-740513, pp. 28-40.
- Orians, G.H. (1975) Diversity, satbility and maturity in natural ecoystems. In W.H. van Dobben and R.H. Lowe-McConnell (eds.), Unifying Concepts in Ecology, First International Congress of Ecology. Dr. W. Junk B. V. Publishers, The Hague, pp. 139-150.
- Page, T., and P.F. Ricci. (1985) A cost-benefit perspective for risk assessment. Chapter 2 in Ricci, P.F. (ed.), Principles of Health Risk Assessment. Prentice-Hall, Englewood Cliffs, New Jersey. pp. 37-65.
- Patten, B.C. (1984) System theory formulation of site-specific water quality standards and protocols. Ecol. Modelling 23:313-340.
- Pearson, K. (1926) On the coefficient of racial likeness. Biometrika 18:105-117.
- Penrose, L.S. (1954) Distance, size and shape. Ann. Eugen. 18:337-343.
- Pimm, S.L. (1984) The complexity and stability of ecosystems. Nature 307:321-326.
- Pokorný, J., J. Květ, J.P. Ondok, Z. Toul, and I. Ostrý. (1984) Production - Ecological analysis of a plant community dominated by Elodea canadensis Michx. Aquat. Bot. 19:263-292.
- SAS Institute, Inc. (1985a) The MATRIX Procedure: Language and Applications, Technical Report P-135, SAS Institute, Inc., Cary, North Carolina.
- SAS Institute, Inc. (1985b) SAS User's Guide: Basics, Version 5 Edition, SAS Institute, Inc., Cary, North Carolina.
- SAS Institute, Inc. (1985c) SAS User's Guide: Statistics, Version 5 Edition, SAS Institute, Inc., Cary, North Carolina.
- Sayler, G.S., T.W. Sherrill, R.E. Perkins, L.M. Mallory, M.P. Shiaris, and D. Pedersen. (1982) Impact of coal-coking effluent on sediment microbial communities: a multivariate approach. Appl. Environ. Microb. 44:1118-1129.

- Sayler, G.S., R.E. Perkins, T.W. Sherrill, B.K. Perkins, M.S. Shields, H.L. Kong, and J.W. Davis. (1983) Microcosm and experimental pond evaluation of microbial community response to synthetic oil contamination in freshwater sediments. *Appl. Environ. Microb.* 46:211-219.
- Shannon, L.J., M.C. Harrass, D.J. Yount and C.T. Walbridge. (1986) A comparison of mixed flask culture and standardized laboratory model ecosystems for toxicity testing. In J. Cairns, Jr. (ed.), *Community Toxicity Testing*. ASTM STP 920, American Society for Testing and Materials, Philadelphia, pp. 135-157.
- Shapiro, S.S., and M.B. Wilk. (1965) An analysis of variance test for normality (complete samples). *Biometrika* 52:591-611.
- Sheehan, P.J. (1984) Effects on community and ecosystem structure and dynamics. In Sheehan, P.J., D.R. Miller, G.C. Butler and P. Bourdeau (eds.), *Effects of Pollutants at the Ecosystem Level*, SCOPE 22. John Wiley and Sons, Chichester, pp. 51-99.
- Shugart, H.H., R.A. Goldstein, and R.V. O'Neill. (1974) TEEM: A terrestrial ecosystem energy model for forests. *Oecol. Plant.* 25:251-284.
- Simpson, P.S., and J.W. Eaton. (1986) Comparative studies of the photosynthesis of the submerged macrophyte Elodea canadensis and the filamentous algae Cladophora glomerata and Spirogyra sp. *Aquat. Bot.* 24:1-12.
- Stebbing, A.R.D. (1982) Hormesis - the stimulation of growth by low levels of inhibitors. *The Science of the Total Environment* 22:213-234.
- Suter II, G.W., L.W. Barnthouse, and R.V. O'Neill. (1987) Treatment of risk in environmental impact assessment. *Environ. Manag.* 11:295-303.
- Tatsuoka, M.M. (1971) *Multivariate Analysis: Techniques for Educational and Psychological Research*. John Wiley and Sons, New York.
- Taub, F.B., and P.L. Read. (1982) *Standardized Aquatic Microcosm Protocol, Vol. II. Final Report: Model ecosystems, design, development, construction and testing*. Contract 223-80-2352. Food and Drug Administration, Washington, D.C.
- Titus, J., R.A. Goldstein, M.S. Adams, J.B. Mankin, R.V. O'Neill, P.R. Weiler, Jr., H.H. Shugart, and R.S. Booth. (1975) A production model for Myriophyllum spicatum L. *Ecology* 56:1129-1138.

- Ulanowicz, R.E. (1978) Modeling environmental stress. In J.H. Thorp, and J.W. Gibbons (eds.), Energy and Environmental Stress in Aquatic Systems. DOE Symposium Series, pp. 1-18.
- Waide, J.B., J.E. Schindler, M.C. Waldron, J.J. Hains, S.P. Schreiner, M.L. Freedman, S.L. Benz, D.R. Pettigrew, L.A. Schissel, and P.J. Clark. (1980) A Microcosm approach to the study of biogeochemical systems. 2. Responses of aquatic laboratory microcosms to physical, chemical, and biological perturbations. In J.P. Giesy (ed.), Microcosms in Ecological Research. DOE Symposium Series 52, pp. 204-223.
- Webster, J.R., J.B. Waide, and B.C. Patten. (1975) Nutrient recycling and the stability of ecosystems. In F.G. Howell, J.B. Gentry and M.H. Smith (eds.), Mineral Cycling in Southeastern Ecosystems. ERDA Symposium Series, CONF-740513, pp. 1-27.
- Westman, W.E. (1978) Measuring the inertia and resilience of ecosystems. BioScience 28:705-710.
- Woltering, D.M. (1985) Population responses to chemical exposure in aquatic multispecies systems. In J. Cairns, Jr. (ed.), Multispecies Toxicity Testing. Pergamon Press, New York, pp. 61-75.
- Zadeh, L.A., and C.A. Desoer. (1963) Linear System Theory: The State Space Approach. McGraw-Hill, New York.



## INTERNAL DISTRIBUTION

- |        |                  |        |                               |
|--------|------------------|--------|-------------------------------|
| 1.     | S. I. Auerbach   | 25.    | A. W. King                    |
| 2.     | L. W. Barnthouse | 26.    | R. V. O'Neill                 |
| 3-7.   | S. M. Bartell    | 27.    | W. M. Post                    |
| 8.     | J. J. Beauchamp  | 28.    | M. L. Poutsma                 |
| 9.     | H. L. Boston     | 29.    | D. E. Reichle                 |
| 10.    | J. A. Cunningham | 30.    | K. A. Rose                    |
| 11.    | D. L. DeAngelis  | 31.    | G. W. Suter II                |
| 12.    | W. R. Emanuel    | 32.    | S. S. Talmage                 |
| 13.    | C. J. Ford       | 33.    | R. S. Turner                  |
| 14.    | R. H. Gardner    | 34.    | W. Van Winkle                 |
| 15.    | C. W. Gehrs      | 35.    | Central Research Library      |
| 16.    | B. Harvey        | 36-50. | ESD Library                   |
| 17.    | S. G. Hildebrand | 51-52. | Laboratory Records Department |
| 18.    | W. Hill          | 53.    | Laboratory Records, RC        |
| 19.    | M. Horn          | 54.    | ORNL Patent Office            |
| 20-24. | A. R. Johnson    | 55.    | ORNL Y-12 Technical Library   |

## EXTERNAL DISTRIBUTION

56. R. P. Berube, Deputy Assistant Secretary for Environment, EH-20, U. S. Department of Energy, Washington, DC 20585
57. C. M. Borgstrom, Director, Office of NEPA Project Assistance, EH-25, U.S. Department of Energy, Washington, D.C. 20585
58. D. L. Bunting, The University of Tennessee, Knoxville, TN 37916-1610
59. J. Burris, E. C. Jordan Co., Corporate Place 128, 107 Audubon Road, Building 11, Suite 301, Wakefield, MA 01880
60. J. Thomas Callahan, Associate Director, Ecosystems Studies Program, Room 336, 1800 G Street, NW, National Science Foundation, Washington, DC 20550
61. R. R. Colwell, Director of Maryland Biotechnology Institute, University of Maryland, Rm. 2A, Elkins Building, College Park, MD 20742
62. W. E. Cooper, Department of Zoology, College of Natural Sciences, Michigan State University, East Lansing, MI 48824
63. G. J. Foley, Office of Environmental Process and Effects Research, U.S. Environmental Protection Agency, 401 M Street, SW, RD-682, Washington, DC 20460
64. J. M. Giddings, Springborn Bionomics, Inc., 790 Main St., Wareham, MA 02571
65. Harvey Holme, U.S. Environmental Protection Agency, Environmental Research Laboratory, Athens, GA 30613
66. L. Hook, Science Applications International Corp., 800 Oak Ridge Turnpike, Oak Ridge, TN 37830

67. J. W. Huckabee, Manager, Ecological Studies Program, Electric Power Research Institute, 3412 Hillview Avenue, P.O. Box 10412, Palo Alto, CA 94303
68. George Y. Jordy, Director, Office of Program Analysis, Office of Energy Research, ER-30, G-226, U.S. Department of Energy, Washington, DC 20545
69. Raymond Lassiter, U.S. Environmental Protection Agency, Environmental Research Laboratory, Athens, GA 30613
70. Simon A. Levin, Department of Ecology and Systematics, Biological Sciences Bldg., E-347, Cornell University, Ithaca, NY 14853
71. G. E. Likens, Director, The New York Botanical Garden, Institute of Ecosystem Studies, The Mary Flagler Cary Arboretum, Box AB, Millbrook, NY 12545
72. C. J. Mankin, Director, Oklahoma Geological Survey, The University of Oklahoma, 830 Van Vleet Oval, Room 163, Norman, OK 73019
73. Helen McCammon, Director, Ecological Research Division, Office of Health and Environmental Research, Office of Energy Research, MS-E201, ER-75, Room E-233, U.S. Department of Energy, Washington, DC 20545
74. G. P. Patil, Statistics Department, 318 Pond Laboratory, Pennsylvania State University, University Park, PA 16802
75. Donald J. Rodier, Environmental Protection Agency, TS-796, 401 M Street, SW, Washington, DC 20460
76. Michael Slimak, Office of Pesticide Programs (TS-796), U.S. Environmental Protection Agency, 401 M Street SW, Washington, DC 20460
77. F. Stay, U.S. Environmental Protection Agency, Environmental Research Laboratory, 6201 Congdon Blvd., Duluth, MN 55804
78. Frank J. Wobber, Division of Ecological Research, Office of Health and Environmental Research, Office of Energy Research, MS-E201, U.S. Department of Energy, Washington, DC 20545
79. M. Gordon Wolman, The Johns Hopkins University, Department of Geography and Environmental Engineering, Baltimore, MD 21218
80. J. D. Yount, U.S. Environmental Protection Agency, Environmental Research Laboratory, 6201 Congdon Blvd., Duluth, MN 55804
81. Office of Assistant Manager for Energy Research and Development, Oak Ridge Operations, P. O. Box 2001, U.S. Department of Energy, Oak Ridge, TN 37831
- 82-91. Office of Scientific and Technical Information, P.O. Box 62, Oak Ridge, TN 37831